Residential Distribution System Power Quality Improvement using DG-Grid Interfacing VSC

by

Md Shirajum Munir

A thesis submitted in partial fulfillment of the requirements for the degree of

Doctor of Philosophy

in

Energy Systems

Department of Electrical and Computer Engineering
University of Alberta

Abstract

The increasing utilization of power electronic loads in today's homes is a growing concern for utility companies due to the increased harmonic distortions. The harmonic problem is further complicated by the harmonic resonance introduced by other system components, such as the power factor correction (PFC) capacitors. At the same time, power industry is experiencing a paradigm shift as more renewable energy based distributed generation (DG) systems are being connected to the power distribution network. These DG systems are connected to the grid through DG-grid interfacing inverters which can be used to address the harmonic issue utilizing the available apparent power rating from the interfacing inverters.

To ensure proper utilization of the available DG rating, this thesis discusses interfacing converter control method that actively mitigates the harmonics in residential distribution systems. The first objective is to determine the harmonic compensation priorities for DG converters in a given distribution system, considering harmonics load locations, PFC capacitors etc. To realize this objective, this thesis conducts an in-depth investigation of different control methods of VSI for power quality improvement. Then a modal analysis based approach is proposed to determine compensation priorities for different harmonics and at different distribution system nodes to improve harmonic compensation performance. The second objective of this thesis is to develop harmonic compensation functions on DC converters that can consider harmonics compensation priority, aggregated available DG ratings, loads, etc. To do so, a priority driven G-S droop based selective harmonic compensation scheme is proposed in this thesis that assigns compensation priorities on DGs with different ratings and operating at different distribution system nodes.

Acknowledgement

I would like to show my sincerest appreciation to Dr. Yunwei Li. I must say that without his endless patience and tireless will to guide and supervise me, I would have never be able to conduct this work. I will always be proud to say that I had the privilege of being his student, and I hope to have learned enough to succeed in my future career. During the tough years when I was very sick, he supported me like my guardian. I will remain forever grateful to him for all the support he gave me.

I thank Alberta Ingenuity Fund for their generous grants provided for more than 5 years. I am also thankful to the University of Alberta, for providing me with one year of the Entrance Scholarship, to the ECE department for providing me with several terms of T.A, and to GSA for providing me with PD travel grants. This collection of financial sources made my student life a lot more enjoyable, and is very much appreciated.

I thank my parents Mosfika and Karim for supporting me in so many different ways. They supported my coming to Canada and my desire to spend another half decade in school.

I am deeply obliged with my wife Rubaba. Without her encouragement, I would not have continued my Ph.D. when I faced some of the major obstacles. Rubaba is the person who most loved and motivated me during the past few years. I wish to lead our family to an eternal, healthy and fulfilling relationship. I would also like to express my gratitude to the love and support from my parents-in-law, Gulshan and Gaffar.

I want to acknowledge all the other members of the power lab as well, whose names are not mentioned here.

Finally, I thank the committee members of this examination for the valuable comments that helped in improving the quality of this thesis: Dr. Yunwei Li, Dr. Yasser Abdel-Rady I. Mohamed, Dr. Qing Zhao, Dr. Hao Liang and Dr. Carl (Ngai Man) Ho.

Table of Contents

Table of Figures

List of Tables

List of Acronym

DG – Distributed Generation

PFC – Power Factor correction

IEA – International Energy Agency

PV – Photovoltaic

CFL – Compact Fluorescent Light

PHF – Passive Harmonic Filter

APF – Active Power Filter

IGBT - Insulated Gate Bipolar Transistors

FFT – Fast Fourier Transform

SDFT – Sliding Discrete Fourier Transform

VSC – Voltage Source Converter

VSI – Voltage Source Inverter

CSI – Current Source Inverter

VCM – Voltage Control Method

CCM – Current Control Method

PR – Proportional Resonant

DSP – Digital Signal Processing

FPGA – Field-Programmable Gate Array

PCC – Point of Common Coupling

SOGI – Second Order Generalized Integrator

THD – Total Harmonic Distortion

TDD – Total Demand Distortion

RES – Renewable Energy Sources

THD – Total Harmonic Distortion

PWM – Pulse Width Modulation

WAC – Weighted Average Control

GCC – Generalized Closed Loop Control

R-APF – Resistive Active Power Filter

MPPT – Maximum Power Point Tracking

PLL – Phase Locked Loop

HVAC – Heating, Ventilation and Air Conditioning

LED – Light Emitting Diode

PWM – Pulse Width Modulation

ASD – Adjustable Speed Drive

DAFS – Distributed Active Filter System

CPV – Compensation Priority Value

Chapter 1

Introduction

1.1 Renewable Energy Based Distributed Generation

Distributed generation is the term used when electricity is generated from renewable energy based small-scale (typically 1 kW – 50 MW) sources, near the point of use instead of centralized generation sources like traditional power plants. The concept of many small scale energy source based DGs dispersed over the grid gained a considerable interest in the recent time. International Energy Agency (IEA) lists five major factors [1] those contributed to this evolution. They are, developments in distributed generation technologies, constraints on the construction of new transmission lines, increased customer demand for reliable electricity, liberalization of the electricity market and concerns regarding the climate change. Vast majority of these DG units operate as grid connected microgeneration units and the number is significantly increasing with the increasing number of residential DG installations. Sitting between microgeneration and utility-scaled centralized generation are microgrids. A microgrid typically consist of multiple DG units those are situated in the midst of a dense load center and supplies electricity to those loads. The DGs those operate as microgeneration units are typically grid connected while DGs in the microgrid can be connected to the main grid and can also operate in the islanded mode.

Although there has been a significant growth of DGs in the recent time, the proliferation of generation sources that are small in scale but potentially significant in the aggregate, and whose operation may not be directly under utility or grid operator control, adds challenges to grid operation. For example, at higher penetration levels, distributed resources can affect reliability. Additionally, DG-grid interfacing converters can cause voltage fluctuations [2], transient disturbances [3] and other conditions that detrimentally affect power quality and impact customers adjacent to the DG source. Also, the DG-grid interfacing converters may introduce harmonics into the power system and cause additional power quality concerns [4]. At the same time, these DG-grid interfacing converters are also able to improve the system efficiency and power quality if designed and controlled properly. To realize this function of DG, besides the primary purpose of real power generation, many ancillary services, such as power factor compensation, voltage support [5], flicker mitigation [6], system harmonic compensation [7-9], unbalance voltage compensation [10], etc. can also be provided through the DGs whenever there is sufficient apparent power rating available. Doing so is feasible as most of the time these inverters are not running at their maximum rated power due to the intermittent nature of renewable energy [11]. Moreover, peak demand in residential areas does not occur at the same time as the peak renewable energy generation. Therefore, when power quality compensation is needed, rating from the renewable energy based DGs are usually available to provide the ancillary services [11, 12]. As a result, utilizing these available rating effectively to ensure optimal power quality improvement performance is an important research topic that should be addressed properly.

Taking this into account, this work aims to optimize the power quality improvement performance of renewable energy based distributed generation units in a residential distribution system. Since PV energy based distributed generation systems are most common in the residential distribution system and worldwide growth of renewable power generation is mainly driven by solar PV growth, this thesis particularly focuses on power quality improvement using PV based DG systems.

1.2 Harmonics in Today's Power System

Typical power system and its components are designed as AC system which operates with pure sinusoidal voltage and current. Ideally, utility companies should provide electric power to the consumers through 50/60 Hz sinusoidal voltage and current waveform. But the proliferation of non linear and power electronics switched residential loads are causing harmonic distortion in the grid voltage and current [14]. Harmonic producing residential loads like TV, compact florescent light (CFL), personal computer, laptop, washing machine etc. are distributed across the power distribution system and inject harmonic currents at every node. At the same time, many countries are placing lighting and appliance standards at a very high priority. As a result, more replacement of such appliances into energy-efficient ones is expected in the next few years. Although their individual harmonic current contribution to the distribution system is insignificant, the wide spread use of such energy efficient appliances contributes a significant amount of harmonic current to the grid collectively [15-17]. As a result, the harmonic distortion in the urban area is significantly increasing as the residential load is increasing [18-21]. This is an alarming situation as the harmonic polluted grid voltage and current may cause a number unwanted effects such as increased loss and vibration of electrical machines [22], transformer overheating [23], premature aging of the distribution transformers [24]. The distorted voltage and current waveform on the distribution grid may cause voltage and current stress on power cables which may lead to dielectric failure [25]. The distribution grid usually contains power factor correction capacitors (PFCs). This PFCs can introduce series and parallel resonances in the distribution grid which can even amplify the harmonic levels and make the distortion even worse [26]. At the same time, increased harmonic current flow may cause dielectric loss and thermal stress when they flow through PFCs as PFCs have low shunt impedance at high-order harmonics. They may cause excessive stress on the PFCs and eventually lead to failure of PFCs [27]. This high level of harmonic distortion also causing telephone interference in the residential distribution system [28].

The modern power electronic based residential loads are introducing harmonic related power quality concerns and at the same time, the use of such appliances will only see growth in the coming days. As a result, the harmonic problem in the distribution system will only increase with time which has raised a widespread concern. Since the use of modern power electronic residential loads can not be avoided, a number of previous works tried to address this harmonic related power quality issue.

1.3 Harmonic Compensation in the Power Distribution System

Harmonic mitigation approaches in the power distribution system can be classified into two main categories: harmonic mitigation at the source and harmonic mitigation at harmonic transmission path [29]. To mitigate the harmonics at the source, design of electronic devices can be improved so that they produce less harmonics. However, this approach can not be used for the existing devices in distribution systems. So the installation of harmonic compensation devices at the distribution system is more suitable to address the harmonic problem. There are two major types of harmonic compensation techniques based on the harmonic mitigation mechanisms, i.e., the traditional passive harmonic mitigation techniques and active harmonic mitigation techniques.

1.3.1 Passive Harmonic Mitigation Techniques

There are a few passive harmonic mitigation techniques available to reduce the level of harmonic pollution in an electrical network, such as connection of series line reactors, passive harmonic filters etc. In these methods, the undesirable harmonic current is prevented from flowing into the grid by either by implementing a high series impedance to block the flow of the harmonic current or diverting the flow of harmonic currents by creating a parallel path with low-impedance. The use of series AC line reactors, which essentially is an inductor, is a common and economical means of reducing harmonics. For example, line reactor at the input rectifier of a motor drive system reduces harmonics. Passive harmonic filter (PHF) involves series or parallel connection of a tuned LC and high-pass filter circuit and forms a low-impedance path for a specific harmonic frequency. The filter is connected in parallel or series with the electrical distribution line to divert the tuned frequency harmonic current away from flowing back to the grid which eliminates a single harmonic frequency. Such L-C passive filters based PHF are widely used to achieve the harmonic suppression and to improve power factor. There are mainly two categories of passive power filters, i.e., tuned filters and high-pass filters depending on their structure. Although PHFs have many advantages such as design simplicity, high efficiency, no control link requirement, ease of maintenance, etc., there are still many drawbacks in practical design and applications [30-33]. For example, the increased cost involved to install PHFs is a significant barrier. A single tuned PHF can mitigate only a single specific harmonic frequency. So additional PHFs are needed to address different harmonics. The harmonic elimination performance of a PHF largely depends on parameters of the passive components and grid impedances. Also, if there is a frequency variation in the system harmonics, the effectiveness of existing PHF to suppress harmonics will be reduced as the PHFs are tuned to specific frequencies. When parallel-connected PHF is connected further upstream in the power network, higher cost accumulates due to the losses in the conductors as they carry harmonic currents. When PHF is series connected with the load, the losses in the filter itself due to the higher series impedance increases.

1.3.2 Active Harmonic Mitigation Techniques

Active harmonic reduction techniques uses active power filters (APF) and improves the power quality by injecting equal and opposite current or voltage distortion into the network which cancels the original distortion. APFs uses power electronic switches, e.g., insulated gate bipolar transistors (IGBT), to produce output current of the required shape such that when injected into the AC lines, it cancels the grid harmonics.

Contrary to passive harmonic mitigation techniques, active harmonic mitigation techniques are more flexible in a number of ways, e.g., the impact of the variation of system harmonics and impedances. The active harmonic mitigation techniques present no risks of introducing additional resonance in the system and dynamic compensation can be realized (compensating different harmonic frequencies). Due to all these advantages, active harmonic mitigation techniques have become one of the most effective means to suppress harmonics and eliminate distortion in voltage and current waveforms in the electrical power system.

The APF control strategies play a very important role on the improvement of the performance and stability of the filter. Contrary to their passive counterparts, APFs contain energy storage elements at the DC link side of the inverters. These elements are usually DC inductor or DC capacitor. Based on the energy storage element present in APFs, it can be of two types, current source inverter based APF and voltage source inverter based APF. The controller of the APFs generates its reference current in two different ways. The first method uses different methods, e.g., fast Fourier transforms (FFT), sliding discrete Fourier transform (SDFT) etc., to calculate the amplitude and phase angle of each harmonic present in the load current. The APF is then controlled to produce current of equal amplitude but opposite phase angle of specific harmonic order(s). The second method of control is referred to as full spectrum cancellation. Here the controller removes the fundamental frequency component from the load current and operates the APF to inject the inverse of the remaining waveform which cancels the distortion.

APFs could be classified as parallel or series APF according to the circuit configuration which is shown in Figure 1.1. In case of the series APF, the controller detects the instantaneous supply current (I_s) and extracts the harmonic current (I_{sh}). the active filter applies the compensating voltage V_{APF} ($= -K I_{sh}$) via the interfacing transformer. This results in a significant reduction in the supply harmonic current (I_{sh}), when the feedback gain K is set to be high enough. In case of the parallel APF, the controller detects the instantaneous load current (I_L), extracts the harmonic current (I_{Lh}) and draws the compensating current I_h ($= -I_{Lh}$).

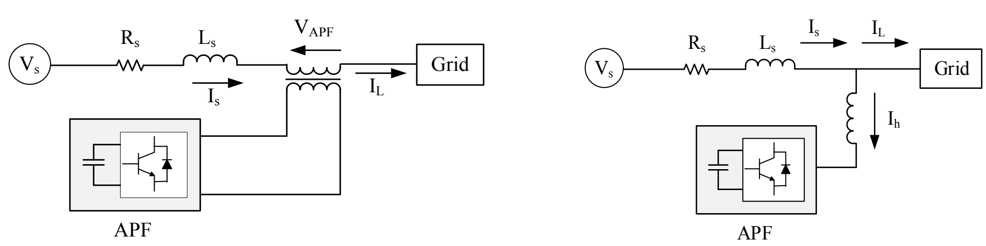

(a) (b)

Figure 1.1. (a) Series and (b) shunt active power filter (APF).

Although the active harmonic mitigation techniques can overcome the shortcomings of passive techniques, this method is expensive due to the dedicated high performance control and power electronic devices used solely to compensate harmonics. Moreover, the effectiveness of this method is limited to the capacity of the APF and cost rises notably with the increasing capacity. On the other hand, renewable energy based DGs are connected to the grid via interfacing inverters. These interfacing inverters can be controlled properly to provide different ancillary services including harmonic compensation. When DG interfacing inverters are used to compensate harmonics, it eliminates the need of separate APF hardware installation and ensures the maximum utilization of the available rating of the DG. As a result, the control of DG-grid interfacing inverters to compensate harmonics have received a lot of research interest recently.

1.4 DG-Grid Interfacing Converter

Typically, the DG units are connected to the electrical network via interfacing inverters. e.g. PV and fuel cell system produce DC voltages at the output and they require DC/AC inverters to AC grid integration. Micro-turbines and wind turbine systems produce variable frequency AC output and they will need AC/AC (typically with front end AC/DC rectifier and grid side DC/AC inverter) for AC grid connection. Various topologies of inverters can be classified broadly into two main types, namely voltage source inverter (VSI) and current source inverter (CSI).

When the input current of an inverter is maintained constant, it is called current source inverter (CSI). In a current source inverter, the DC current is kept constant with a small ripple using a large inductor, thus forming a current source on the DC side. CSI based DC-AC interfacing converters are not very popular in DG grid integration. But there have been used in PV, fuel cell and battery storage where the boost capability of CSI converter enable single stage DC/AC conversion instead of the two stage DC/DC+DC/AC conversion.

When the input DC voltage of an inverter is maintained constant, it is called voltage source inverter (VSI). In a voltage source inverter, the input DC voltage is kept constant with small ripple using a large capacitor, thus forming a constant voltage source on the DC side. VSI based interface has been dominantly used in DG grid integrations.

When the DG is interfaced to the grid, fast dynamic response is desired. Hence, VSIs are mostly used to interface DG with the grid which can be controlled properly to provide additional ancillary services. Control mechanisms of the VSIs are mainly of two types, namely current control method (CCM) and voltage control method (VCM).

The control can be realized in synchronous frame, stationary frame or natural frame. In synchronous reference frame control, a frame transformation is used to transform the input current and voltage signals into a reference frame that rotates synchronously with the grid voltage. As a result, sinusoidal voltage and current quantities become DC quantities. This type of control is also referred as *dq* frame control. As the input voltage and current signals are converted into DC quantities, it offers the benefit of easier filtering and controlling. Also, the phase of the voltage and current remain unaffected after being filtered since they are DC quantities. In stationary reference frame control scheme, a frame transformation is used to transform the input current and voltage signals into a reference frame that is stationary using an abc-αβ frame transformation module. Since the reference frame is stationary, the transformed voltage and current signals are also sinusoidal. As the input qualities are sinusoidal in this case, a PI controller fails to remove steady state error when controlling such sinusoidal signal. To control such waveform, proportional resonant (PR) controllers are used. In case of PR controllers, the gain at the resonant frequencies is very high and consequently they remove any steady state error between the reference and feedback signals. In case of natural frame control scheme, three separate controllers are employed for each phase. For natural frame controllers, usually nonlinear controllers such as hysteresis and dead beat controllers are used. The performance of such controllers improves with increase of switching frequency. With the advancement of power electronics technology, this control scheme is becoming more attractive to implement with DSP and FPGA.

1.4.1.1 Voltage Control Method (VCM) of VSI

For autonomous islanded microgrid applications where DG-grid interfacing VSI has to provide direct voltage support, voltage control method of VSI are used [34-36]. To enable load sharing in an islanding microgrid with multiple DG units, VCM of VSI usually employs V-f droop control. To implement V-f droop control, real power-frequency droop (P-f) and reactive power-voltage magnitude droop (Q-E) is usually adopted. Here, the DG interfacing converter is controlled to behave like synchronous generators. An advantage of this method that the DG units that are controlled to emulate synchronous generator, can also collaborate with real distributed synchronous generators. A VCM based VSI control scheme is shown in Figure 1.2. Here the VSI is connected to the PCC with an LCL filter. The capacitor voltage of the LCL filter is controlled to integrate the DG system to grid.

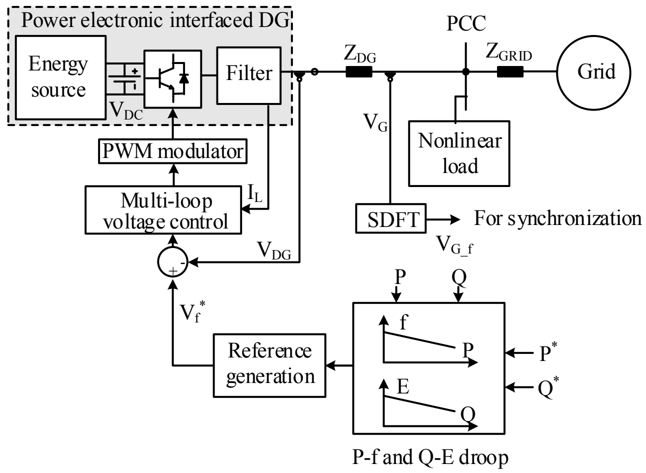

Figure 1.2. Voltage control method (VCM) based VSI control scheme

Although VCM based VSI has the unique application in islanding microgrid operation, this method does not have any direct control of inverter line current which is essential to provide ancillary services with DG. In [37], a novel method to compensate harmonics using the VCM based VSI is proposed based on the virtual impedance concept.

1.4.1.2 Current Control Method (CCM) of VSI

Figure 1.3 illustrates the configuration of a CCM based DG-grid interfacing VSI. The CCM based VSIs are adopted for most grid connected DG systems.

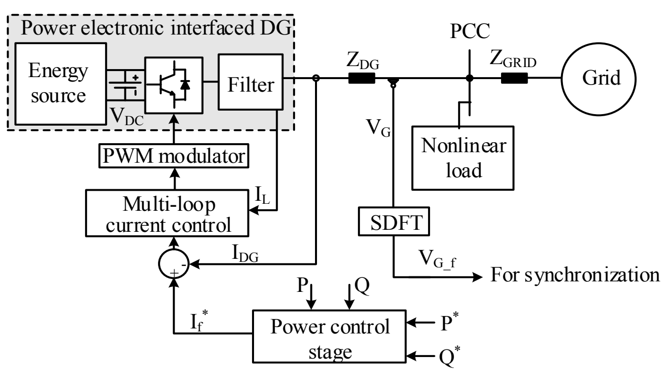

Figure 1.3. CCM based VSI control scheme

As illustrated, the fundamental reference current (I_f^*) is obtained from the power control loop. The real power reference can be produced using the maximum power point tracking like in a wind or a photovoltaic system, the maximum system efficiency control like in a fuel cell system, or the command value from a microgrid energy management center. The reactive power command can be produced from voltage support requirements. If unity-power-factor injection from a DG is desired, this reactive power command can be simply set to zero.

1.5 Distribution System Harmonic Compensation Using DG

As mentioned earlier, due to the limitations of passive harmonic mitigation techniques and APFs and with the significant advances in power electronics technology, distribution system harmonic compensation using DG has been gaining a lot of attentions recently. Due to the dispersed nature of DG installations across the distribution system, DG-grid interfacing converter can be used to compensate harmonics in two scenarios.

1.5.1 Compensation of Harmonic Current from Local Load

Figure 1.4 shows an interfacing converter with a local nonlinear load connected to the output terminal of the LCL filter. When the interfacing converter just injects real power to the grid without any harmonic compensation, the inverter output current is sinusoidal. As a result, the harmonic current from the local load flows to the grid side. In the presence of line impedance, this distorted line current distorts line voltage along the distribution feeder. On the other hand, this local load harmonic current can be absorbed by the interfacing converter which will make the line voltage and current distortion free.

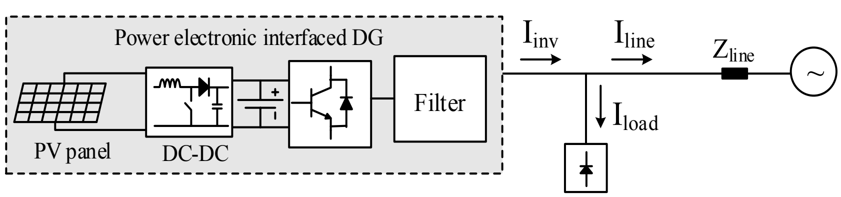

(a)

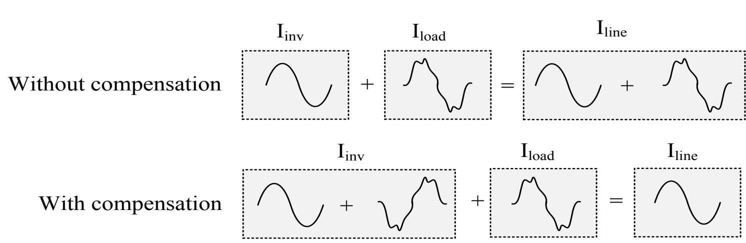

(b)

Figure 1.4. Local non linear load harmonic compensation

To realize this task, an accurate detection of the local load harmonic current and a rapid tracking of the harmonic current reference in the interfacing converter are important. Figure 1.5 shows a diagram of the local load harmonic compensation scheme in an interfacing converter. First, the local load current is measured and a digital filter is used to extract the harmonic component. Various types of digital filters have been proposed in literature, e.g., Fourier transformation based detection method [38], instantaneous real and reactive power based detection theory [39], a second-order generalized integrator (SOGI) [40], detection method based on delayed signal cancellation [41] etc. In the inner current tracking loop, the local load harmonic current component is used as a reference (I_h^*) while wide bandwidth controllers such as proportional and multiple resonant (PR) controllers, a deadbeat controller, etc., can ensure rapid current tracking.

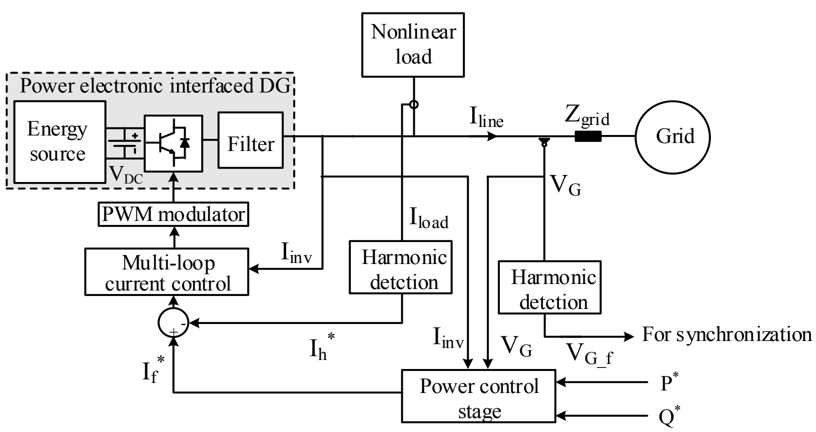

Figure 1.5. Control scheme of local load harmonics compensation

1.5.2 Compensation of Distribution System Voltage Harmonics

As shown in Figure 1.6, when the DG is connected to a distribution grid where non linear loads are dispersed across the system, it is difficult to measure the non linear load current. In such scenario, DG-grid interfacing converters are utilized to actively improve the voltage quality of a power distribution system via harmonic voltage detection at the point of common coupling (PCC). To do so, the harmonic voltage at the PCC (V_{PCC}) is extracted and used as a reference to control the DG unit as a small damping resistor at those selected harmonic frequencies [42]. The emulated small resistors provide paths for the flow of load harmonic current and indirectly improve the quality of the PCC voltage. These emulated resistors are called virtual resistances.

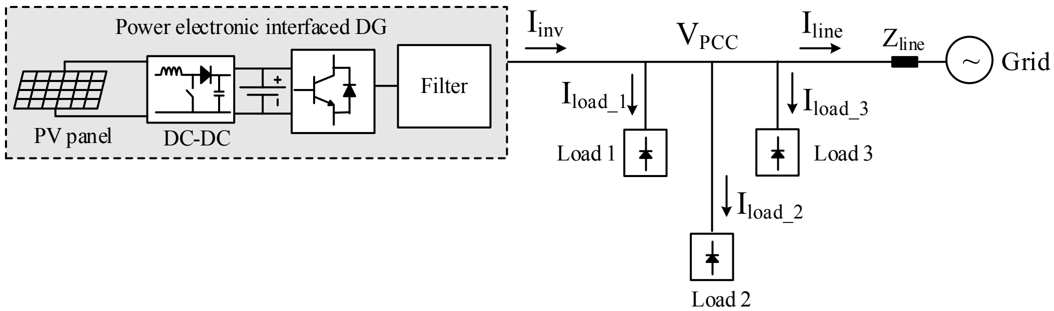

Figure 1.6. PCC voltage harmonics compensation using DG

The control diagram of PCC harmonic voltage compensation is shown in Figure 1. 7. The main difference between the control diagram shown in Figure 1.5 and 1.7 is the harmonic current reference generation block. When a DG unit is deployed to compensate PCC voltage distortion, the harmonic current reference is generated from the PCC harmonic voltage (V_{PCC_h}). Accordingly, the interfacing converter behaves as a damping resistor at those selected harmonic frequencies.

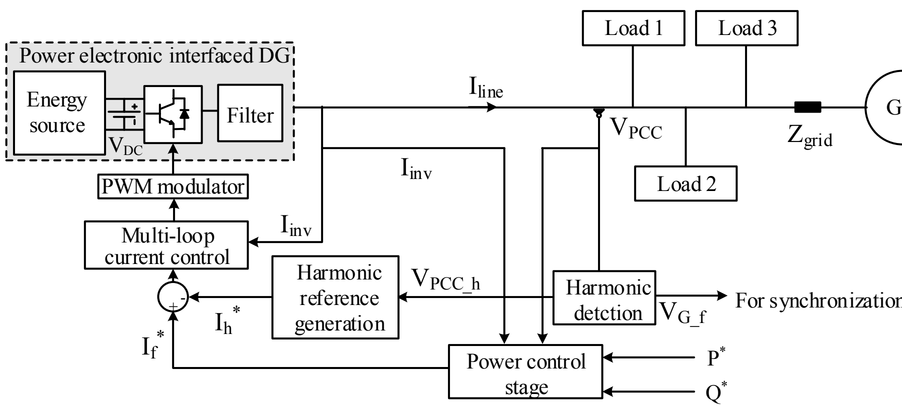

Figure 1.7. Control diagram of PCC voltage harmonics compensation using DG

Traditionally, emphasis is put on the even sharing of harmonic compensation workload among different DGs when multiple DG units are connected in the distribution system. But depending on the location of the distribution system components, power factor correction capacitors (PFCs), non linear load etc., compensating harmonics at some specific location of the distribution system may provide better result. So far, this issue has not been addressed properly in the literature and there is a promising scope to greatly improve the compensation performance.

1.6 Research Objectives

Main objective of this thesis work is to improved distribution system harmonics compensation performance using the DG-grid interfacing converters. As discussed earlier, the wide spread use of power electronics based energy-efficient appliance is contributing a significant amount of harmonic current to the grid collectively and as a result, harmonic distortion in the electrical grid of the residential area is rapidly increasing. At the same time, renewable energy based on PV sources saw record additions in the recent years [13]. A significant portion of this PV growth was due to the rising popularity and declining cost of residential rooftop solar PV which be utilized to mitigate the power quality concerns introduced by these residential loads. Therefore, in this work the residential distribution system is considered and the PV inverters are adopted for the study. For distributed harmonics compensation using DG-interfacing converters, there are two main challenges which are needed to be addressed properly:

1) How to determine the compensation priority of different DG converters, particularly considering the distribution system harmonics resonance and DG converter available rating for harmonics compensation.
2) How to implement the harmonic compensation control in the DG converter that can adaptively adjust the converter's compensation priority without communicating with other DC converters.

To address these two issues, the following objectives are considered in this work:

- Review and compare different VCM and CCM based interfacing converter control schemes in terms of system harmonics compensation performance. This study and comparison is necessary to determine which control strategy can generate better performance from ancillary services (harmonics compensation) point of view.
- Determine harmonics compensation priority for DG converters in a given distribution system, considering locations of harmonic loads and PFCs. This compensation priority will be determined for different harmonics and at different nodes on a radial residential distribution system to facilitate selected harmonic compensation.
- Develop harmonics compensation scheme using DG-grid interfacing converters that can consider harmonic compensation priority, aggregated available DG rating for harmonics

compensation, loads, etc. while ensuring that the scheme can be easily implemented without the need of constant communication among DG converters.

1.7 Research Contributions and Thesis Layout

The research in this thesis aims to develop a coordinated control of the DGs operating at different locations of the distribution system that can compensate system harmonics and ensure the effective use of available DG rating. To do so, two priority driven selective harmonic compensation schemes based on modal analysis is developed, discussed and verified in this work. A summary of the research contributions in each chapter is listed here.

Different control methods of VSI for power quality improvement are investigated in Chapter 2. Two alternative DG control methods, namely current controlled DG and voltage controlled DG are considered. Then harmonic compensation strategies using both these methods are investigated. A comparative study of those harmonic compensation strategies is presented to identify the strength and weakness of each method. The study identifies that while the current control method can only operate in the compensation mode, voltage control method can operate in three different modes namely compensation, rejection and uncontrolled mode. Since most grid connected DG systems use current controlled VSI and this thesis focuses on residential power quality improvement, the analysis on different current control methods is then extended. When current control methods are used, the VSI acts as a current source within the current loop bandwidth of the current controller. The stability and dynamic performance variation of different closed-loop control schemes are then discussed. To do so, a criteria is proposed in this chapter that facilitates fair comparison of different closed-loop current control method for a VSI with output LCL filters. Effect of system parameter variation on their stability is also investigated and verified. Simulation and experimental results are provided to support the findings of this chapter.

Chapters 3 and 4 address the harmonics compensation priority determination. Particularly, two popular harmonics compensation strategies are evaluated and compared in Chapter 3 – end of line and distributed. To address the harmonic problem in the distribution system, different variations of end-of-line and distributed harmonic compensation schemes are proposed in literature. While these methods are very different from each other, both methods were claimed to be the better compensation scheme in different literatures. Chapter 3 mainly focuses on identifying the effects of the DG locations on harmonic compensation performance by investigating different compensation schemes and identifying the reason behind the conflicting claims about compensation performance. An analysis was carried out using state space model of an N node distribution system which is then extended to include the resonance effects introduced by power factor correction (PFC) capacitors. This analysis then identifies the compensation method that should be used under different grid condition by proposing the idea of a crossover frequency that separates effective compensation methods to different frequency zones. The effects of capacitor size, line impedance, and length on the introduced crossover frequency were also analyzed in this chapter. All these observations were verified using time domain simulation of an 11 node distribution system.

Distributed harmonics compensation is identified as superior strategy in Chapter 3, particularly when harmonic resonance occurs due to PFC in the distribution system. While Chapter 3 presents a guideline to assign harmonic compensation priorities on DGs, the considered possibilities are end-of-line or distributed compensation where distributed compensation scheme is implemented utilizing same virtual resistance for all DGs and at all frequencies. This is a simplified case of distributed compensation which assumes that DG is available at each distribution system nodes and each DG have the same rating. Chapter 4 further improve the work through the study of the compensation priority of DG converters. A selective harmonic compensation scheme based on modal analysis is proposed to assign compensation priorities on DGs operating at different distribution system nodes for improved compensation performance. The method proposed here improves the system level performance as the priority values are identified considering the location of each DGs in the distribution system. A modeled residential distribution system containing distribution components such as distribution line, PFC capacitors, transformers and household appliances along with DG units is used to verify the improvement of compensation performance.

In order to implement the harmonics compensation strategies to the DG converters, a droop based harmonics compensation implementation scheme is proposed in Chapter 5. To implement the selective harmonic compensation scheme proposed in Chapter 4, the virtual resistances of DGs at different locations are controlled for improved compensation performance. But controlling DG harmonic current may cause overrating and the direct virtual harmonic tuning in Chapter 4 is not a very straightforward way for DG harmonic compensation level control. To address these issues, a novel priority driven G-S droop based selective harmonic compensation scheme is developed in this chapter to assign compensation priorities on DGs with different ratings and operating at different distribution system nodes. This method uses a droop relationship between the harmonic conductance and VA consumption of each individual inverter, to ensure over current is avoided automatically. The droop characteristic of different DG inverter is designed according to the compensation priority level as developed in Chapter 4.

Finally, the conclusions of the research and future work recommendations are presented in Chapter 6.

Chapter 2

Opportunities for Power Quality Improvement using DG-Grid Interfacing VSI

2.1 Introduction

With the increasing concerns on conventional energy costs, energy security and greenhouse gas emissions, the energy industry is experiencing fundamental changes as more and more distributed energy resource based distributed generation (DG) units are being connected to the gird. These DG systems are seen as a means for facilitating climate friendly renewable energy sources (RES) and to enable efficient use of electricity. This increased penetration of DG introduced a number of challenges, such as harmonics, protection interference, voltage regulation problems, etc [43]. As a result, the power quality as well as power regulation requirements are becoming more stringent as have already been reflected in a few grid codes. IEEE 1547 [44] and its recent series of application guidelines require that the total demand distortion (TDD) of harmonic current injection by the DG into the grid should be less than 5% (individual harmonic lower than 11th should be less than 4% and the even order harmonics should be even lower than half of this number). A DG unit of more than 250kVA rating must have the provision for monitoring its output power and voltage at the point of connection. A DG unit should be disconnected from the grid within 0.16s in a grid voltage quality event (e.g. under grid frequency or voltage variations). Besides the IEEE standard for interconnecting the DER with power system,

---

Publication out of this chapter:

J. He, Y. Li and S. Munir, "A Flexible Harmonic Control Approach through Voltage Controlled DG-Grid Interfacing Converters," IEEE Transactions on Industrial Electronics, vol.59, no.1, pp.444-455, Jan. 2012.

S. Munir, J. He and Y. Li, "Comparative Analysis of Closed-Loop Current Control of Grid Connected Converter with LCL Filter", in Conf. Rec. IEEE International Electric Machines and Drives Conference (IEMDC'11), Niagara Falls, pp 1678-1683, 2011.

there are also many country-wide DG interconnection standards, which specifies similar requirement regarding the DG current harmonics and the ability to disconnect itself from the grid in case of a disturbance. As a result, although maintaining good power quality is the responsibility of the utility, it has become a difficult task with the increasing use of unbalanced loads, nonlinear loads and sensitive loads in today's distribution system. For example, IEEE 519 [45] requires that the utility should make sure the voltage total harmonic distortion (THD) at the point of common coupling (PCC) with each customer be less than 5%, with individual harmonic voltage less than 3% which is a difficult task with all the non linear loads present in today's distribution system.

On the other hand, while the DG interfacing converters may introduce harmonics into the power system and cause power quality concerns, they are also able to improve the system efficiency and power quality if designed and controlled properly. To realize this function of DG, besides the primary purpose of real power generation, many ancillary services, such as power factor compensation, voltage support [46], flicker mitigation [47], system harmonic compensation [48-50], unbalance voltage compensation [51], etc. can also be provided through the DGs whenever there is sufficient apparent power rating available. Furthermore, with the recent development of smart grid and microgrid concepts, and the associated advancement of communication, instrumentation and control techniques for power electronics interfaced DG systems, systematically controlling the DGs to improve the distribution system power quality is becoming be a very promising topic. Most of these power electronics interfaced DG systems use voltage source inverters (VSI) as the interfacing inverter. The control mechanism of the VSI is mainly of two types, namely current control method (CCM) and voltage control method (VCM). In this chapter, both control methods are considered first and the associated power quality improvement strategies by compensating harmonics are discussed. The observations obtained from the study of these two methods for harmonic compensation is validated using simulation and experimental results.

Since most grid connected DG systems use current controlled VSI, the analysis on different current control method is then extended in this chapter. The current control schemes of VSI can be classified into two groups: (a) Direct error tracking control with PWM, and (b) Closed-loop feedback control. The first group of control methods is based on direct current error control and includes predictive control [52], hysteresis control [53], parabolic PWM [54] etc. The drawbacks of these methods, such as system parameter sensitivity or variable switching frequencies, have limited the use of these methods to some extent. The second group of control methods includes single-loop [55, 56] and multiple-loop feedback control [57, 58]. The closed-loop current control can also be classified as single current sensor feedback and two sensors feedback. Generally, the closed-loop feedback method eliminates many drawback of the direct error tracking control, but its stability and dynamic performance is limited due to the low bandwidth of the current control loop especially for single-loop control. This low control loop bandwidth is mainly due to the output LCL filter resonance. To overcome this problem, split capacitor method referred as LCCL method is presented in [56]. But this control method requires capacitor with specific calculated values which is difficult to obtain practically and requires physical change of capacitors in case of line parameter variation. To overcome this problem, weighted average control referred as WAC is proposed in [57] which eliminates LCL resonance and increases controller bandwidth. The WAC is essentially a single-loop control with combination of inverter and grid side current feedback. On the other hand, with two current feedbacks, a double-loop feedback control is introduced in [58]. To have a clear understanding of the performance differences from different control schemes and the reasons behind it, this chapter conducts a comparative analysis of closed-loop current control methods of grid connected VSI with LCL filter. To facilitate a fair comparison among different control methods, a comparison criteria is proposed first. The analysis of different controllers are then carried out according to the proposed criteria and the effects of LCL filter parameter variation on system stability due to the presence of LCL resonance is then investigated. Comparative analysis results are explained using the recently proposed generalized closed-loop control (GCC) platform [59]. Simulation and experimental results of different VSI control systems are also presented to support the findings of comparative analysis.

2.2 Current Controlled DG

Many grid-connected DG systems (such as PV systems) adopt the current control method (CCM) for the interfacing inverter, where the DG output current is synchronized with the grid voltage, and the current magnitude is generated through the output power control.

The idea of PCC voltage quality improvement using the current controlled grid-connected inverter has been reported in [49, 50]. This method functions by controlling the DG as a shunt active power filter (APF) where the DG absorbs the harmonic current from the nonlinear loads, leaving an improved source current and PCC voltage with low THD. One way to achieve this is to control each DG as an R-APF [18], where the grid side voltage is measured and the harmonic components are extracted to produce the reference harmonic current for a DG ($I_h^* = V_{G\_h}/R_h$), and therefore the DG acts as a small resistance (R_h) only at the harmonic frequencies.

The block diagram of the power quality improvement method with current controlled interfacing inverter is shown in Figure 2.1. As illustrated, the fundamental reference current magnitude (I_f^*) is obtained from the power control loop, where the real power reference can be produced from the maximum power point tracking (MPPT) like in a wind or PV system, the maximum system efficiency control like in a fuel cell system or from the command value of the energy management center. The reactive power command can be produced from the voltage support or load power factor compensation algorithms. If unity power factor injection from a DG is desired, this reactive power demand can be simply set to zero. To improve the transient performance, a current magnitude feedforward loop can be added, where the feedforward current is calculated from the reference power and grid side voltage magnitude. With the grid voltage angle information from a phase-locked-loop (PLL), the reference inverter output current synchronized to the fundamental grid voltage can be obtained. In order to properly compensate the grid side voltage harmonics, and at the same time to avoid any conflicts with the primary function of real power injection of a DG system, the reference harmonic current generation and the current control loop need to be carefully designed.

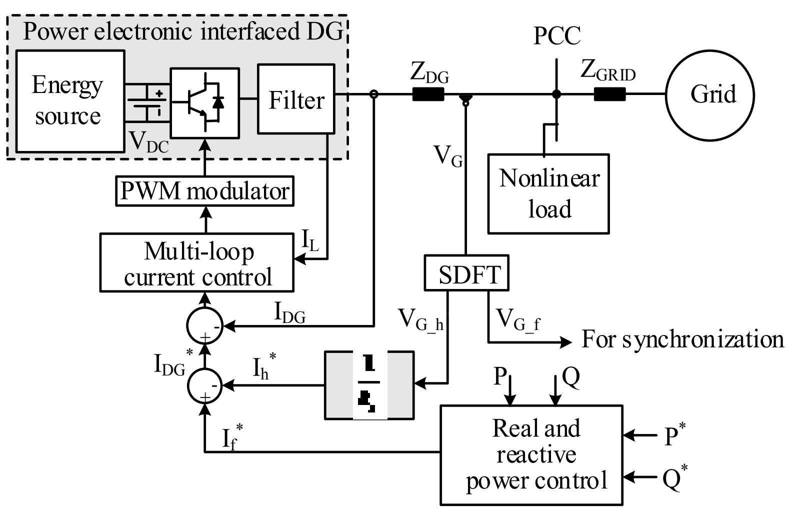

Figure 2.1. Interfacing inverter control scheme for current controlled DG.

Traditionally, the harmonic components and fundamental component are separated by using low pass or high pass filters in either the stationary or synchronous frames [61]. However, this filtering usually introduces magnitude and phase errors in the extracted signals, which subsequently leads to inaccurate compensation performance. On the other hand, it is also important to avoid high order harmonic tracking due to limited current control bandwidth (usually, tracking of harmonics higher than 13^{th} is difficult with an inverter operated at around 2 kHz switching frequency). The inaccurate control may introduce amplification of these harmonics, or even lead to instability of the system. With the above considerations, selected compensation of the most significant low order harmonics in a system (such as 5^{th}, 7^{th}, 11^{th}) would be more appropriate.

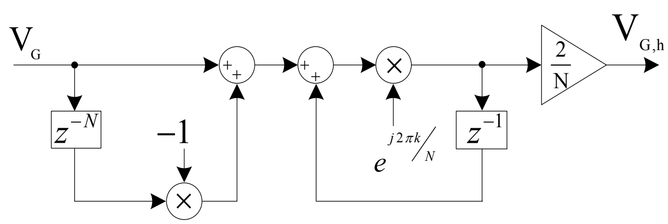

Figure 2.2. SDFT for fundamental and harmonic component extraction.

To selectively extract the harmonics, resonant filters are used in [50]. However, the resonant filter has sudden change of phase angle at the resonant frequencies, which means that slight variation of the resonant frequency may introduce substantial phase error in the extracted signals. To accurately extract the harmonics, the sliding discrete Fourier transform (SDFT) was used in this work [20]. The SDFT features a sliding window and can be easily implemented in a DSP for real time calculation. The z-domain transfer function for the h^{th} harmonic can be descried as,

$$G_{SDFT} = \frac{1 - Z^{-N}}{1 - e^{\frac{j2\pi h}{N}} Z^{-1}} \tag{2-1}$$

where N is the number of samples in one fundamental period, and h is the harmonic order. The implementation diagram of the SDFT is illustrated in Figure 2.2. Note that with SDFT, the grid voltage fundamental component ($h = 1$) can also be extracted and it is used for the grid synchronization of the current control scheme.

Once the harmonic voltage is obtained, the harmonic current reference can be produced by using the desired virtual resistance R_h. Here, the value of R_h will affect the compensation performance. Generally, a smaller R_h gives better compensation, but tends to reduce the system stability. Additionally, the value of R_h should also be determined according to the available rating of a DG, to avoid any conflict of the primary function of real power generation. This control of the R_h according to the DG's available rating can be realized through an adaptive control algorithm [49] or simply by an integral controller.

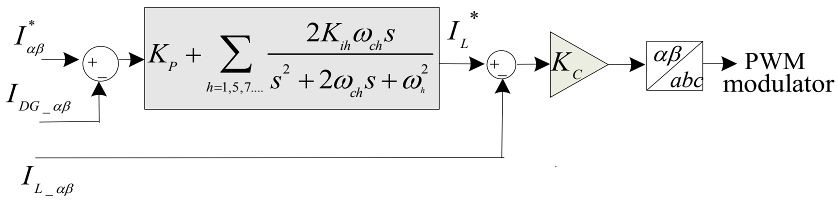

Figure 2.3. Closed-loop current control diagram.

Finally, the DG reference current can be obtained by adding the fundamental reference from power control loop and the harmonic current reference. The DG output current closed-loop control scheme is shown in Figure 2.3 where $I^*_{\alpha\beta}$ and $I_{DG\_\alpha\beta}$ are the α-β frame DG reference and feedback currents respectively. For good fundamental current tracking and harmonic current control, a current controller based on parallel P$^+$ resonant controllers (at fundamental frequency and the harmonic frequencies of interest) and used [63, 64]:

$$G_c = K_P + \sum_{h=1,5,7\ldots} \frac{2K_{ih}\omega_{ch}s}{s^2 + 2\omega_{ch}s + \omega_h^2} \tag{2-2}$$

where ω_h is system fundamental and harmonic frequency, ω_{ch} is the cut-off bandwidth at each frequency, K_{ih} is the integral gain at each frequency, and K_p is the proportional control gain at all frequencies. To further improve the damping and stability of the control loop, an inner filter inductor current feedback loop with proportional controller is also added as shown in Figure 2.3. It should be noted that if the distributed line impedance is very small, and DG is connected to the grid with an LCL filter (or with a coupling transformer), the grid side voltage measured for harmonic compensation is very close to PCC voltage, and therefore remote measurement is not necessary for this compensation scheme.

2.3 Voltage Controlled DG

While the current controlled DG is mostly employed for grid connected inverters, the voltage controlled DG can also be used [65, 66]. The voltage control method (VCM) produces seamless transient if a DG is to be operated in intentional islanding mode, as VCM is necessary in the islanding operation to provide voltage and frequency support for the microgrid.

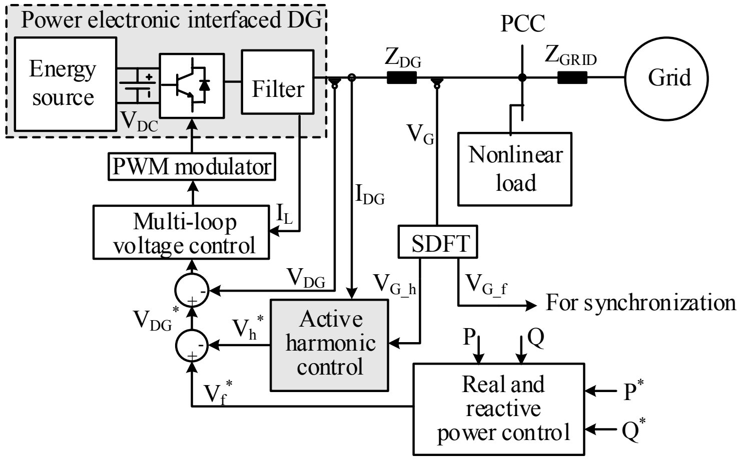

Figure 2.4. Interfacing inverter control scheme for voltage controlled DG.

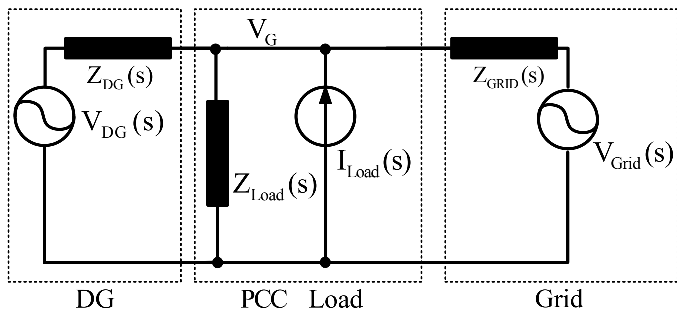

Figure 2.5. Equivalent circuit of DG-grid system with voltage control.

The block diagram of the power quality improvement method with current controlled interfacing inverter is shown in Figure 2.4 while the equivalent circuit of a DG-grid system with VCM is shown in Figure 2.5, where the DG is described as a controlled voltage source V_{DG} and a DG impedance Z_{DG}, and the grid is represented as a voltage V_{Grid} and a grid impedance Z_{Grid}. The PCC nonlinear load is shown in the middle as a harmonic current source and passive loads. If the DG harmonic voltage is controlled as,

$$V_{DG}(s) = -GV_G(s) \tag{2-3}$$

the equivalent harmonic impedance can be accordingly expressed as,

$$Z_{DG,eq} = Z_{DG}/(1+G) \tag{2-4}$$

where $V_G(s)$ is measured voltage after the DG impedance $Z_{DG}(s)$. Similarly, considering the low line impedance, it is valid to assume that $V_G(s)$ is the PCC voltage.

From the above analysis, it is obvious that by properly controlling the DG output voltage with a feedback gain of G, the harmonic impedance at DG side can be scaled down by a factor of $(1+G)$

and therefore it can be substantially lower than that at the grid side. As a result most of the nonlinear load current can be absorbed by the DG, leaving an improved grid current and the PCC voltage. Obviously, a higher G value will further reduce the PCC voltage harmonics. With $G=0$, the DG will be a standard voltage controlled DG unit without any compensation. This is in contrast to the current controlled method, where the whole DG system is controlled as a resistor R_h at the harmonic frequencies.

Furthermore, if desired, this method can also control the DG output current with low harmonics and better THD. This can be done by using a negative feedback gain $(-1<G<0)$, and therefore the DG output impedance will be increased at the harmonic frequencies. As a result, the PCC harmonic voltage will be amplified comparing with conventional voltage controlled mode. Actually, if DG harmonic current can be properly attenuated with a negative G, the performance will be the same as current controlled DG unit. Therefore, with different system compensation requirements or DG operation objectives, the value of G can be controlled adaptively (with a theoretical range from -1 to ∞). Since a high value of G tends to make the system unstable, a practical top limit of G is around 10-20. Finally, it is important to note that G should not be less than -1, as this will introduce capacitive equivalent impedance, which may induce some system resonance. In this work, $G>0$ is named harmonic compensation mode and $G<0$ is named as harmonic rejection mode.

This control strategy is implemented as shown in Figure 2.4. Similar to the CCM control method, a SDFT block first separates the fundamental and the harmonic components of the PCC voltage. The fundamental voltage is used for grid voltage synchronization and DG output real and reactive power calculation, while the harmonic components are used for the inverter reference harmonic voltage generation. In the control scheme, the real and reactive power control block produces the fundamental reference of DG voltage while the active harmonic control block generates the reference harmonic voltages. The power control can be realized by using the droop control [65-67], where the reactive power control should be updated by using a PI controller to remove any control errors [66, 67].

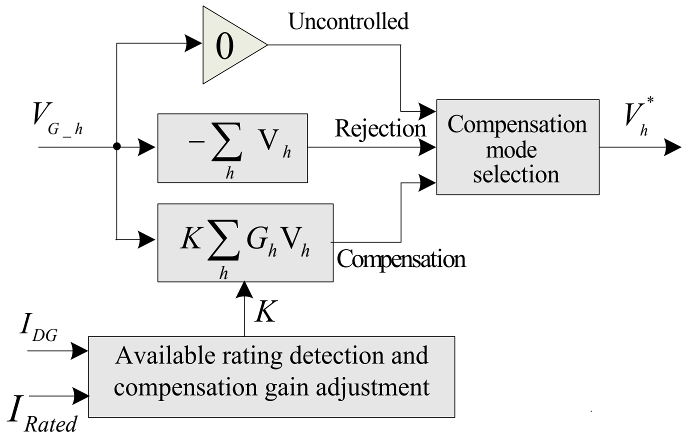

Figure 2.6. Active harmonic control algorithm.

The active harmonic control is illustrated in Figure 2.6. As discussed before, this control block can operate at compensation, rejection or uncontrolled mode. To avoid over-rating operation and possible conflict with the primary function of power control, a control algorithm named "available DG rating detection and compensation gain adjustment" is added. By using either the adaptive controller [49] or a simple integral controller [50], this algorithm adjusts the value of K, which subsequently changes the effective gain used for each harmonic. To achieve optimal compensation, the feedback gain G_h for each harmonic components is not necessarily to be the same. Generally, G_h is lower for high order harmonics. Note that for harmonic rejection mode, $G_h = -1$ for all the harmonics.

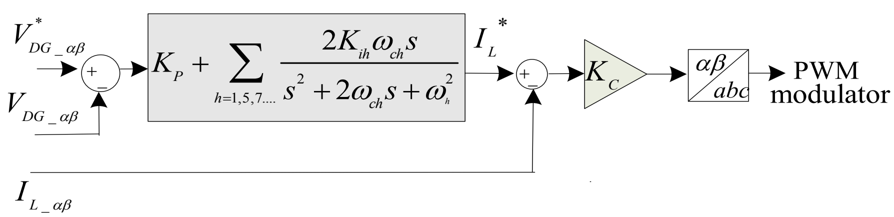

Figure 2.7. Muli-loop voltage control diagram.

The final multi-loop DG voltage control block is shown in Figure 2.7, where the parallel P^+ Resonant controller for fundamental and different harmonic components are used as the outer loop voltage controller, and the inner current loop uses the filter inductor current feedback and a proportional controller (K_c).

2.4 Comparison between CCM and VCM

While both VSI control methods can effectively control the DG output real and reactive power and compensate the PCC harmonic voltage, a further comparison of both methods gives the following conclusions:

- Without harmonic compensation, CCM pushes all the harmonic currents to the grid side. Leading to polluted PCC voltage due to harmonic voltage drops on source impedance. To the contrary, even without harmonic compensation, the voltage controlled DG shares the nonlinear load current with the source according to their respective impedance. This leads to better PCC voltage compared to CCM.
- With PCC harmonic compensation, the CCM works as a shunt low resistance (R-APF) to absorb the harmonic currents. In case of multiple DG systems, this method ensures that the harmonic current flowing to each DG is of the same phase angle even different Rh is used for different DG units, meaning that no circulating current exist among DG units. However, harmonic components extraction without phase shift is very important here, as any phase error (such as those can be introduced by the resonant filters) will lead to inductive or capacitive impedance in series with R_h, causing the circulating current among DG systems.
- When VCM is used for multiple DG systems, since each DG will act as an impedance of $Z_{DG}/(1+G)$, the harmonic current flowing into each DG is related to Z_{DG} and G for each DG unit. Seemingly causing circulating current among DGs, a further look into this issue reveals that the harmonic impedance Z_{DG} is mainly inductive (even for directly coupled DG without grid side inductance, the line impedance will be inductive at harmonic frequencies). As a result, the harmonic current circulation among DG unit is not a real issue with VCM, as long as the harmonic reference can be generated without phase error.
- Considering that a DG system may operate in grid connected mode and intentional islanding mode (to form a self contained microgrid), the VCM has the advantages of seamless control transition, since the same control scheme can be used for both operation modes. In contrast, the CCM has difficulties in islanding operation, as it is not directly controlling the load voltage and frequency.

- The VCM is more flexible with compensation, rejection and uncontrolled modes, where the harmonic reject operation essentially gives similar performance as the current control method.

2.4.1 Simulation and Experimental Results

Both these harmonic compensation strategies were compared using Matlab/Simulink simulation and experimentally on a *5* kVA grid connected DG system. The system parameters used in the simulation and experiments are almost identical and are listed in Table 3.1. In the simulation and experiment, the nonlinear load at PCC is a diode rectifier with parallel connected capacitor (*1000* uF) and resistor (*25* Ω) at the dc side. Table 3.1 lists the parameters used for simulations and experiment.

Table 2.1. System Parameters in Simulation and Experiment.

Parameters	Simulations	Experiments
Grid voltage	*104V, 60Hz (3 phase)*	*104V, 60Hz (3 phase)*
DC link voltage	*260V*	*260V*
DC link capacitance	Ideal DC source	*1900uF*
LC filter	$L = 2.5mH, C = 40\mu F$	$L = 2.5mH, C = 40\mu F$
DG Impedance	$R = 1\Omega, L = 2.5mH$	$R = 1\Omega, L = 5mH$
Grid impedance	$R = 1\Omega, L = 2.5mH$	$R = 1\Omega, L = 5mH$
Switching frequency	*12kHz*	*12kHz*
Power reference	$P^*=300W, Q^*=125Var$	$P^*=120W, Q^*=75Var$

2.4.1.1 Current Control Method

The current controlled interfacing inverter is first tested in the simulation with the 5^{th} and 7^{th} harmonic compensated. Figure 2.8 and 3.9 show the performance of current controlled DG without implementation of the PCC voltage harmonic compensation. As can be seen from Figure 2.8, the DG output current has no harmonics (as it is only controlled to produce real and reactive power), and the nonlinear load current is supplied through the grid. As a result, the PCC voltage is distorted due to the harmonic voltage drop on the grid impedance. As illustrated in Figure 2.9, the PCC voltage has a THD of 10.22%.

The situation with PCC voltage harmonic compensation is shown in Figure 2.10 and 2.11. As expected, by acting as a low resistance R_h at the harmonic frequencies, the DG unit absorbed most of the nonlinear load currents, leading to an improved grid current and PCC voltage as shown in Figure 2.10 (a) and (b). As shown in Figure 2.11, the low order harmonics of PCC voltage are significantly reduced, which results in a THD of 2.5%.

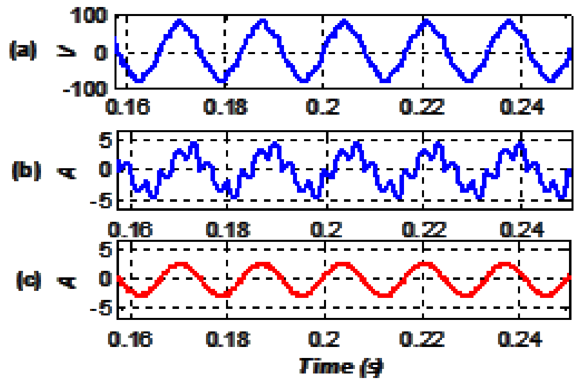

Figure 2.8. Current controlled method without harmonic compensation: (a) PCC phase voltage, (b) grid current, (c) DG current.

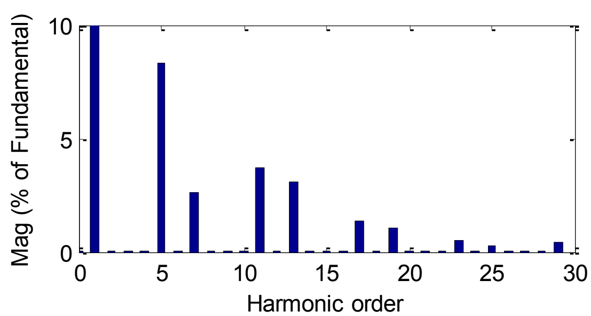

Figure 2.9. Harmonic analysis of PCC voltage under current controlled DG without harmonic compensation (THD =10.22%)

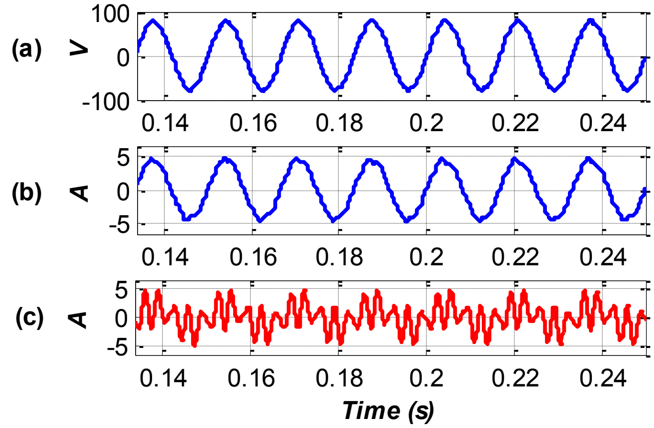

Figure 2.10. Current control method with harmonic compensation: (a) PCC phase voltage, (b) grid current, (c) DG current.

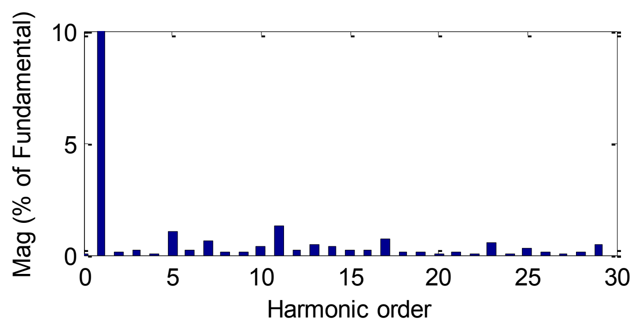

Figure 2.11. Harmonic analysis of PCC voltage under current controlled DG with harmonic compensation (THD =2.50%)

2.4.1.2 Voltage Control Method

The voltage controlled DG and different compensation modes are also tested in the simulation, and the results are shown in Figure 2.12 to 2.15. Figure 2.12 and 2.13 show the results without any harmonic compensation, i.e. the DG unit is controlled with pure sinusoidal output voltage (Figure 2.12(b)). In this case, the DG and grid equally share the nonlinear load current as seen from Figure 2.12 (c) and (d). As a result, the PCC voltage is distorted due to the nonlinear current flow on the grid impedance. Figure 2.13 shows that the PCC voltage has almost 6% 5th harmonic and the THD is 6.72%.

To improve the PCC voltage, the harmonic compensation is implemented (with $G_5=12$, $G_7=12$, $G_{11}=5$). As the DG output impedance at harmonics frequencies is reduced by a factor of $(1+G_h)$, the DG unit absorbs most of the load nonlinear current as can be seen in Figure 2.14(d).

As a result, the grid current and PCC voltage are improved. As shown in Figure 2.15, the 5th harmonic voltage at PCC is reduced to about 1.5% and the THD is reduced to 2.42%.

Finally, the harmonic rejection mode is tested and the results are shown in Figure 2.16 and 2.17. As expected, with *G=-1*, the DG output current is controlled to be sinusoidal (Figure 2.16(d)) due to the very high DG impedance at harmonic frequencies. In this case, the grid will provide all the nonlinear load current, and therefore the grid current and voltage are further distorted. The PCC voltage has 8% 5th harmonic, and the THD is 10.08% as shown in Figure 2.17. As expected, this performance is similar to the current control mode without PCC harmonic compensation.

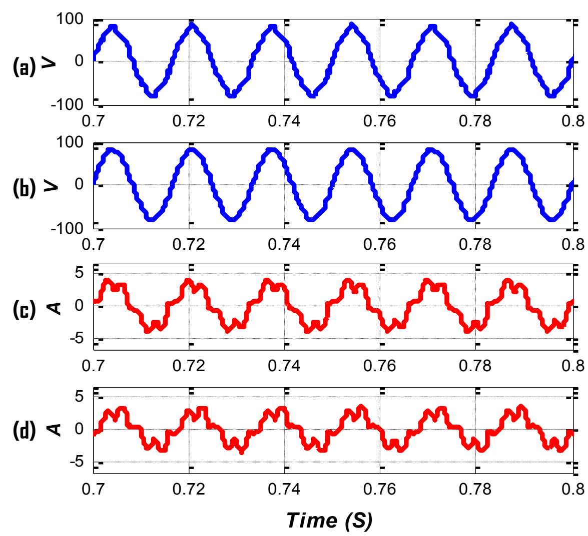

Figure 2.12. Voltage control method without compensation: (a) PCC phase voltage, (b) DG phase voltage, (c) grid current, (d) DG current.

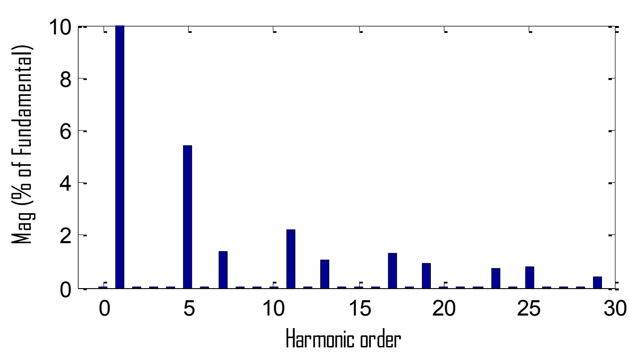

Figure 2.13. Harmonic analysis of PCC phase voltage under voltage controlled DG without harmonic compensation (THD =6.72%)

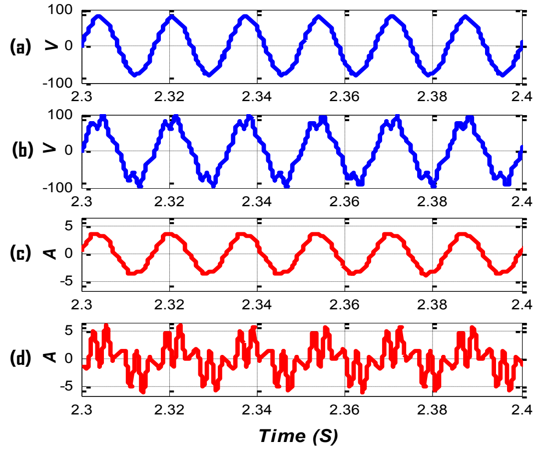

Figure 2.14. Voltage control method with harmonic compensation: (a) PCC phase voltage, (b) DG phase voltage, (c) grid current, (d) DG current.

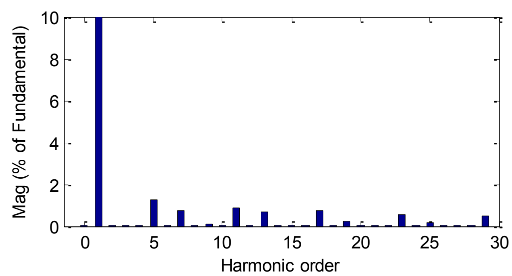

Figure 2.15. Harmonic analysis of PCC voltage under voltage controlled DG with harmonic compensation (THD =2.42%)

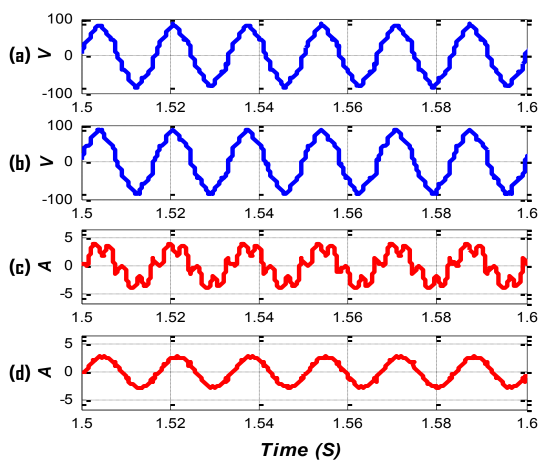

Figure 2.16. Voltage control method with harmonic rejection: (a) PCC phase voltage, (b) DG phase voltage, (c) grid current, (d) DG current.

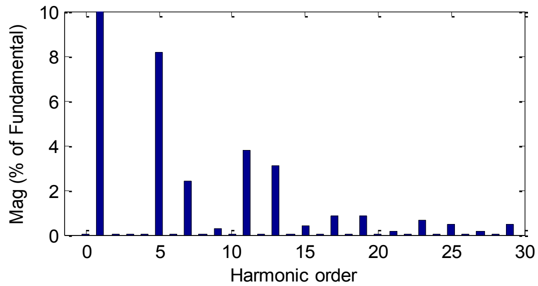

Figure 2.17. Harmonic analysis of PCC voltage under voltage controlled DG with harmonic rejection (THD =10.08 %)

2.4.1.3 Experimental Verifications

Experiments are also conducted on a 5kVA grid connected DG system to verify the observations. In the experiment, a three-phase programmable power supply is used to represent the grid, and the three-phase DG system is controlled with a DSP-FPGA system. In the experiment, the 5th and 7th harmonics are compensated. The experimental parameters are listed in Table 2.1, and the results are shown in Figure 2.18 to 2.20.

The performance of uncontrolled mode (without harmonic compensation) is shown in Figure 2.18, where it can be seen that the DG and grid share the nonlinear load current. Since the DG real and reactive power references is smaller in the experiment (Table 2.1), the grid current contains higher fundamental current. Without harmonic compensation, the THD of PCC voltage and grid current is 10.5% and 16.9% respectively.

When PCC harmonic compensation is implemented, the DG absorbs the nonlinear load current and as a result, both the source current and PCC voltage are improved as shown in Figure 2.19. In this case, the THD of PCC voltage and grid current is improved to 5.2% and 7% respectively.

Finally, for the harmonic rejection mode, the DG output current is controlled to contain very few harmonics as the DG output impedance is increased significantly at harmonic frequencies. As a result, most of the nonlinear load current is supplied through the source and the PCC voltage is further deteriorated. With harmonic rejection, the THD of PCC voltage and grid current is 15.3% and 26.3% respectively. Note that the increase of harmonics compared to simulations is introduced by using higher DG and grid impedance in the experiment. This is shown in Figure 2.20.

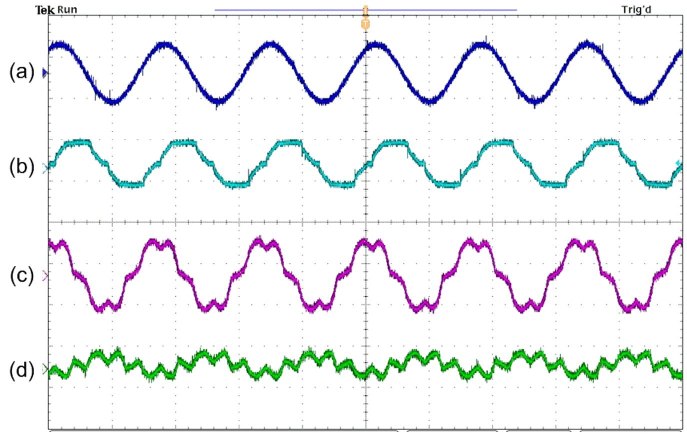

Figure 2.18. Voltage control method without harmonic compensation: (a) DG line voltage (200V/div), (b) PCC line voltage (250V/div), (c) grid current (5A/div), (d) DG current (5A/div).

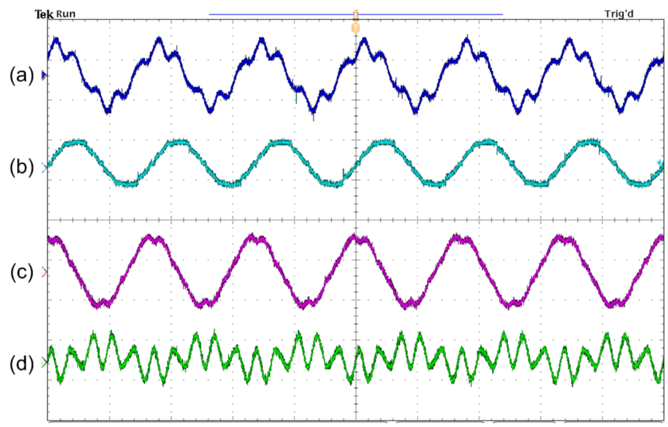

Figure 2.19. Voltage control method with harmonic compensation: : (a) DG line voltage (200V/div), (b) PCC line voltage (250V/div), (c) grid current (5A/div), (d) DG current (5A/div).

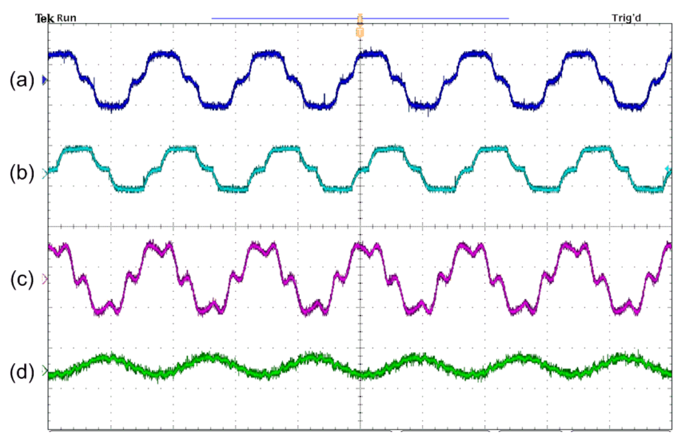

Figure 2.20. Voltage control method with harmonic rejection: : (a) DG line voltage (200V/div), (b) PCC line voltage (250V/div), (c) grid current (5A/div), (d) DG current (5A/div).

2.5 Feedback Methods of Current Controlled VSI

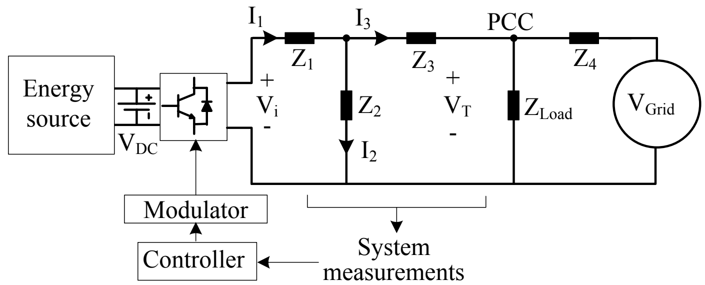

Figure 2.21. DG-Grid interfacing inverter with LCL filter

Figure 2.21 shows DG-grid interfacing inverter with an LCL filter. Here, V_i is the inverter output voltage and V_T is the grid voltage. The DG is connected to the grid with an LCL filter or with an LC filter with output coupling transformer. The LCL filter is mainly used for decreasing switching ripple originated from the inverter. The impedance components of the LCL filter are,

$$Z_1 = R_1 + L_1 s \tag{2-5}$$

$$Z_2 = R_2 + (1/C_2 s) \tag{2-6}$$

$$Z_3 = R_3 + L_3 s \tag{2-7}$$

According to the equivalent filter system, transfer function of DG output voltage (V_i) and currents (I_1, I_2 and I_3) would be,

$$G(I_1/V_i) = (Z_2 + Z_3)/(Z_1 Z_2 + Z_2 Z_3 + Z_3 Z_1) \tag{2-8}$$

$$G(I_2/V_i) = Z_3/(Z_1 Z_2 + Z_2 Z_3 + Z_3 Z_1) \tag{2-9}$$

$$G(I_3/V_i) = Z_2/(Z_1 Z_2 + Z_2 Z_3 + Z_3 Z_1) \tag{2-10}$$

In literature, these current feedbacks are used in different configuration for inverter control. Single current sensor feedback control system includes conventional single-loop and split capacitor inverter control system. Two current sensors feedback system includes WAC, multiple-loop with inductor current (I_L) feedback and multiple-loop with capacitor current (I_C) feedback inverter control system.

2.5.1 Inverter Control with Single Current Sensor

2.5.1.1 Conventional single-loop inverter control:

Conventionally, LCL filter output current is used for single-loop inverter control as shown in Figure 2.22. In such cases, the resonance of the output LCL filter affects the control loop gain. Due to the resonance, the controller bandwidth decreases and gain becomes limited.

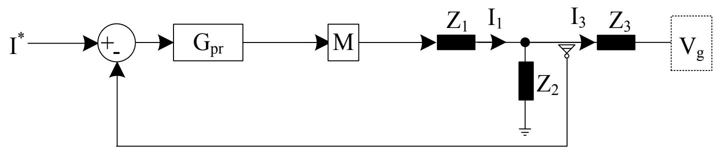

Figure 2.22. Equivalent circuit of single-loop inverter control

Here the open-loop transfer functions of the VSI system is,

$$G_{OL,I_3} = G_{pr} \cdot M \cdot G(I_3/V_i) \tag{2-11}$$

where, M is modulation and G_{PR} is proportional resonant (PR) controller shown in (2-12).

$$G_{pr} = K_p + \sum_{h=1,3,5,7....} \frac{2K_{ih}\omega_{ch}s}{s^2 + 2\omega_{ch}s + \omega_h^2} \tag{2-12}$$

where ω_h is system fundamental and harmonic frequency, ω_{ch} is the cut-off bandwidth at each harmonic frequency, K_{ih} is the integral gain at each harmonic frequency, and K_P is the proportional control gain at all frequencies.

The controller gain range of (2-10) is limited due to the resonance introduced by the LCL filter. The Bode plot of the open-loop transfer function (2-10) without the current controller is shown in Figure 2.23. As shown in Figure 2.23, the resonance amplitude peak limits the control loop gain. Due to this limited gain, usually the controller cannot track reference correctly.

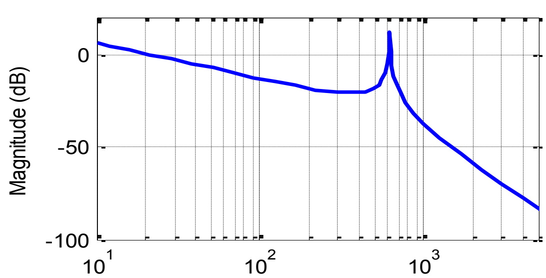

Figure 2.23. Open-loop Bode plot of the single-loop controlled system.

2.5.1.2 Inverter control with LCCL feedback:

To overcome the bandwidth limitation of single-loop inverter controller, split capacitor current feedback is presented in [56] and referred as LCCL method. In this method, capacitor of LCL filter is split into two parts and current flowing between them is used as feedback of the controller. With properly designed capacitor values, this method eliminates the resonance problem and increases the controller bandwidth. Figure 2.24 shows the LCCL feedback method.

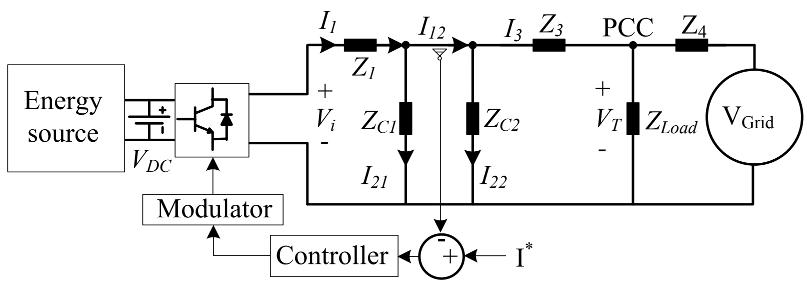

Figure 2.24. Split capacitor current feedback system.

With properly selected values of Z_{C1} and Z_{C2}, transfer function of inverter output voltage (V_i) to feedback current (I_{12}) becomes $G(I_{12}/V_i)=1/Ls$. Here L is the total inductance in Z_1 and Z_3. Then the open-loop transfer function becomes,

$$G_{OL,LCCL} = G_{pr} \cdot M \cdot G(I_{12}/V_i) = G_{pr} \cdot M \cdot (1/Ls) \tag{2-13}$$

Now it can be seen from (2-13) that the resonance problem is eliminated by transforming the inverter control system into a first order system. But this method requires capacitor with specific calculated values which is difficult to obtain practically. Moreover in case of line parameter variation, this method requires physical change of capacitors.

2.5.2 Inverter Control with Two Current Sensors

2.5.2.1 Inverter control with WAC feedback:

In [57], a new control method with weighted feedback is presented as shown in Figure 2.25. This method removes LCL resonance problem and at the same time eliminates specific valued capacitor and physical change of capacitor requirement of LCCL method.

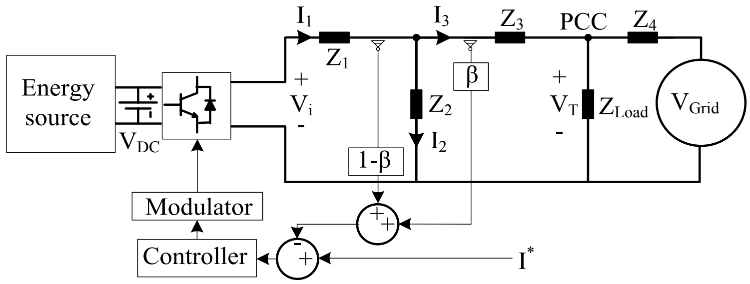

Figure 2.25. WAC feedback system.

In this method a weighted average of the inverter and LCL filter output current is used as feedback. From Figure 2.25, the feedback current I_f can be written as,

$$G\left(I_{f,WAC}/V_i\right) = (1-\beta)\cdot G(I_1/V_i) + \beta \cdot G(I_3/V_i) \tag{2-14}$$

If, $L = L_1 + L_3$ and $\gamma = L_1/L$ then (2-14) becomes,

$$G\left(I_{f,WAC}/V_i\right) = \frac{(1-\beta)\{(1-\gamma)LCs^2 + R_2Cs + 1\} + \beta(R_2Cs+1)}{\gamma(1-\gamma)LCs^3 + R_2LCs^2 + Ls} \tag{2-15}$$

If, $\beta = 1 - \gamma$ then feedback to inverter output voltage transfer function becomes $G\left(I_{f,WAC}/V_i\right) = 1/Ls$. As $G\left(I_{f,WAC}/V_i\right)$ is converted into first order equation eliminating resonance problem and open-loop transfer function becomes (2-16).

$$G_{OL,I_{WAC}} = M \cdot G_{pr} \cdot G\left(I_{f,WAC}/V_i\right) = M \cdot G_{pr} \cdot (1/Ls) \tag{2-16}$$

2.5.2.2 Multiple-loop inverter control with I_1 and I_3 feedback:

The first multiple-loop inverter control configuration uses inverter output (I_1) and filter output current (I_3) feedback as shown in Figure 2.26 [58]. This feedback method is referred as inductor current (I_L) feedback system.

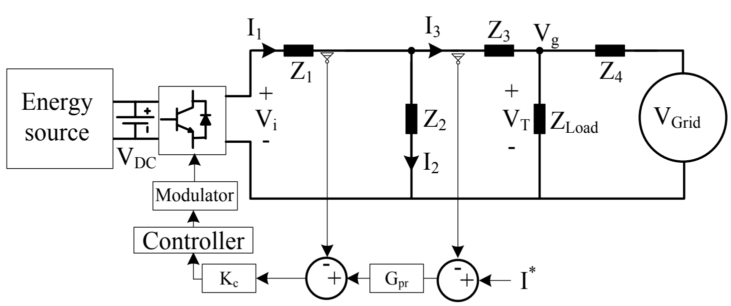

Figure 2.26. Multiple-loop inverter control with I_1 and I_3 feedbacks.

In this inverter control method, LCL filter output current (I_3) is used as feedback in the outer loop of the current controller while the inverter output current (I_1) is used as feedback in the inner loop of the current controller. Furthermore, a proportional controller (K_c) is also used in the inner loop. Now from Figure 2.26, the feedback current I_f can be written as,

$$I_{f,I_1} = I_1/G_{pr} + I_3 \tag{2-17}$$

Then the open-loop transfer function of inverter controller becomes,

$$G_{OL,I_1} = M \cdot G_{pr} \cdot K_c \cdot \{G(I_1/V_i)/G_{pr} + G(I_3/V_i)\} \tag{2-18}$$

2.5.2.3 Multiple-loop inverter control with I_2 and I_3 feedback:

This multiple-loop inverter control configuration uses filter capacitor current (I_2) and the filter output current (I_3) feedback as shown in Figure. 2.27. This feedback method is referred as capacitor current (I_C) feedback system.

In this inverter control method, LCL filter output current (I_3) is used as feedback in the outer loop of the current controller while the capacitor current (I_2) is used as feedback in the inner loop of the current controller. Furthermore, a proportional controller (K_c) is also used in the inner loop.

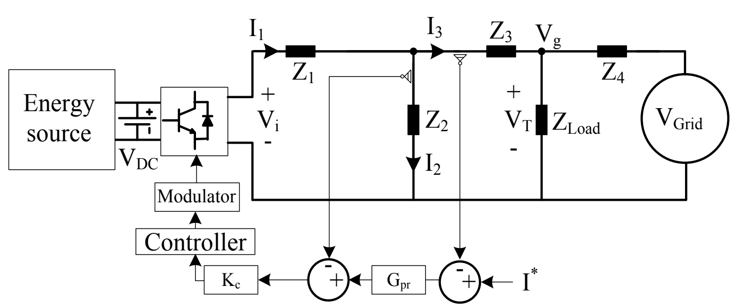

Figure 2.27. Multiple-loop inverter control with I_2 and I_3 feedbacks.

Now from Figure 2.27, feedback current I_f can be written as,

$$I_{f,I_2} = I_2/G_{pr} + I_3 \tag{2-19}$$

Then open-loop transfer function of the controller becomes,

$$G_{OL,I_2} = M \cdot G_{pr} \cdot K_c \cdot \{G(I_2/V_i)/G_{pr} + G(I_3/V_i)\} \tag{2-20}$$

2.6 Comparison Between two Current Sensors Feedback Methods

In this section, a comparison between different inverter control schemes with two current sensors is carried out. The conventional single-loop inverter control is not compared for their limited control loop gain and LCCL method for their practical applicability constraint.

To facilitate a fair comparison between different inverter controllers with two sensors, their open-loop transfer functions shown in (2-16), (2-18) and (2-20) are compared to identify similarity. Comparing (2-16), (2-18) and (2-20), a design criteria (2-21) is identified in this work which would make control bandwidth and gains at controller resonance frequency of both multiple-loop controller configuration and WAC same.

$$G_{pr,WAC} = G_{pr,multi,I_1} \cdot K_c = G_{pr,multi,I_2} \cdot K_c \tag{2-21}$$

Here G_{pr} represents PR controller parameter for corresponding inverter controller and K_C is the inner loop proportional controller of both multiple-loop inverter controllers.

2.6.1 Comparison I: Stability analysis

At first, stability analysis of all three controllers with two sensors is carried out with the help of root locus analysis. The system transfer functions of all three controllers are derived from their open-loop transfer function.

To derive the closed-loop transfer function of the WAC controller, the open-loop transfer function of the controller (2-16) is used and the obtained denominator of the closed-loop transfer function is (2-22).

$$[C_2 s\,\{Z_1 + G_{PR}(1-\beta)\} + 1]Z_3 \;+ G_{PR}\beta + Z_1 + G_{PR}(1-\beta) \tag{2-22}$$

Similarly, to derive the closed-loop transfer function of the multiple-loop controllers with inductor and capacitor current feedback, the open-loop transfer function of the controllers (2-18) and (2-20) is used and the obtained denominator of the closed-loop transfer function for inductor current feedback is (2-23) and capacitor current feedback is (2-24).

$$\{C_2 s\,(Z_1 + K_C M) + 1\}Z_3 + K_C M(PR + 1) + Z_1 \tag{2-23}$$

$$\{C_2 s\,(Z_1 + K_C M) + 1\}Z_3 + PRK_C M + Z_1 \tag{2-24}$$

From (2-22), (2-23) and (2-24); root locus plot of the three different inverter control method is shown in Figure 2.28 under line parameter variation. At first the controllers are designed for inverter side inductance = *2.5*mH and grid side inductance = *7*mH. To demonstrate the effect of line parameter variation on stability, root locus plot is shown in Figure 2.28 where inverter side inductance is varied from *1.5*mH to *4.5*mH and grid side inductance is varied from *2*mH to *7*mH.

From the root locus plots of Figure 2.28 it can be concluded that multiple-loop inverter controller with both feedback configuration is stable against line parameter variation. But the WAC controller is sensitive to line parameter variation and becomes unstable if line inductance is changed, e.g. changing inverter side inductance from *2.5*mH to *4.5*mH or grid side inductance from *7.0*mH to *2.0*mH, makes the system unstable. Here equivalent series resistances of the inductors are considered to be 0.2Ω. To compare the inductor and capacitor feedback system, their closed-loop Bode plot is shown in Figure 2.29. From Figure 2.29 it is seen that the inverter control system with capacitor current feedback has higher gain at low frequency than inductor current feedback system. As a result, the transient performance of the capacitor current feedback system is better than inductor current feedback system. Figure 2.29 also shows that multiple-loop inverter control with both feedback configuration have similar gain at fundamental frequency (*50Hz*) and both controller has similar bandwidth. But the lower low frequency gain of the inductor current feedback means that the controller will have better DC rejection capability. This will also be shown with the experimental results. The feedback configuration of multiple-loop VSI control also suggest that it has less steady state error than single-loop VSI control with single sensor or two sensors. For example, LCCL method uses current through the capacitor as feedback where I_{21} and I_{22} appear as a steady state error at the VSI output. Again, WAC uses combination of I_2 and I_3 as feedback and I_2 introduces a steady state error at the VSI output. But only I_3 feedback is used for multiple-loop VSI control that minimizes steady state error.

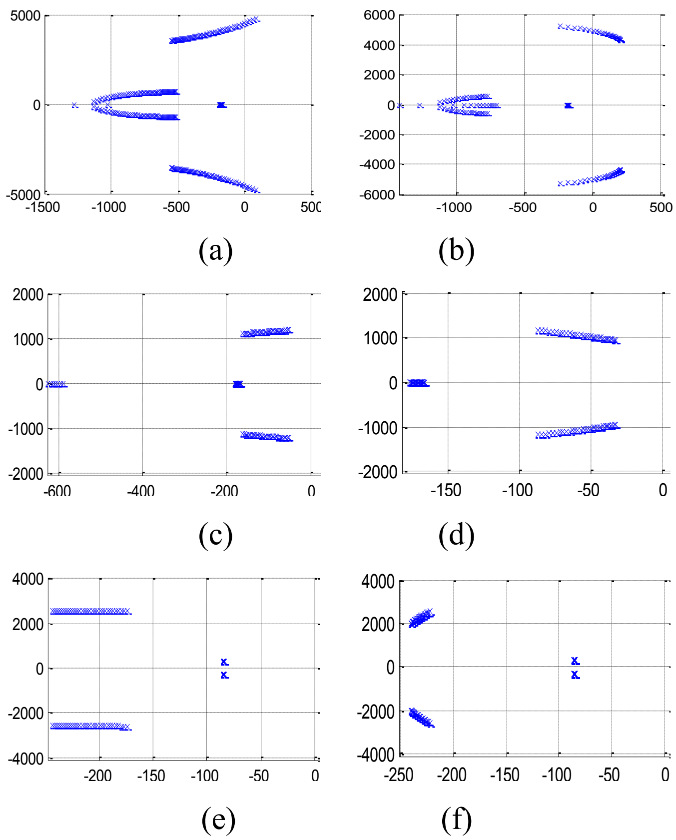

Figure 2.28. Root locus of different systems under inverter side (left column) and grid side (right column) parameter variation. (a) and (b): WAC control. (c) and (d): multiple-loop control system with I_C as inner loop feedback. (e) and (f): multiple-loop control system with I_L as inner loop feedback.

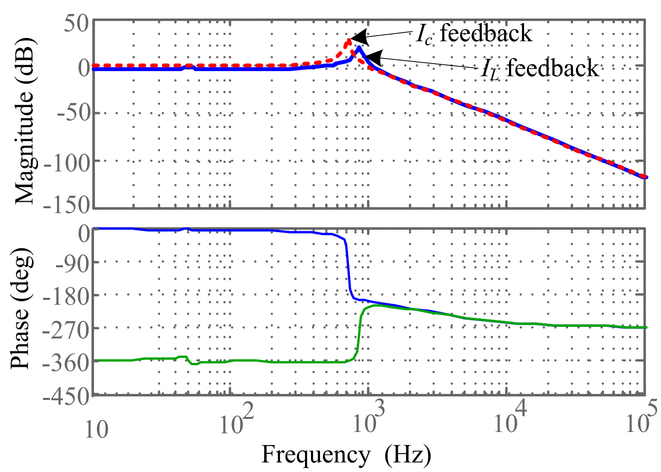

Figure 2.29. Closed-loop Bode plot for double-loop control with I_C or I_L as inner loop feedback.

2.6.2 Comparison II: Explanation of the Performance Difference

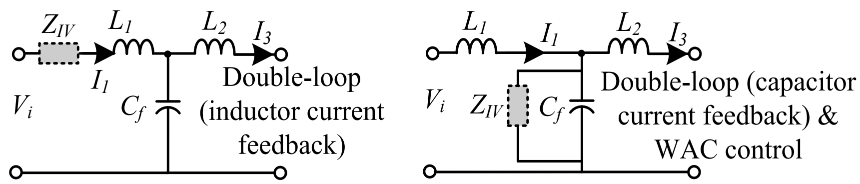

Figure 2.30. Position of damping impedance with different controllers

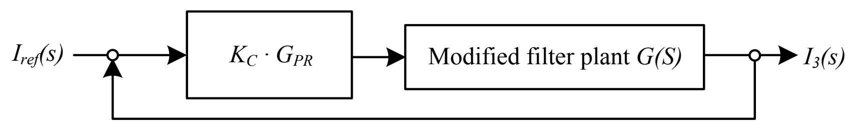

Figure 2.31. DG-Grid interfacing inverter with LCL filter

The performance differences of the aforementioned controllers can also be investigated using recently proposed Generalized Closed Loop Control (GCC) scheme [50]. In the GCC scheme, the double-loop and WAC controllers are unified as a single closed-loop control and an additional internal damping impedance term, where the effect of the internal damping impedance is to place a virtual impedance Z_{IV} with the original LCL filter plant. As shown in Figure 2.30, for double-loop control using inductor current inner loop feedback, the damping impedance is placed in series with filter inductor L_1. On the other hand, the double-loop control with capacitor current inner loop is equivalent to placing a damping impedance in parallel with filter capacitor. Finally, the WAC controller can also be incorporated into the GCC scheme, where the equivalent damping impedance is a nonlinear impedance associated with the filter capacitor branch. The expressions of the damping impedance with different controllers are obtained here as:

$$Z_{IV}(s) = \begin{cases} K_C \\ L_1/\left(C_f \cdot K_C\right) \\ L_1/\left\{C_f \cdot (1-\beta) \cdot G_{PR}(s)\right\} \end{cases} \tag{2-25}$$

where the top one in (2-25) is for double-loop with inductor current inner loop, the expression in the middle is for double-loop with capacitor current inner loop. The bottom one is for WAC control. The detailed analysis of this virtual impedance can be found in [59].

With the modified LCL filter plant, Figure 2.31 demonstrates the closed-loop diagram of the grid-connected system. As shown, the system is composed of a single-loop equivalent PR controller and a modified filter plant. The gain of the PR controller is maintained to be the same for different controllers, and the only difference here is the modified filter plants. Therefore, the performance differences of double-loop and WAC controllers can be analyzed through open-loop transfer function of the modified filter plant as:

$$G(s) = I_3(s)/V_i(s) \tag{2-26}$$

where $V_i(s)$ is the PWM voltage at the modified filter plant.

The Bode plots of the modified filter plants are shown in Figure 2.32 to 2.34. Figure 2.32 shows the dampened filter plant with double-loop capacitor current inner loop, where the originally resonant peak in LCL filters is properly mitigated in different grid side conditions (both 7mH and 2mH). The Bode plots with double-loop inductor current inner loop are also presented in Figure 2.33. In this case, although the resonance introduced by PWM voltage can be dampened, the magnitude around low frequency region is significantly lower than its capacitor current counterpart. That means the dynamic response is also slower in this situation. Finally, the Bode plots with WAC control are shown in Figure 2.34. Comparing to the double-loop controllers, the WAC control achieves inherent damping through single-loop control. In addition, the filter plant has a relatively wider constant phase angle region around fundamental frequency. Therefore, it may benefit the PR controller design. However, the weighting factor of WAC control here is designed based on weak grid situations with 7mH grid side inductance. When grid side impedance reduces to 2mH, the system becomes more sensitive to harmonic voltage disturbances, as the resonance peak is higher than with double controllers. Therefore, it can be concluded that the filter parameter mismatch shall be avoided in WAC control.

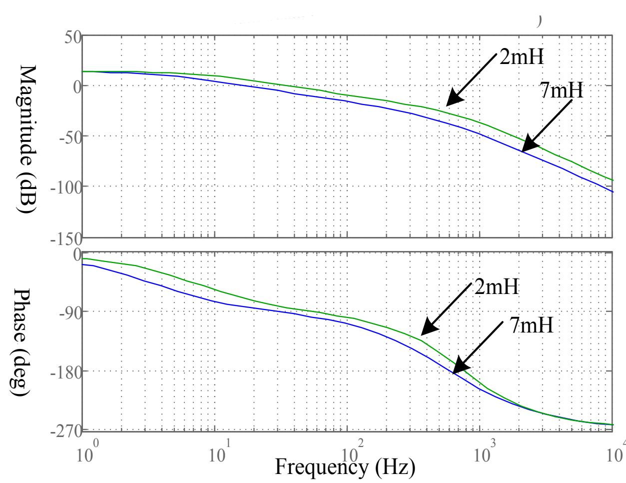

Figure 2.32. *G(s)* with double-loop controller using capacitor current inner loop.

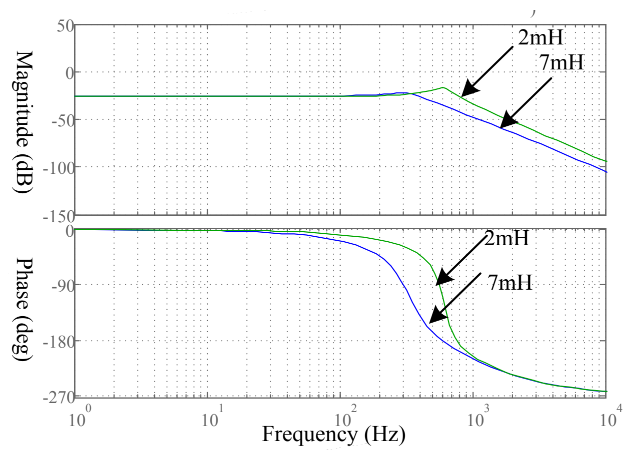

Figure 2.33. *G(s)* with double-loop controller using inductor current inner loop.

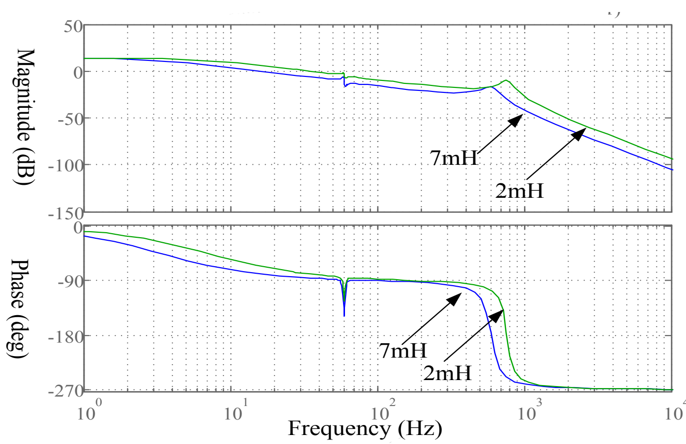

Figure 2.34. *G(s)* with WAC controller.

2.6.3 Simulation and Experimental Results

Performance of the three two sensor feedback VSI control methods are compared with simulation using Matlab/Simulink and experimentally on a 5kVA grid connected DG system. The control methods are tested in presence of line parameter variation. The system parameters used in simulation and experiment are identical and listed in Table 2.2.

Table 2.2.2. System Parameters

Parameters	Simulation and Experiment
Grid voltage	81V
DC link voltage	260V
L_1, R_1	2.5mH, .1Ω
C_2, R_2	40µF
L_3, $R3$	2mH, .1Ω
Switching frequency	9kHz

To see the performance of inverter control methods under line parameter variation, the inverter side inductance is changed from 2.5mH to 4.5mH and grid side inductance is changed from *7*mH to *2.5*mH during simulation. The simulation results are shown in Figure 2.35. The simulation results suggest that unlike WAC, multiple-loop controllers are not sensitive to system parameter variation.

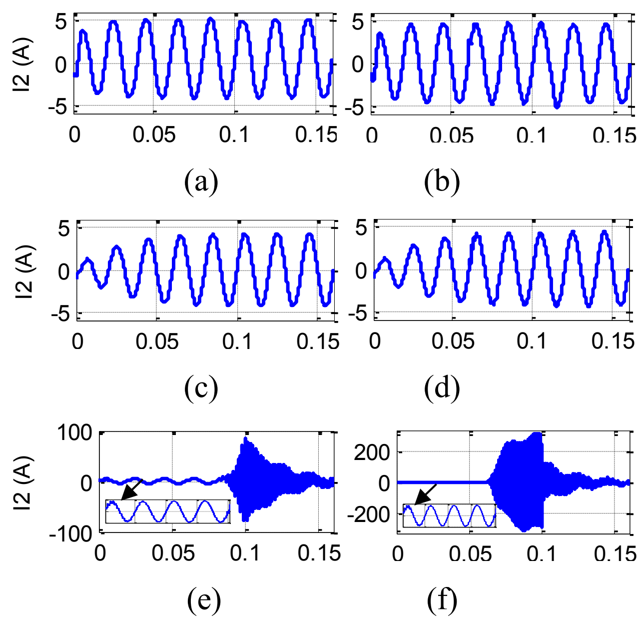

Figure 2.35. Simulation results under inverter side (left column) and grid side (right column) parameter variation. (a) and (b): double-loop with I_c as inner loop feedback, (c) and (d): double-loop with I_L as inner loop feedback, (e) and (f): WAC feedback.

Previously it was mentioned that I_L feedback has better DC rejection capability than I_C feedback system but its transient performance is worse. To verify the DC rejection performance, 10% DC value was added intentionally with the grid side current feedback to emulate an exaggerated measurement DC offset. Then, frequency analysis of output current shows that I_L feedback has better DC rejection capability than I_C feedback. This is shown in Figure 2.36. To verify the transient performance, reference was intentionally changed from 5A to 20A during simulation. Then, the output current shows that the transient performance of I_C feedback is better than I_L feedback. This is shown in Figure 2.37.

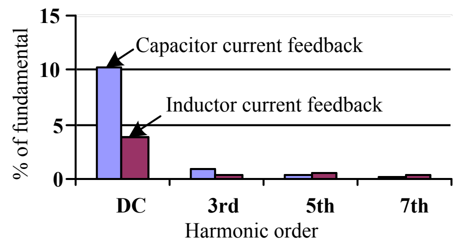

Figure 2.36. DC rejection capability of double-loop control with I_C or I_L feedback.

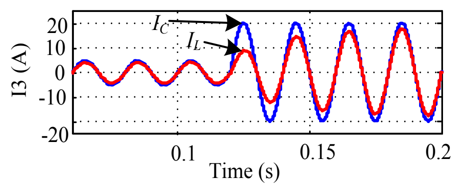

Figure 2.37. Transient performance of double-loop control with I_C or I_L feedback

To see the performance of line inverter control methods under line parameter variation, the grid side inductance is changed from *7*mH to *2.5*mH during experiment. The experimental results are shown in Figure 2.38.

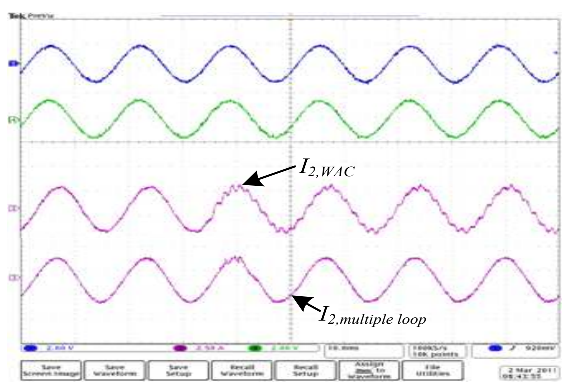

Figure 2.38. Experimental result under grid side parameter variation of WAC system and multiple-loop control with I_c feedback.

From the experimental result, it is evident that the multiple-loop inverter control system with both feedback configurations is more stable under grid parameter variation than WAC. The stability of both multiple-loop inverter control system with capacitor and inductor current feedback under line parameter variation is similar. From Figure 2.39, it can be seen that the transient performance of the multiple-loop inverter control system with capacitor feedback is better than inductor current feedback. In Figure 2.39, the reference is changed from 1A to 5A during the experiment and transient performance of both multiple-loop feedback systems is recorded. The experiment result shows that the capacitor current feedback system becomes stable within 1 cycle of operation following a change whereas inductor current feedback takes 3 cycles to reach steady state.

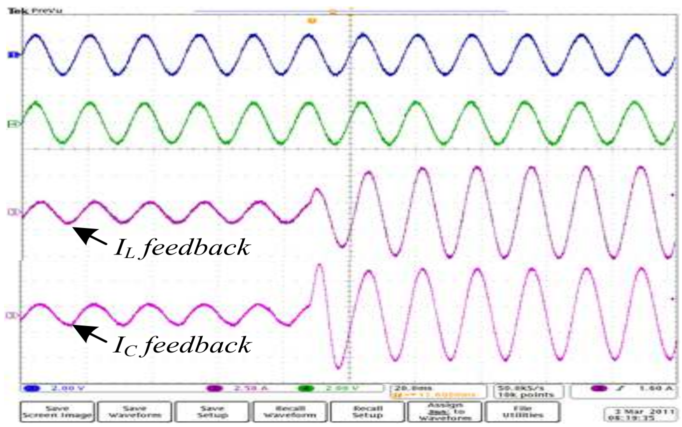

Figure 2.39. Transient performance of double-loop control with I_C or I_L as inner loop feedback.

2.7 Conclusions

In this chapter, the opportunities of distribution system power quality improvement using the DG interfacing inverters are investigated. Both the current controlled method and the voltage controlled method are considered and their associated power quality compensation schemes are investigated. The current controlled DG is suitable to be used in the grid connected system while voltage controlled DG can be used in the islanded microgrid as it can provide the required voltage support. The voltage controlled DG can be operated with compensation, rejection and uncontrolled mode, where the harmonic compensation and rejection modes produce similar performance as with the current controlled DG. The analysis of the control strategies and the observations of the comparison of these two methods have been verified in both time domain simulations and experiments. Since most grid connected DG systems use current controlled VSI, the analysis on different current control method is then extended and a comparative analysis of VSI control systems with single and two current sensors are presented. A design criteria for single and multiple-loop feedback method is proposed here to facilitate fair comparison among different control methods. The analysis shows that multiple-loop feedback system has low line parameter sensitivity which makes the controller suitable to be used in a system with line parameter variation. Finally, Table 2.3 summarizes the comparison results obtained from analysis, simulation and experiment. According to the study and comparison in this Chapter, when CCM based VSI is used as DG interface, the two current sensor scheme with inductor current feedback is recommended considering it superior performance and ability to provide quick protection due to the direct measurement of inverter output current.

Table 2.3. Comparison Summary

Comparison criteria	Single current sensor		Two current sensors		
	Single-loop	**LCCL feedback**	**I_L feedback**	**I_C feedback**	**WAC feedback**
Steady state error	Poor	Fair	Good[1]	Good[1]	Fair[1]
Transient response	Poor	Good[2]	Good	Best	Good[2]
Parameter sensitivity	Fair	Poor	Good	Good	Poor
Implementation complexity	Good	Poor[3]	Fair	Fair	Fair

[1] WAC uses combination of I_2 and I_3 as feedback and I_2 appears as a steady state error at the output. Whereas only I_3 feedback is used for multiple-loop control that minimizes steady state error.

[2] Properly designed LCCL or WAC system has high controller bandwidth. But line parameter variation during operation reduces controller bandwidth and compromises transient performance.

[3] LCCL method needs exact valued capacitor.

Chapter 3

Residential Harmonic Mitigation: Distributed and End-of-Line Compensation

3.1 Introduction

In recent years, the use of power electronics driven home appliances have increased significantly due to the consideration of energy efficiency. For example, lighting and heating systems were mostly resistive in the past which are replaced by CFLs (compact fluorescent light) LEDs, and HVAC (Heat, Ventilation and Air Conditioning) [68]. Although these appliances consume considerably less power than their older counterparts, they are a significant source of harmonics in today's power grid [68-71]. This increasing utilization of power electronic loads in today's homes is a growing concern for utility companies due to the increased harmonic distortions. The harmonic problem could be further complicated by the harmonic resonance introduced by other system components, such as the power factor correction (PFC) capacitors. It is predicted that the residential system voltage harmonics will increase rapidly and could reach 5% total harmonic distortion (THD) soon if no remedial actions are taken [72]. Besides the degrading power quality, the harmonic current flow is also a concern for the telecommunication industry as this harmonic current flow may interfere with the adjacent telephone lines [72, 73]. Compensating the harmonics in a residential system is difficult because of the dispersed nature of the residential loads. Therefore, lump compensation at a few locations is not every effective [74]. As a result, finding an effective way to compensate the dispersed load harmonics and improve the residential distribution system power quality is an important topic.

Publication out of this chapter:

S. Munir and Y. W. Li, "Residential Distribution System Harmonic Compensation Using PV Interfacing Inverter," in IEEE Transactions on Smart Grid, vol. 4, no. 2, pp. 816-827, June 2013.

At the same time, the power industry is experiencing a paradigm shift as more renewable energy based distributed generation (DG) systems are being connected to the power distribution network [75, 76]. A typical example is the increasing installation of rooftop photovoltaic (PV) systems in residential areas. As shown in Figure 4.1, these PV systems are connected to the grid through DG-grid interfacing inverters, which are used mainly to convert the voltage from the energy source to the voltage that can be readily connected to the grid, and to transfer the real power to the grid. As stated in the previous two chapters, these DG-grid interfacing converters are able to provide a number of ancillary functions in addition to the primary function of real power injection if controlled properly. This potential for ancillary services can be realized by properly utilizing the available apparent power rating from the interfacing inverters. Doing so is feasible as most of the time these inverters are not running at their maximum power due to the intermittent nature of renewable energy (such as PV) [77]. Moreover, peak demand in residential areas does not occur at the same time as the PV peak power hours. Therefore, when power quality compensation is needed, rating from the PV inverters will be available to provide the ancillary services [77, 78].

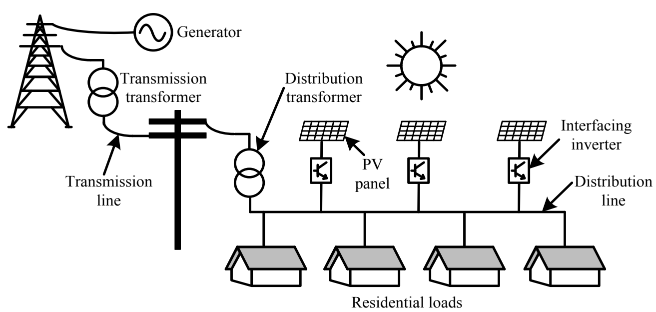

Figure 3.1. Residential system with PV installations

The concept of system harmonic compensation in a residential distribution system using grid interfacing PV inverter has been reported in the literature [79-81]. However, the system considered in the previous work is usually too simple (e.g., the system is often comprised of only a few lines and loads) to provide realistic results. Also, the effects of harmonic resonance with other power system components, such as capacitors, are not sufficiently considered in the previous work. Additionally, for a system with distributed loads and DG systems, assigning the harmonic compensation priority to different DG units to achieve the best compensation result is an important topic that has not been addressed in the literature.

The above mentioned issues are addressed in this chapter. A residential distribution system with line impedances, distribution transformers and typical house loads is modeled first. The house load model is created from the aggregated load characteristics of typical residential appliances [82, 83]. This house load model is used to investigate the effect of non-linear residential loads on the power quality of the modeled distribution system. Then the PV grid-interfacing inverters are connected to the distribution system model and are controlled to improve the power quality by acting as harmonics-damping virtual impedance. The effects of the PV locations on harmonic compensation such as end-of-line [74] and distributed compensation [84, 85] are investigated. An in-depth analysis and explanation of the performance differences are also carried out to provide a guide for properly assigning the harmonics compensation priorities to PV inverters at different locations of the distribution system considering DG is available at every location of the distributed system. These analysis results are verified by simulations of a sample residential distribution system.

3.2 Control Scheme of PV Inverter with Virtual Harmonic Resistance

In this work, the PV inverters are controlled as virtual harmonic impedance at the harmonic frequencies to compensate the residential system harmonics. Therefore, before the residential system model and harmonic compensation performances are discussed, the virtual impedance control concept is introduced in this section.

3.2.1 Virtual Harmonic Impedances

Virtual impedance emulates the effect of physical impedance, without the need to connect any physical component to the system. In the DG inverter control, the virtual impedance is implemented by modifying the voltage or current reference or the PWM signal, through digital control of the inverters. Virtual impedance can be either at the fundamental frequency or at the harmonic frequencies. The fundamental frequency virtual impedance is used mainly to facilitate DG power flow control [86, 87] and grid disturbance ride through [88]. The harmonic virtual impedance is mainly used for active damping [89, 90] and distribution system harmonic compensation [91].

A harmonic compensation method by a voltage-controlled DG unit is proposed in [91], where the DG unit is represented as a controlled voltage source (V_{DG}) with output series impedance (Z_{DG-}

$_h$). The harmonic components of the controlled voltage source, V_{DG-h}, is controlled according to the harmonic voltage of the point of common coupling (PCC), V_{PCC-h}, with a positive feedback gain G so that V_{DG-h} = -G×V_{PCC-h}. As a result, the equivalent harmonic impedance of the DG becomes $Z_{DG-h}/(1+G)$. Here, G can be in the range of -1 to ∞. A virtual inductive equivalent impedance is introduced in this method to compensate the system harmonics, since the impedance is mainly inductive at harmonic frequencies. This method is quite attractive for use in a microgrid, where the voltage-controlled DG is important for providing the microgrid voltage and frequency control.

In [92] and [93], distribution system harmonics improvement using a current-controlled grid-interfacing inverter is discussed where DG operates like a shunt active power~~s~~ filter (APF) and absorbs the harmonic current generated by the non-linear load. As a result, the source current becomes harmonic-free and the PCC voltage THD decreases. A popular way to achieve this function is to operate the DG as resistive-APF (R-APF) [94]. Here, the harmonic components of the grid side voltage, V_{Grid-h}, are extracted and the reference harmonic current of the DG is produced by using $I^*_{DG} = V_{Grid-h}/R_h$. As a result, the DG acts as a virtual resistance, R_h, only at the harmonic frequencies. As most residential rooftop PV inverters are current-controlled, the virtual harmonic resistance method is adopted in this work.

3.2.2 Control Scheme of PV Inverter with Virtual Harmonic Resistance

With the virtual harmonic resistance control, the PV inverters work as R-APF. A block diagram of the system harmonic damping control is shown in Figure 3.2. The PV system in this example is a two-stage conversion system, which includes a DC-DC converter that steps up the PV output to the DC link voltage level with maximum power point tracking (MPPT) control, and an inverter that connects the system to the grid. The PV system output current reference (I^*_{DG}) has two components: (i) the fundamental component (I^*_f), which is produced from the DC link voltage control and power factor control loops (which are not shown in Figure 3.2 as the focus here is harmonics compensation), and (ii) the harmonic components (I^*_h), which are used for harmonic compensation.

For virtual resistance realization, the reference harmonic current of the PV system is produced by using $I^*_h = V_{G\_h}/R_h$. Then the reference current of DG is obtained by combining the fundamental reference (I^*_f) and the harmonic current reference (I^*_h). Finally, the PV system output current is controlled with double control loops~~,~~ containing an outer output current (I_{DG}) control loop and an inner (LC) filter inductor current (I_L) control loop [90], which has better performance than many other two sensor feedback control schemes as shown in Chapter 2.

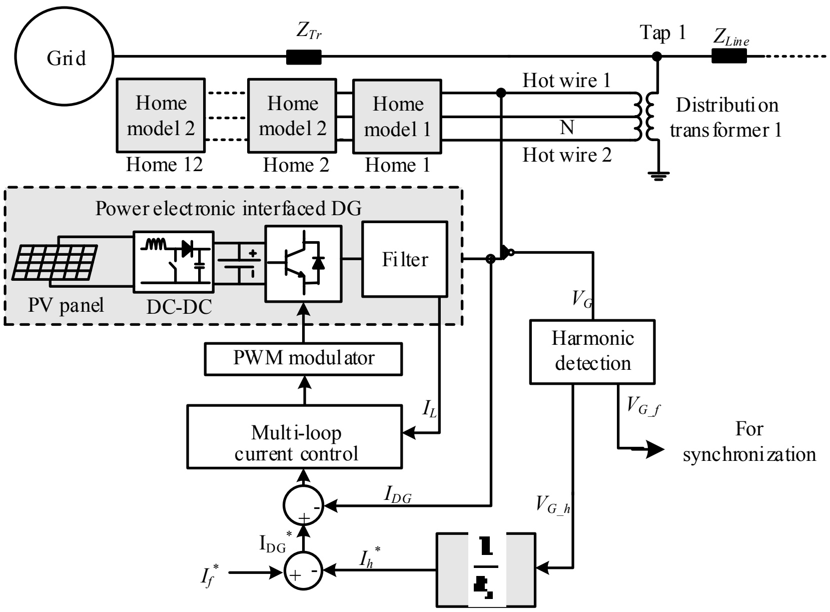

Figure 3.2. Harmonic damping with R-APF based DG.

For fundamental current tracking and harmonic current control, proportional resonant controllers are used (3-1) [95, 96].

$$G_c = K_P + \sum_{h=1,5,7\ldots} \frac{2K_{ih}\omega_{ch}s}{s^2 + 2\omega_{ch}s + \omega_h^2} \tag{3-1}$$

where ω_h is the system fundamental and harmonic frequency, ω_{ch} is the cut-off bandwidth at each frequency, K_{ih} is the integral gain at each frequency, and K_p is the proportional control gain at all frequencies. To improve the dynamic response and stability of the control loop, a proportional controller is usually adopted for the inner filter inductor current feedback loop [90].

The modeling of the distribution system is presented in the following section, and the aforementioned PV inverter system is then connected to the developed distribution system model to investigate the harmonic compensation performance. To avoid the effects of different current control techniques on the PV inverter, controlled current sources at the desired harmonic frequencies are used in the rest of this chapter to model the PV inverter with virtual impedance control.

3.3 System Modeling

In this section, the system model including the residential house load, distribution systems with PFC capacitors, and PV inverters (with virtual harmonic impedance control) is first developed. The developed models are then used for the analysis of harmonic distortions and compensation performances by using different approaches.

3.3.1 Residential Load Modeling

To model a home, different home appliances are modeled as a harmonic current source in parallel with the fundamental impedance as shown in Figure 3.3.

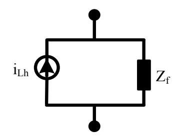

Figure 3.3. House load model with harmonic current source and fundamental impedance.

$$i_{Lh} = \sum_{h=3,5,7\ldots} i_h \tag{3-1}$$

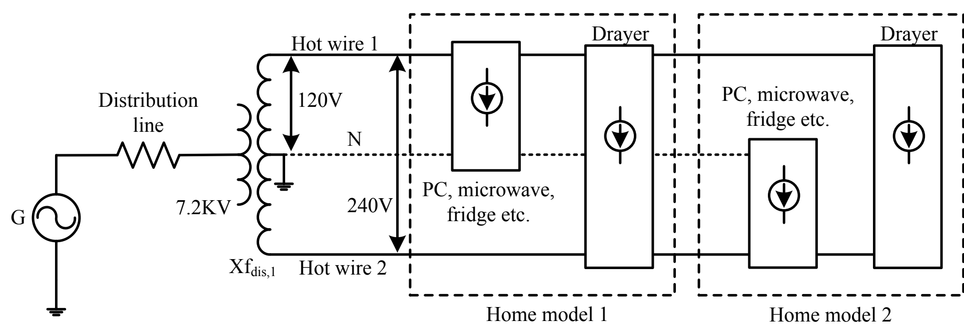

Figure 3.4. Connection configuration of home model 1

To obtain such a home model, individual home appliance models, including personal computer (PC), compact fluorescent light (CFL), adjustable speed drive (ASD) fridge, TV, refrigerator, washer, and dryer are generated first. As an example, the harmonic load current data for the CFL and PC are shown in Table 3.1. Note that these data are taken from [82, 97] where the appliance harmonic load current data are measured practically. To construct the home model, these appliances are then connected to hot wire 1, hot wire 2 and neutral (*N*) as shown in Figure 3.4. Finally, the constructed home models are connected to a distribution system model as shown in Figure 3.5 [83].

Table 3.1. Harmonic Load Current Data for Home Appliances

Appliance model of	Data type	Harmonic Load Current Data						
		1st	3rd	5th	7th	9th	11th	13th
CFL	Mag	.15	.13	.09	.07	.07	.06	.039
	Ang	21.2	53.9	105.5	169.4	-134.8	-84.2	-21.8
PC	Mag	.83	.65	.41	.16	.10	.12	.12
	Ang	.50	1.6	3.6	8.6	58.1	168.7	178.0

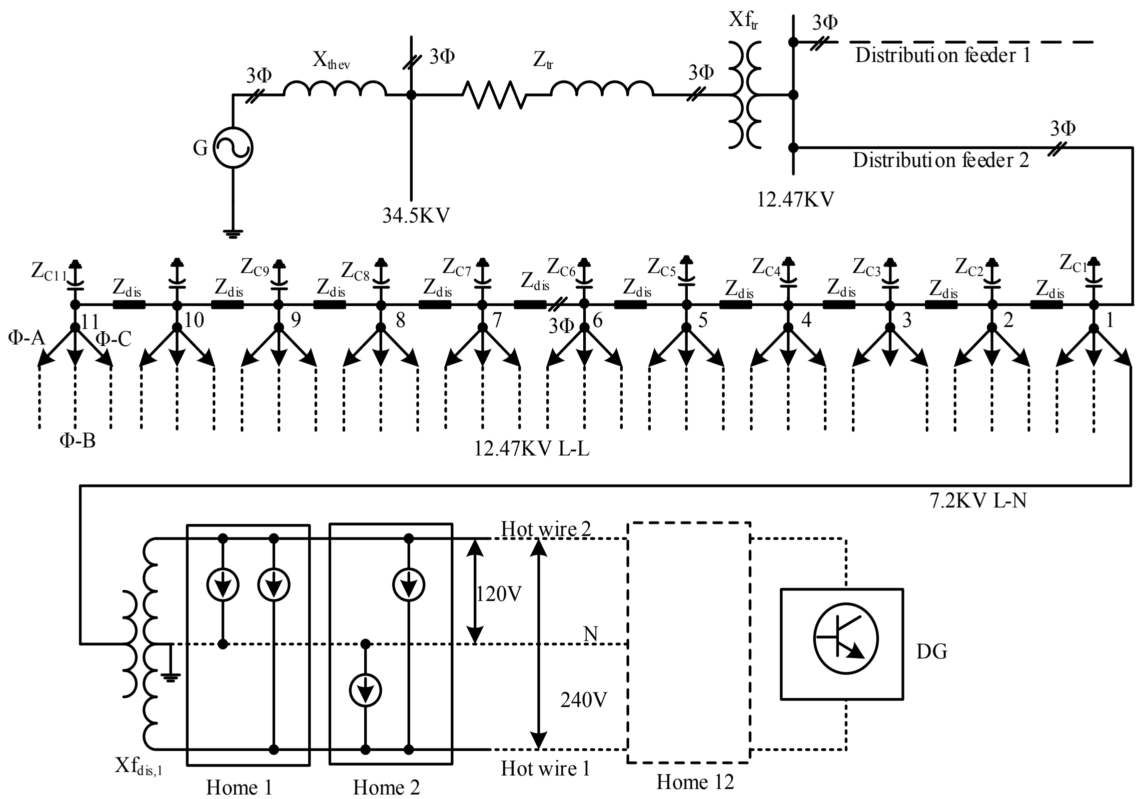

Figure 3.5. Distribution system model.

All the appliance models except the dryer are connected between hot wire 1 and the neutral for home model 1, whereas the appliance models are connected between the neutral and hot wire 2 for home model 2. The dryer model is connected between hot wire 1 and hot wire 2 for both home model 1 and home model 2. The parameters used in this work to model the distribution system are listed in Table 3.2 [83].

Table 3.2: System Parameters

Parameter	Value
Distribution feeder voltage	7200V (line-neutral)
Distribution transformer	7200V/120V, 0.015+0.03j p.u.
Distribution line impedance	.43Ω/km, 150μH/km
Number of distribution node	11
House load in each node	12
PFC capacitor	4μF to 12μF

The distribution system has a *34.4*kV transmission line connected to the *12.47*kV distribution feeders through transmission transformer (Xf_{tr}). The 3-phase distribution feeder has 11 nodes. On each node, a group of 12 houses is connected to the distribution feeder through distribution transformer (Xf_{dis}) in a way that the load current is balanced (6 home model 1 and 6 home model 2).

3.3.2 Distribution System Modeling without Capacitor Bank

Figure 3.6 shows the simplified distribution feeder of the distribution system shown in Figure 3.5 with DG connected at the secondary side of the distribution transformer. Here, n = 1, 2, 3……N represents the n^{th} node. Z_{Xn} ($R_{Xn} + j\omega L_{Xn}$) represents the distribution line impedance of the n^{th} node, Z_{Yn} ($R_{Yn} + j\omega L_{Yn}$) represents the distribution transformer impedance at the n^{th} node, Z_{Ln} ($R_{Ln} + j\omega L_{Ln}$) represents the fundamental load impedance at the n^{th} node, DG_n represents the DG current at the n^{th} node, and I_{hn} represents the harmonic current of the non-linear load at the n^{th} node.

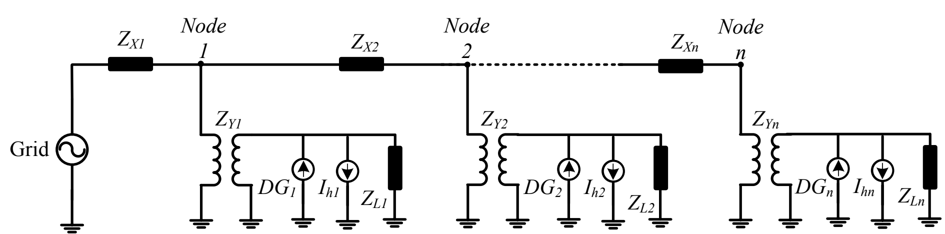

Figure 3.6. Typical distribution feeder with DG.

Referring the system to the primary side of the transformer, the equivalent circuit of such a system is shown in Figure 3.7 (note that the same symbols as in Figure 3.6 are used in Figure 3.7 to represent the system. Also, as the analysis here focuses on harmonic frequencies, the source is shorted in Figure 3.7). Additionally, V_n is the voltage at the n^{th} node. x_1, $x_4 \ldots x_{3N-2}$ are the currents through Z_{L1}, $Z_{L2} \ldots Z_{Ln}$. x_2, $x_5 \ldots x_{3N-1}$ are the currents through Z_{Yn}. x_3, $x_6 \ldots x_{3N}$ are the currents through Z_{Xn}.

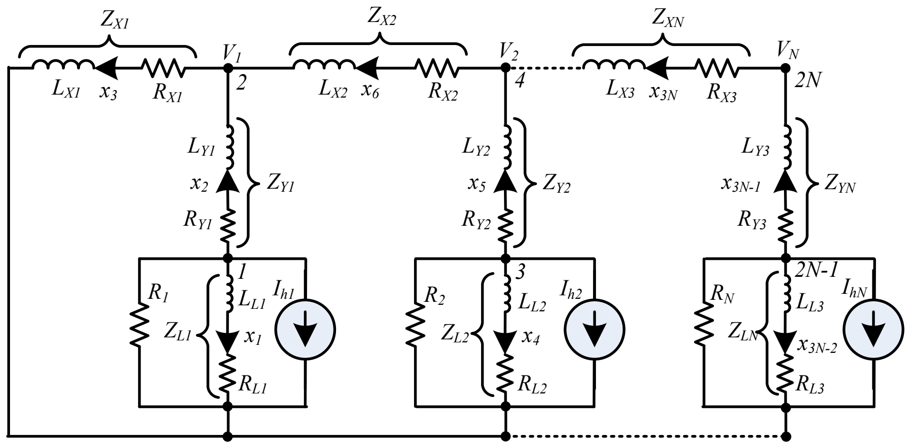

Figure 3.7. Equivalent circuit of an N node distribution feeder.

Here, x_1, $x_2 \ldots x_{3N}$ are taken to be the state variables, I_{hn} is the input, and V_n is the output of the state space model of the system. Then for a N-node system, there are 3N equations based on KCL-KVL methods. The 1-N, N+1 to 2N, and 2N+1 to 3N equations are shown in (3-3)-(3-5), respectively:

$$I_{h\cdot n} = x_{3n-2} + x_{3n-1} + \frac{x_{3n-2}R_{L\cdot n} + \dot{x}_{3n-2}L_{L\cdot n}}{R_n} \tag{3-3}$$

$$\begin{gathered}\sum_{n=1}^{N}(x_{3\cdot n}R_{X\cdot n} + \dot{x}_{3n}L_{X\cdot n}) - x_{3n-1}R_{Y\cdot n} - \dot{x}_{3n-1}L_{Y\cdot n} \\ = x_{3n-2}R_{Y\cdot n} + \dot{x}_{3n-2}L_{L\cdot n}\end{gathered} \tag{3-4}$$

$$x_{3n-1} + x_{3n+3} = x_{3n} \tag{3-5}$$

Solving (3-3) to (3-5) yields the A_N and B_N matrices of the state space model while the equation of the system output (3-6) yields the C_N and D_N matrices of the state space model.

$$v_n = v_{n-1} + x_{3n}R_{Xn} + \dot{x}_{3n}L_{Xn} \tag{3-6}$$

Hence, the state space model of the system can be obtained as shown in (3-7) and (3-8). From the state space model, the transfer function of the system can be easily found by using (3-9).

$$\dot{x} = A_N \begin{bmatrix} x_1 \\ x_2 \\ \cdot \\ \cdot \\ x_{3N} \end{bmatrix} + B_N \begin{bmatrix} I_{h1} \\ I_{h2} \\ \cdot \\ \cdot \\ I_{hN} \end{bmatrix} \tag{3-7}$$

$$\begin{bmatrix} v_1 \\ v_2 \\ \cdot \\ \cdot \\ v_N \end{bmatrix} = C_N \begin{bmatrix} x_1 \\ x_2 \\ \cdot \\ \cdot \\ x_{3N} \end{bmatrix} + D_N \begin{bmatrix} I_{h1} \\ I_{h2} \\ \cdot \\ \cdot \\ I_{hN} \end{bmatrix} \tag{3-8}$$

$$\frac{v_n(s)}{I_{hn}(s)} = C_N \emptyset B_N + D_N \tag{3-8}$$

where, $\emptyset = (sI - A_N)^{-1}$, n = 1, 2…N, and I is a 3NX3N identity matrix.

3.3.3 Distribution System Modeling with PFC Capacitors

The installation of the power factor correction (PFC) capacitor in the distribution system makes the harmonic issues complex, and some harmonics can be amplified [98]. Although installing an active power filter may mitigate the harmonics at the point of installation in such a situation, the harmonics may be amplified on the other busses due to the whack and mole effects [74, 99]. To investigate the effectiveness of different harmonic compensation schemes in such a situation, a distribution bus with capacitors connected has to be modeled. Figure 3.8 shows the equivalent distribution feeder of the distribution system with PFC capacitors. It also includes DG systems connected at the secondary side of the distribution transformer. Referring the system to the primary side of the transformer, the equivalent circuit of such a system is shown in Figure 3.9.

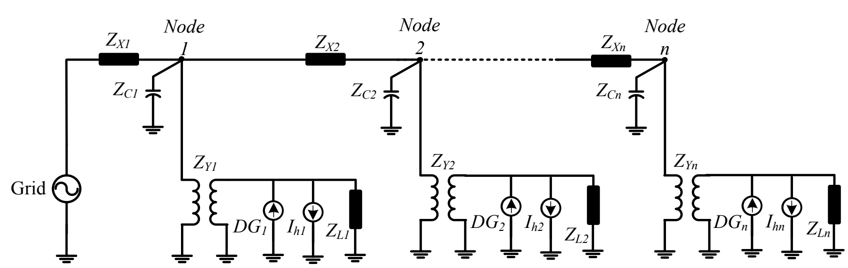

Figure 3.8. Typical distribution feeder with DG and PFC capacitors.

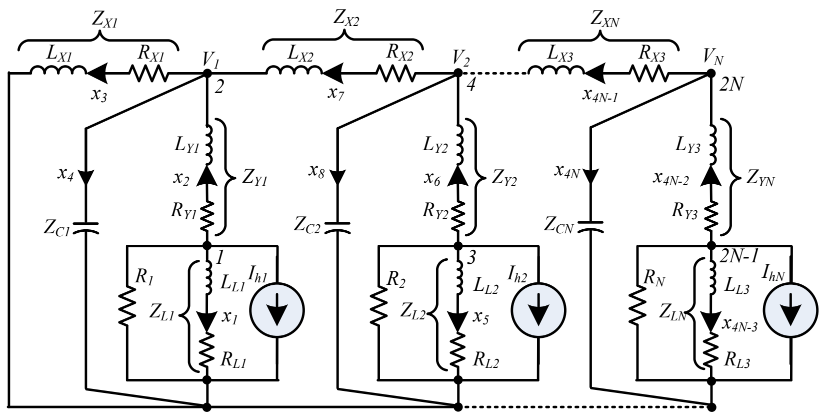

Figure 3.9. Equivalent circuit of an N node distribution feeder with PFC capacitors.

The symbols shown in the distribution system of Figure 3.8 and 3.9 are similar to those of Figure 3.6 and 3.7. Additionally, $Z_{C1}, Z_{C2}\ldots Z_{Cn}$ are the impedances of the PFC capacitors ($C_{C1}, C_{C2}\ldots C_{Cn}$), respectively, at the n^{th} node, and x_4, $x_{8\ldots}$ x_{4N} is the voltage across Z_{Cn}. Here, x_1, $x_{2\ldots}$ x_{4N} are taken to be the state variables, I_{hn} is the input, and V_n is the output of the state space model of the system. For a N-node system, there are 4N equations based on KCL and KVL. The 1-N, N+1 to 2N, 2N+1 to 3N, and 3N+1 to 4N equations are shown in (3-10)-(3-13), respectively:

$$I_{h\cdot n} = x_{3n-2} + x_{3n-1} + \frac{x_{3n-2}R_{L\cdot n} + \dot{x}_{3n-2}L_{L\cdot n}}{R_n} \tag{3-10}$$

$$\sum_{n=1}^{N}(x_{3\cdot n}R_{X\cdot n} + \dot{x}_{3n}L_{X\cdot n}) - x_{3n-1}R_{Y\cdot n} - \dot{x}_{3n-1}L_{Y\cdot n} = x_{3n-2}R_{Y\cdot n} + \dot{x}_{3n-2}L_{L\cdot n} \tag{3-11}$$

$$x_{3n-1} + x_{3n+3} = x_{3n} \tag{3-12}$$

$$\sum_{n=1}^{N}(x_{4\cdot n-1}R_{X\cdot n} + \dot{x}_{4\cdot n-1}L_{X\cdot n}) = x_{4n} \tag{3-13}$$

Solving (3-10) to (3-13) yields the A_N and B_N matrices of the state space model while the equation of the system output (3-14) yields the C_N and D_N matrices of the state space model.

$$v_n = v_{n-1} + x_{4n}R_{Xn} + \dot{x}_{4n-1}L_{Xn} \tag{3-14}$$

Hence, the state space model of the system can be obtained as shown in (3-15) and (3-16). From the state space model, the transfer function of the system can be found by using (3-17).

$$\dot{x} = A_N \begin{bmatrix} x_1 \\ x_2 \\ \cdot \\ \cdot \\ x_{3N} \end{bmatrix} + B_N \begin{bmatrix} I_{h1} \\ I_{h2} \\ \cdot \\ \cdot \\ I_{hN} \end{bmatrix} \tag{3-15}$$

$$\begin{bmatrix} v_1 \\ v_2 \\ \cdot \\ \cdot \\ v_N \end{bmatrix} = C_N \begin{bmatrix} x_1 \\ x_2 \\ \cdot \\ \cdot \\ x_{3N} \end{bmatrix} + D_N \begin{bmatrix} I_{h1} \\ I_{h2} \\ \cdot \\ \cdot \\ I_{hN} \end{bmatrix} \tag{3-16}$$

$$\frac{v_n(s)}{I_{hn}(s)} = C_N \emptyset B_N + D_N \tag{3-17}$$

Again, $\emptyset = (sI - A_N)^{-1}$, n = 1, 2…N, and I is a 3N×3N identity matrix.

With the obtained residential distribution system models, the performance of harmonic compensation using PV inverters will be investigated in the following sections.

3.4 Distribution System Harmonic Compensation Using DG

This section discusses the harmonic compensation effects using PV inverters. A simple two-node system is used for the initial investigation. The results are then extended for an 11-node distribution system and then a system with capacitors is considered.

Residential PV system locations are usually not controllable as they depends on which residence has the system installed. However, coordinated control of the PV inverters in a system is possible, and an optimal compensation strategy should be identified to obtain the best harmonic compensation result. The two strategies for harmonic compensation using the DG interfacing inverters are the end-of-distribution-feeder (or end-of-line) compensation [74], and distributed compensation [84, 85]. In a distribution system with multiple PV systems, the end-of-line compensation strategy can be implemented by assigning harmonic compensation priority to the PV inverters connected at the end of the feeder. On the other hand, the distributed compensation approach can be implemented by operating all PV inverters in the harmonic compensation mode with equal priority.

To study the effects of different compensation approaches, a two-node system is used as an example in this section. This system gives $N = 2$ in Figure 3.9. To simplify the analysis, it is assumed that both node 1 and 2 have identical loads ($Z_{L,1} = Z_{L,2}$, $i = I_{h1} = I_{h2}$), the same line parameters ($Z_{line,1} = Z_{line,2} = Z_Y$), and the same transformers ($Z_{Xf,1} = Z_{Xf,2} = Z_X$). Then the equivalent circuit for analysis can be obtained as with $N = 2$. In this case, we can take x_1, x_2, x_3, x_4 and x_5 as the state variables, i to be the input, and V_1 and V_2 to be the output of the state space model of the system. Using the distribution system modeling technique shown in Section 3.3, V_1/i and V_2/i are derived in (3-18) and (3-19), respectively:

$$\frac{V_1}{i} = \frac{Z_X(Z_1 + Z_2) + Z_1(2Z_2 + Z_Y)}{Z_X^2(Z_1 + Z_2 + 3Z_Y + Z_X) + Z_X(Z_1Z_2 + 2Z_1Z_Y + Z_2Z_Y + Z_Y^2)} \tag{3-18}$$

$$\frac{V_2}{i} = \frac{Z_Y\{3Z_1Z_2 + Z_X(Z_1 + 2Z_2) + Z_YZ_2\}}{Z_X\,(Z_1 + Z_2) + Z_X^2 + Z_Y^2 + Z_Y(Z_2 + 2Z_1) + 3Z_XZ_Y + Z_1Z_2} \tag{3-19}$$

where $Z_1 = Z_{VR1}||Z_L$, and $Z_2 = Z_{VR2}||Z_L$. Figure 3.10(a) and 3.10(b) show the Bode plot of (3-18) and (3-19), respectively. Figure 3.10(a) reveals that harmonic compensation at a single node (node 1 or node 2) will better damp the harmonic voltage at node 1 compared to distributed compensation for harmonics, $h < 25$. However, when $h > 25$, distributed compensation provides better damping at node 1. A similar observation is true for node 2 voltage as shown in Figure 3.10(b), which reveals that the distributed compensation method provides better harmonic damping in the high-frequency region. Therefore the decision about the optimal compensation strategy can be different depending on the dominant harmonics of the load. This finding provides an explanation for the literature's conflicting claims about the optimal compensation strategy [74, 84, 85], as different system and load characteristics are considered in different works.

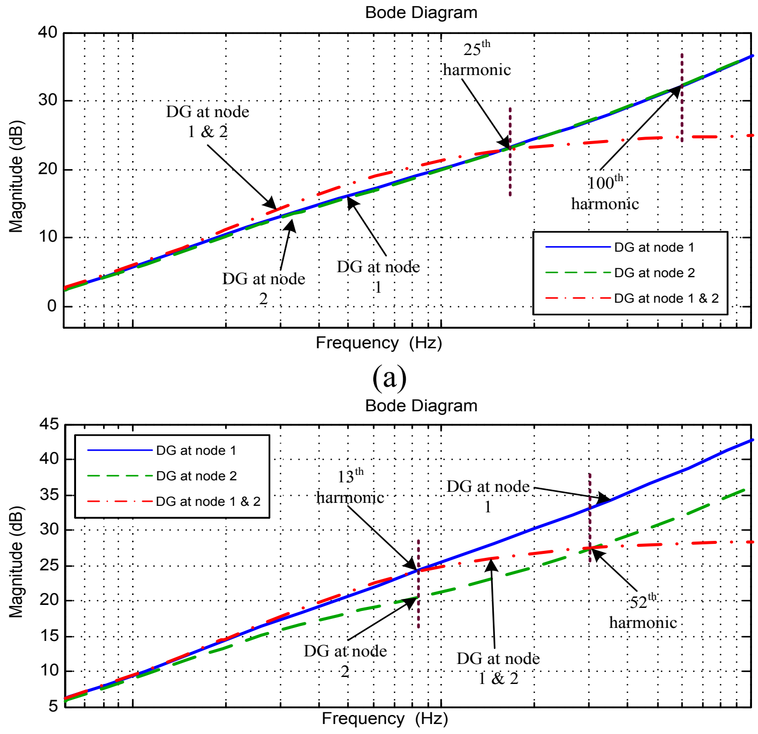

Figure 3.10. (a) Bode plot of V_1/i for compensation at different nodes and (b) Bode plot of V_2/i for compensation at different nodes.

This frequency-related performance of different compensation methods can be intuitively explained by the equivalent circuit shown in Figure 3.11.

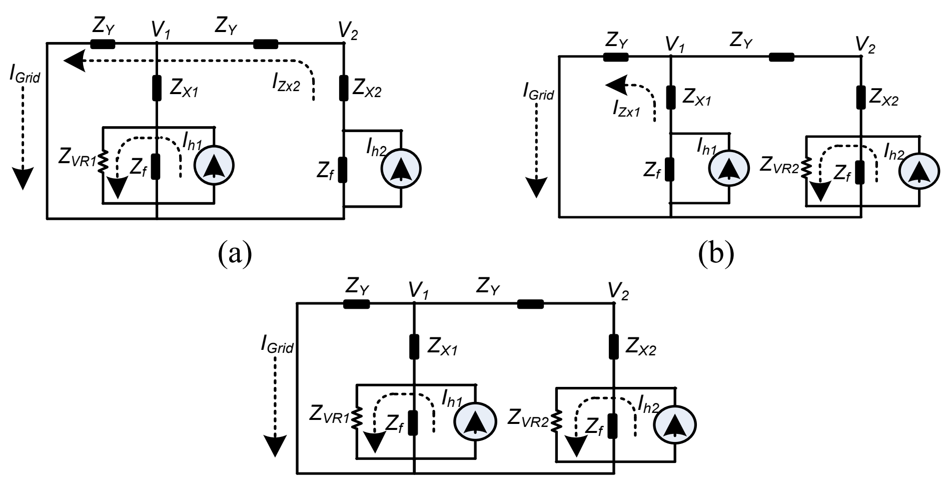

Figure 3.11. Equivalent circuit of (a) DG at node 1, (b) DG at node 2 and (c) DG at nodes 1 and 2

At high frequencies, the impedances Z_f, Z_X and Z_Y are much higher than the inverter virtual harmonic impedance Z_{VR1} and Z_{VR2}. As a result, if Z_{VR1} and Z_{VR2} are connected, most of the adjacent harmonic load current will flow through Z_{VR1} and Z_{VR2}. For example, in the case of DG at node 1 (Figure 3.11(a)), most of I_{h1} will be absorbed by Z_{VR1}, but I_{h2} will flow through nodes 1 and 2. This process will result in a higher V_{THD} at nodes 1 and 2. The situation will be similar when a single DG is at node 2 (Figure 3.11(b)). However, in the case of DG at both nodes 1 and 2 (Figure 3.11(c)), most of the harmonic content of I_{h1} and I_{h2} will be locally absorbed by Z_{VR1} and Z_{VR}, respectively. As a result, the voltages at nodes 1 and 2 will be less polluted. When the harmonic frequency increases, Z_X and Z_Y also increase but the virtual resistance Z_{VR1} and Z_{VR2} remains the same, providing the same level of damping to the load harmonics. This result also explains the constant damping at the high frequency range in the case of DG at nodes 1 and 2.

Another observation from Figure 3.10(a) and 3.10(b) is that, at high frequencies the gain of V_1 is almost identical for DG at node 1 or node 2, but V_2 has a lower gain in the case of DG at node 2 compared to the gain at node 1. The reason is that, regardless of the DG location (node 1 or 2), the harmonic current flowing to node 1 is almost identical in both cases (especially since the feeder impedance is lower than the transformer impedance with $Z_Y << Z_X$). However, in the case of DG at node 2, the harmonic current flowing through V_2 is much lower. In this case, most of I_{h2} is absorbed by Z_{VR2}, and most of I_{h1} flows through grid side impedance Z_Y.

For the compensation at a low-frequency range, the virtual damping resistances of DGs are comparable to Z_X. Therefore, more harmonic current will flow to the source through the feeders, causing relatively high harmonic voltages in the system.

The performance difference of distributed compensation and single DG compensation at low harmonic frequencies is also related to the system impedance. As discussed earlier, with $Z_Y << Z_X$, we can assume $Z_X \approx Z_Y + Z_X$. Therefore, in the case of distributed compensation, the impedances at I_{h1} and I_{h2} will be almost identical if the virtual impedances of all DGs are the same. However, in the case of a single DG at node 1 or node 2, the impedances at I_{h1} and I_{h2} will be different. Therefore, for distributed compensation, the current flowing to the source will be $|I_{Zx1}| + |I_{Zx2}|$, while it will be $|I_{Zx1} + I_{Zx2}|$ for single DG compensation. For single DG compensation at a high frequency, I_{Zx1} (or I_{Zx2}) is very small when compensation at node 1 (or node 2) is used due to the small damping resistance from the DG. As a result, $|I_{Grid}| \approx |I_{Zx1}| + |I_{Zx2}|$ even if I_{Zx1} and I_{Zx2} have different phases. However, at a low frequency, the damping resistance of the DG is comparable to

Z_X, and therefore, single DG compensation at node 1 or 2 will lead to $|I_{Grid}| < |I_{Zx1}| + |I_{Zx2}|$ due to the current phase angle difference. Therefore, even though the current I_{Zx1} or I_{Zx2} will be higher compared to the distributed compensation, the total current flowing to the source can be lower, leading to better performances with single DG compensation in the low-frequency region. This phenomenon can be seen in Table 3.3, where the magnitude and phase of the harmonic current flowing through Z_{x1} and Z_{x2} (I_{Zx1} and I_{Zx2}, respectively) are almost identical for both the 7th and 57th harmonics for distributed compensation. In contrast in the case of single DG at node 1 or 2, I_{Zx1} and I_{Zx2} are not same for the 7th and 57th harmonics. For the 7th harmonics, the total current flowing to the source is lower compared to the distributed compensation. Moreover, it is obvious that for single DG compensation, end-of-line compensation is the best option as it resulted in the lowest feeder harmonic voltage drops. Note that the virtual impedance for different compensation strategies is tuned to ensure an equal total RMS current requirement from the DG units involved. Also, the 57th harmonic current, which is a bit too high in practice, is used here only for explaining the situation at high frequency.

Table 3.3: Harmonic Current Flow for Different Compensation Strategies

Harmonic order [nth]	**DG at node**	I_{Grid} **[mag∠ang]**	I_{Zx1} **[mag∠ang]**	I_{Zx2} **[mag∠ang]**
7	1	13.4∠-26.2	5.1∠-57.3	9.5∠-10.0
7	2	13.4∠-26.1	9.5∠-9.9	5.0∠-57.7
7	1, 2	14.9∠-37.6	7.5∠-37.4	7.4∠-37.8
57	1	5.9-23.1	.79∠-88.5	5.6-15.8
57	2	5.9∠-22.9	5.6∠-15.7	.78∠-88.5
57	1, 2	3.4∠-72.8	1.7∠-72.8	1.7∠-72.9

The above analysis results were obtained from a simple 2-node distribution system. The analysis is extended to a more practical 11-node system in the following sections.

3.5 Harmonic Compensation in an 11-Node Distribution System

In this section, the performance with different harmonic compensation approaches under an 11-node residential distribution system is investigated. To provide a fair comparison of different harmonic compensation methods, the criterion that the total harmonic RMS current from all the DGs in the system is kept the same irrespective of the compensation scheme and distribution system configuration is adopted for this study. With this criterion, the virtual resistance $Z_{VR} = 1/.58\Omega$ is initially selected in the case of distributed compensation in an 11-node system. This resistance leads to a total 76.4A RMS DG harmonic current and about 2% of the total load RMS current. The equal equivalent rating for different compensation strategies and different systems is then calculated from this base DG RMS current. The Bode plot of V_h/i_h (obtained by using the system model developed in Section 3.3) with different compensation methods but the equal equivalent rating, is shown in Figure 3.12.

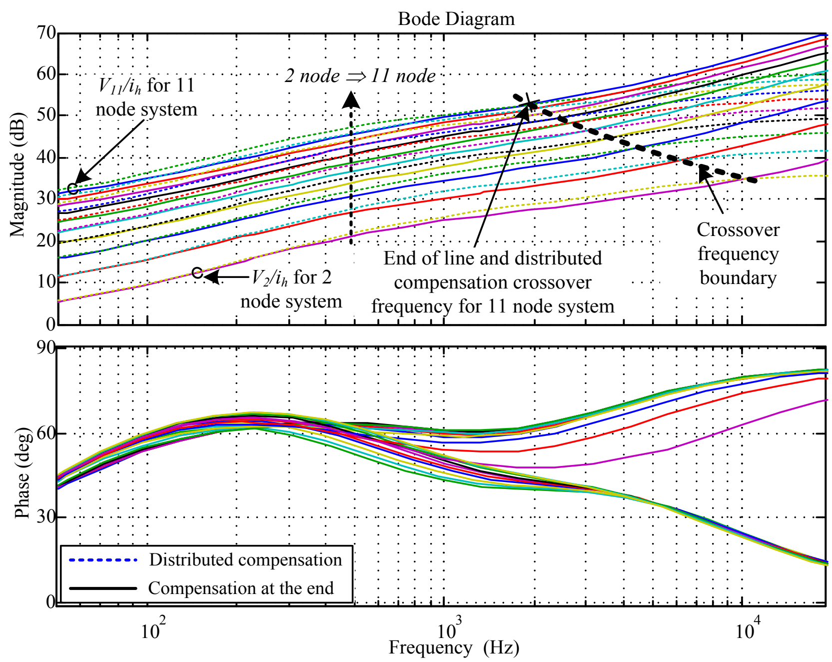

Figure 3.12. Bode plot of V_h/i_h at end node under different compensation strategies and distribution system configurations with equal equivalent DG rating.

As expected, Figure 3.12 reveals that the end-of-line and distributed compensation has a crossover frequency for a N-node distribution feeder. End-of-line compensation is better in the low-frequency region before the crossover frequency, and distributed compensation is better in the high-frequency region after the crossover frequency. As the feeder node (length) increases, this crossover frequency moves to the lower-frequency region.

Time domain simulations of an 11-node system were ~~is~~ also conducted by using Matlab/Simulink to verify the above analysis using the developed models. In the time domain simulations, the home model has harmonics up to the 13th, so the situation will involve the relatively low frequency range. The harmonic current and voltage content throughout the distribution line for different compensation strategies are shown in Figure 3.13(a) to (c), which show that the low-order harmonics are lower throughout the entire distribution line for end-of-line compensation. This finding is consistent with the previous analysis. As a result, V_{THD} throughout the distribution feeder is also lower in the case of end-of-line compensation as shown in Figure 3.13(d). The time domain waveforms with end-of-line compensation in an 11-node distribution system are shown in Figure 3.14.

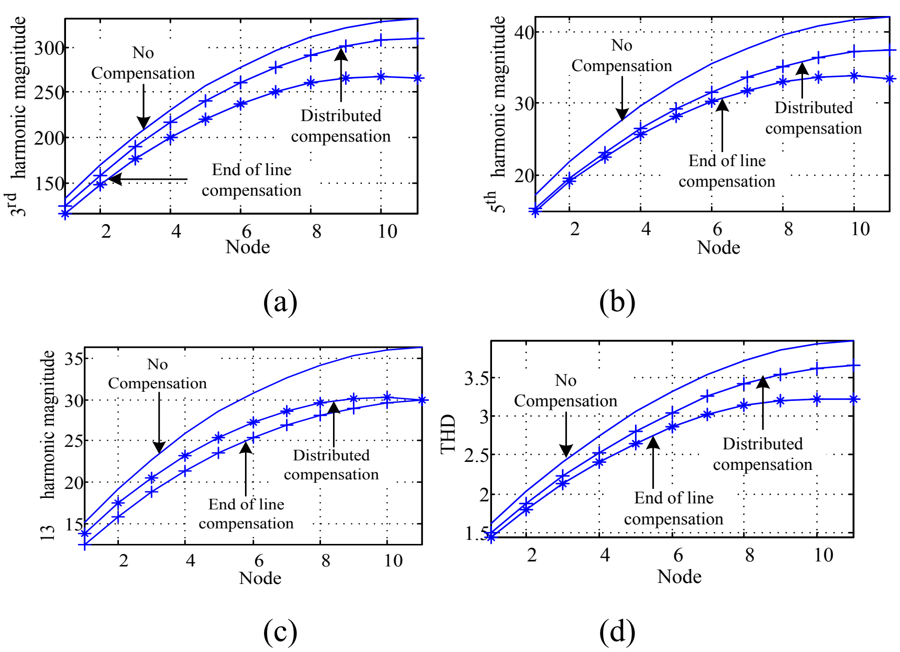

Figure 3.13. Voltage magnitude of (a) 3rd order harmonic content, (b) 5th order harmonic content, (c) 13th order harmonic content and (d) V_{THD} throughout the distribution feeder for different compensation strategies.

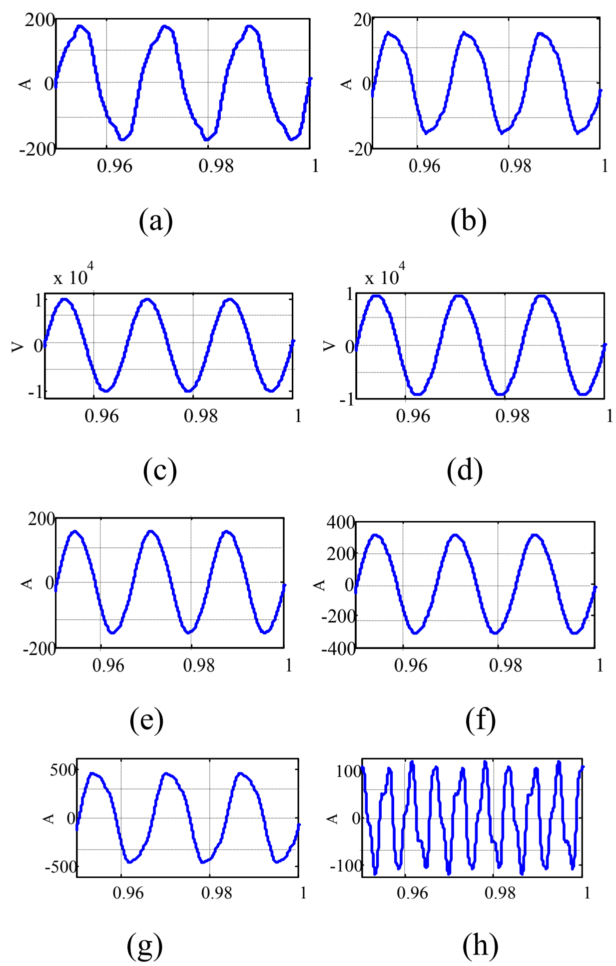

Figure 3.14. (a) Current through distribution line, (b) Current flowing from node 11 to primary side of distribution transformer 11, (c) Distribution voltage at node 1, (d) Voltage at node 11, (e) Hot wire 1 to neutral voltage of distribution transformer 11, (f) Hot wire 1 to hot wire 2 voltage of distribution transformer 11, (g) Current flowing through hot wire 1 of distribution transformer 11 and (h) DG harmonic current at 11th node.

The distribution system considered so far in this section does not have a PFC capacitor connected to it. The impact of harmonic resonance introduced by the PFC capacitor will be discussed in the next section.

3.6 Harmonic Compensation with the Presence of PFC Capacitors

Capacitors are often installed in distribution systems for voltage regulation and reactive power compensation. These capacitors may cause harmonic resonances and affect the harmonic compensation performance. This section extends the analysis in the previous sections to include the effects of PFC capacitors.

The voltage profile along the distribution line with a capacitor is influenced by the capacitor location and the capacitor's reactance value. Generally, a capacitor connected at the end of a distribution network~~s~~ provides the best performance for improving the voltage profile along the distribution line by improving the power transfer capability, voltage regulation, and power factor [100]. However, the most efficient capacitor placement also depends on the load, load power factor, line parameters of the distribution network, and reactance value [101].

To investigate the effects of capacitors on harmonic compensation, different capacitor positions are first analyzed by using the system model developed in Section 3.3. The corresponding Bode plot of V_h/i_h (using the system model developed in Section 3.3) is shown in Figure 3.15. The Bode plot of V_h/i_h in Figure 3.15 shows that the end-of-line compensation performs better before the crossover frequency and the distributed compensation performs better after the crossover frequency. However, as Figure 3.15 shows, the crossover frequency moves towards the low-frequency region as the capacitor is moved towards the end of the distribution line. When the capacitor is connected at node 11, the crossover frequency moves close to the 7^{th} harmonics. Therefore, the optimum harmonic compensation scheme has to be carefully chosen in situation.

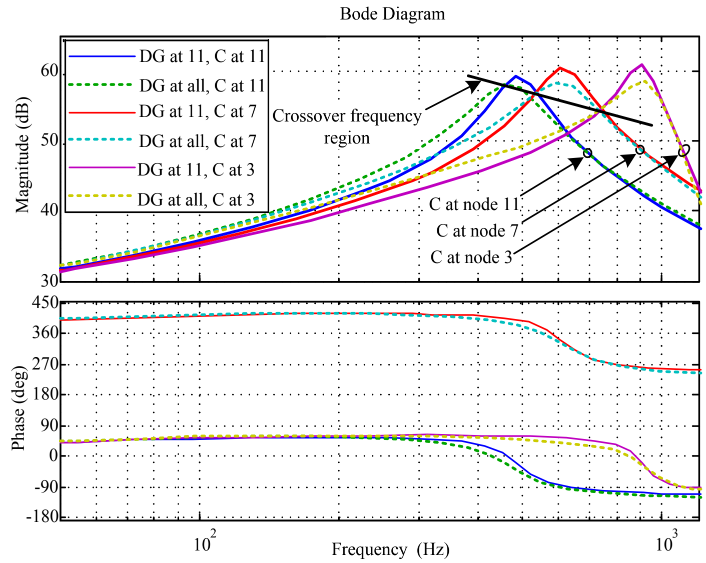

Figure 3.15. Analysis results with different compensation schemes under line capacitance at different nodes (Bode plot of V_h/i_h).

In addition, time domain simulations were also conducted and the results are summarized in Table 3.4. This table shows that the capacitor connected at the end node is more effective in reducing the percentage voltage drop but increases the V_{THD} across the distribution line [93]. For example, when no DG is connected, V_{THD} at node 11 increases from 4.54% to 6.86% when the PFC capacitor is moved from node 3 to 11, while the percentage voltage drop at node 11 decreases from 4.07% to 2.90% in this case. Table 3.4 also shows that V_{THD} along the distribution line is lower when end-of-line compensation (DG at node 11) is used, confirming the previous Bode plot analysis using the developed mathematical models.

Table 3.4. THD_v Along Distribution Feeder 2 Using Different Compensation Schemes and Line Capacitance Positions

***THDv* at [%]**				**I_{DG} [A]**	**DG on node [n^{th}]**	**Virtual impedance [Ω]**	**8μF C on node [n^{th}]**	**%V drop at node 11 [%]**
Node 1	**Node 4**	**Node 8**	**Node 11**					
1.61	2.75	3.71	3.98	0	--	0	--	4.95
2.03	3.66	5.57	6.86	0	No	0	11	2.90
1.80	**3.19**	**4.73**	**5.71**	**76.35**	**11**	**1/10.3**	**11**	**2.90**
1.81	3.22	4.84	5.90	75.67	All	1/0.48	11	2.90
2.11	3.81	5.80	5.94	0	No	0	7	3.46

1.93	**3.44**	**4.80**	**4.78**	**76.19**	**11**	**1/11.5**	**7**	**3.46**
1.90	3.40	4.81	4.95	76.92	All	1/.48	7	3.46
2.09	3.50	4.30	4.54	0	No	0	3	4.07
1.88	**3.09**	**3.66**	**3.70**	**76.21**	**11**	**1/13.2**	**3**	**4.06**
1.88	3.12	3.87	4.08	75.52	All	1/0.48	3	4.06

The effects of capacitor size on the harmonic compensation were also investigated. Different capacitors were connected at the 7th node of the distribution system. The Bode plot of V_h/i_h was then obtained by using the model developed in Section 3.3 and is shown in Figure 3.16, which reveals that as the capacitor size is increased, the crossover frequency for the DG distributed compensation and end-of-line compensation moves towards the lower-frequency region.

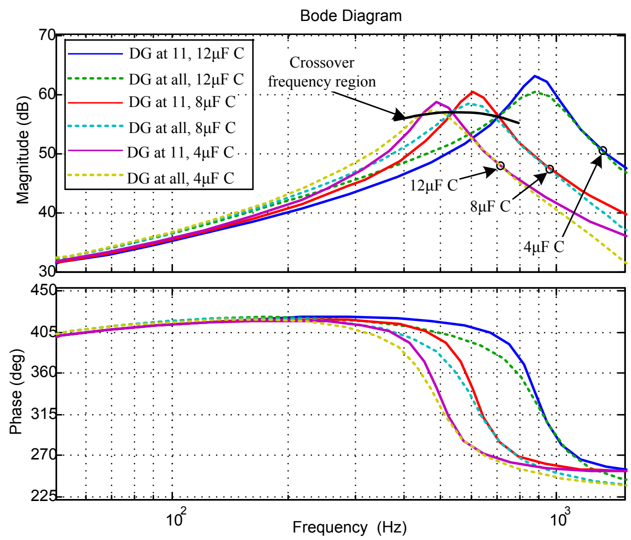

Figure 3.16. Analysis results with different compensation schemes under different line capacitances at node 7 (Bode plot of V_h/i_h).

The time domain simulation results for this case are listed in Table 3.5. As expected, the use of a bigger capacitor bank results in a reduced percentage voltage drop on the line, but V_{THD} is further increased. For example, when no DG is connected, V_{THD} at node 7 increases from 4.77% to 5.29% when the 7th node PFC capacitor value is increased from 4µF to 12µF, while the percentage voltage drop at the 11th node decreases from 4.20% to 2.77%. Table V also shows that the THD values along the distribution line are lower when end-of-line compensation (DG at node 11) is used with 4µF and 8µF PFC capacitors. However, since the crossover frequency moves to the low-frequency region when a 12µF PFC capacitor is used, the distributed compensation performs similarly to the end-of-line compensation. If the PFC capacitor value is further increased, distributed compensation will perform better.

Table 3.5. THD_v Along Distribution Feeder 2 Using Different Compensation Schemes and Line Capacitances at Node 7

***THDv* at [%]**				**I_{DG} [A]**	**DG on node [n^{th}]**	**Virtual impedance [Ω]**	**Line C at 7^{th} node [μF]**	**%V drop at node 11 [%]**
Node 1	**Node 4**	**Node 8**	**Node 11**					
1.61	2.75	3.71	3.98	0	--	0	--	4.95
2.28	4.20	6.07	6.16	0	No	0	12μF	2.77
2.07	**3.77**	**5.36**	**5.29**	**76.01**	**11**	**1/10.7**	**12μF**	**2.77**
2.02	**3.67**	**5.25**	**5.35**	**76.24**	**All**	**0/0.48**	**12μF**	**2.77**
2.15	3.89	5.54	5.69	0	No	0	8μF	3.46
1.93	**3.44**	**4.80**	**4.78**	**76.19**	**11**	**1/11.5**	**8μF**	**3.46**
1.90	3.40	4.81	4.95	76.92	All	1/.48	8μF	3.46
1.87	3.28	4.56	4.77	0	No	0	4μF	4.20
1.66	**2.87**	**3.87**	**3.90**	**76.35**	**11**	**1/13**	**4μF**	**4.20**
1.69	2.93	4.04	4.26	75.9	All	1/.48	4μF	4.20

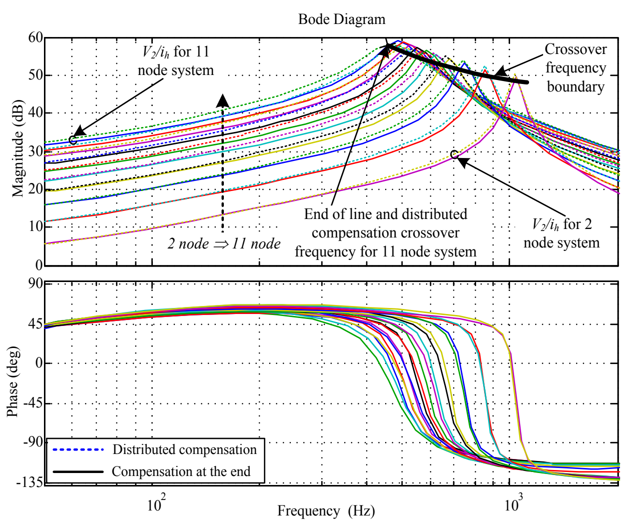

Figure 3.17. Bode plot of V_h/i_h at end node under different compensation strategies and distribution system configuration with capacitor bank connected.

To study the effects of the number of nodes (feeder lengths) on the harmonic compensation performance, different DG compensation strategies were implemented in a distribution system with capacitor banks connected to it (with an equal equivalent rating). The Bode plot of V_h/i_h (obtained from the developed models) in this scenario is shown in Figure 3.17, which reveals that the crossover frequency moves to the lower-frequency region as the node number in the distribution system is increased. Note that the crossover frequency can be as low as the 7th harmonic in the case of an 11-node system. Therefore, attention must be given to this situation during the harmonic compensation operation, and the appropriate compensation strategy must be chosen according to the load harmonic characteristics.

Time domain simulations with a PFC capacitor connected to node 11 were also conducted. Figure 3.18 shows the time domain simulation waveforms while Figure 3.19 shows the harmonics voltage magnitude and V_{THD} across the distribution line under different compensation strategies. In Figure 3.19(a) to 3.19(c), the harmonic content throughout the distribution line for different compensation strategies reveals that the low-order harmonics are lower throughout the entire distribution line for end-of-line compensation. In contrast, at high frequency, the harmonics are amplified with end-of-line compensation. This conclusion is similar to that derived from Figure 3.17. Although V_{THD} throughout the distribution feeder is lower in the case of end-of-line compensation as shown in Figure 3.19(d), a load model with higher high-frequency components could change the compensation result.

To investigate what happens if the load model changes and the high-frequency components of the load are increased, all the harmonic components of the home load model were removed except for the exaggerated 9th harmonic and fundamental components. The simulation was run again with different compensation strategies, and the results are listed in Table 3.6, which shows that the V_{THD} along the distribution line is increased by the end-of-line compensation but decreased by distributed compensation compared to the no-compensation condition. For example, when is no DG compensation is present, V_{THD} at node 8 is 5.27%. This percentage increases to 5.44% with end-of-line compensation, and decreases to 4.78% with distributed compensation. As the load in this case contains only a high-frequency component, distributed compensation performs far better than end-of-line compensation. This result is in line with the observation obtained from Figure 3.17.

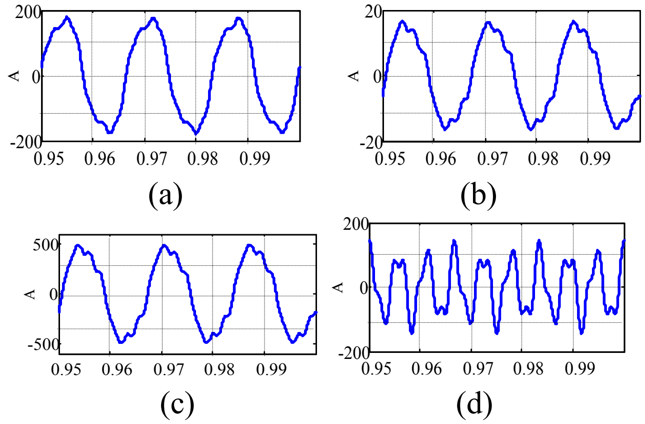

Figure 3.18. (a) Current through distribution line, (b) Current flowing from node 11 to primary side of distribution transformer 11, (c) Current flowing through hot wire 1 of distribution transformer 11 and (d) DG harmonic current at 11th node.

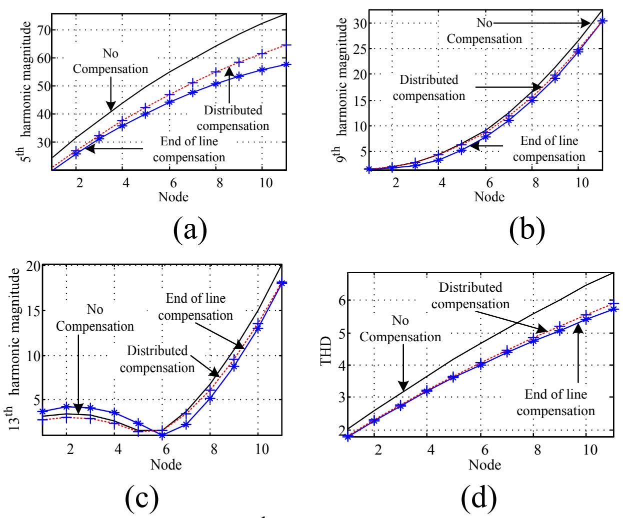

Figure 3.19. Voltage magnitude of (a) 5th order harmonic content, (b) 9th order harmonic content, (c) 13th order harmonic content and (d) V_{THD} throughout the distribution feeder for different compensation strategies.

Table 3.6. THD_v along distribution feeder 2 Using 9th Harmonic and Fundamental Load Only

***THDv* at [%]**				**I_{DG} [A]**	**DG on node [nth]**	**Virtual impedance [Ω]**
Node 1	**Node4**	**Node8**	**Node111**			
1.16	2.52	5.27	8.13	0	No	∞
1.38	2.82	5.44	8.07	55.2	11	1/5.70
1.14	**2.38**	**4.78**	**7.31**	**55.7**	**All**	**1/0.85**

To demonstrate the effect of line parameter variation on a distribution system with a PFC capacitor, the Bode plot of V_h/i_h in the no compensation condition with different line parameter combinations is shown in Figure 3.20, which shows that the effect of a line inductance change has a much greater effect on harmonic propagation along the distribution line, while a line resistance change has little or no effect. With an increase in the line inductance, the resonance frequency and compensation crossover frequency will be reduced. This result is consistent with the analysis of the number of nodes (the line-length effects).

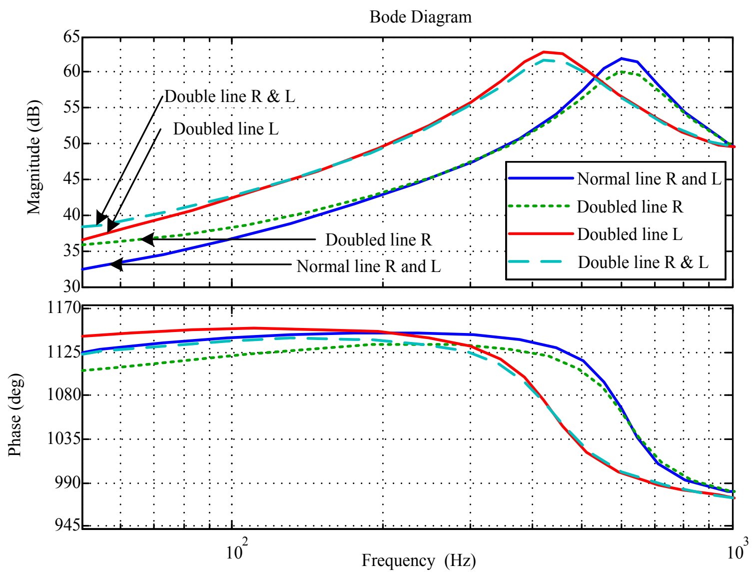

Figure 3.20. Analysis result with different line resistance and inductance combination with PFC capacitors.

Finally, the relationships between the compensation strategy crossover frequency and the different system parameters are summarized in Table 4.7.

Table 3.7. Analysis Summary

Condition	Observation
End-of-line compensation is better	At frequency lower than the crossover frequency
Distributed compensation is better	At frequency higher than the crossover frequency
Increase of PFC capacitor	Crossover frequency lowers
Increase of line impedance (Z_{line})	Crossover frequency lowers
Increase of nodes (line length)	Crossover frequency lowers

3.7 Conclusion

In this chapter, we explored the idea of using residential system DG-grid interfacing inverters as virtual harmonic resistances to damp the system harmonics and improve the power quality. An in-depth analysis and comparison of different harmonic compensation schemes were conducted to investigate the effects of the PV locations on harmonic compensation performance. This analysis then identifies the compensation method that should be used under different grid conditions which lays the groundwork for a priority based improved compensation scheme.

Specifically, the analysis and simulation results showed that the end-of-line compensation provided better damping for low-order harmonics, whereas distributed compensation provided better damping for high-order harmonics if the equal equivalent rating of the DG was maintained. In the system without PFC capacitors, this crossover frequency was quite high, and end-of-line compensation performed better. However, the presence of capacitor in the system could significantly reduce this crossover frequency to around the 7^{th} order harmonic, so the decision about which compensation strategy to use must be made according to the system load characteristics. Moreover, the effects of capacitor sizes, line impedance, and length on the crossover frequency were also analyzed in this work. With the information about a distribution system, the crossover frequency between the two compensation strategies can be determined by using the model developed in this work, and proper priority can be assigned to the PV inverters at different locations.

Chapter 4

Selective Harmonic Compensation for Improved Compensation Performance

4.1 Introduction

In the previous chapter, performance of different harmonic compensation methods namely, end-of-line [74] and distributed compensation [84, 85] are compared. It shows that, every system has a crossover frequency depending on the system configuration and parameters. End-of-line compensation is better at frequencies lower than the crossover frequency and distributed compensation is better at frequencies higher than the crossover frequencies. Although a guideline to assign harmonic compensation priorities on DGs operating at different locations of the distribution system has been identified in the previous chapter, the considered possibilities are only two, end-of-line or distributed compensation. Moreover, the distributed compensation scheme is implemented utilizing same virtual resistance for all DGs and at all frequencies. This is a simplified case of distributed compensation which assumes DG availability at each distribution system nodes and each DG having the same rating [84, 85]. In a practical system, DG(s) can be connected anywhere in the distribution system. With compensation priority defined (off line or online), DGs at different locations can be assigned with associate priorities for harmonic compensation. To achieve improved harmonic compensation result in such a practical scenario, finding an effective way to determine harmonic compensation priorities of each DG and at each harmonic is an

Publication out of this chapter:

M.S. Munir, Y.W. Li, H. Tian, "Improved residential distribution system harmonic compensation scheme using power electronics interfaced DGs", IEEE Trans. Smart Grid, vol. 7, no. 3, pp. 1191-1203, Mar. 2016.

important topic that has not been addressed sufficiently in the literature. Such improved compensation priority determination process becomes more complex in the presence of resonance introduced by PFC capacitors. In this chapter, a selective harmonic compensation scheme is developed to assign compensation priorities on DGs operating at different distribution system nodes and at different harmonic frequencies for improved compensation performance. This is implemented using system wide different virtual resistance for DGs operating at different nodes and at different harmonic frequencies which is not been reported in literature so far to the author's knowledge.

Currently the most widely used method to determine resonance in power network is the frequency scan method [102]. But the frequency scan method fails to address a number of concerns. For example, the frequency scan method cannot identify the bus or component which excites a particular resonance easily. This method also cannot determine whether the resonance observed at different buses are originated from the same bus or not. To overcome this problem, a method based on modal analysis was proposed in [103]. Using the method presented in [103], bus and component sensitivity to resonance excitation can be determined. Later on in [104], the proposed modal analysis was used to solve harmonic resonance problem of an offshore wind power plant using additional filters.

In this chapter, resonance analysis is first carried out in the distribution system model using modal analysis. Then the harmonic compensation priorities of DGs at different nodes are identified. A selective compensation scheme is used for assigning the calculated harmonic compensation priorities on DG(s) at different position and at different harmonics for improved compensation performance. One way to implement such distributed compensation scheme is to use different virtual harmonic resistances for DGs at different position and at different harmonic frequencies [105]. In this work, this type of distributed compensation scheme will be further improved and implemented.

4.2 Resonance Mode Analysis in a Residential Distribution System

Traditionally, frequency scan analysis is used in an electrical network to identify resonance phenomena and resonance frequency. To carry out frequency scan analysis, an electrical network of n node is represented by an $n \times n$ admittance matrix $[Y]$ at first. Then voltage vector of the system is calculated from the following equation:

$$[V]_f = [Z_N]_f [I]_f \tag{4-1}$$

$$\text{or, } \begin{bmatrix} V_1 \\ V_2 \\ \vdots \\ V_N \end{bmatrix}_f = \begin{bmatrix} Y_{11} & Y_{12} & \vdots & \cdots \\ Y_{21} & Y_{22} & \vdots & \cdots \\ \vdots & \vdots & \vdots & \vdots \\ Y_{N1} & Y_{n2} & \vdots & \cdots \end{bmatrix}_f \begin{bmatrix} I_1 \\ I_2 \\ \vdots \\ I_N \end{bmatrix}_f \tag{4-2}$$

Here, $[V]$, $[Z_N]$ and $[I]$ are nodal voltage vector, nodal impedance and nodal current vector respectively while subscript f denotes the frequency. For every frequency, the voltage vector can be calculated for 1 p.u. current injection. The voltage vector that has very high value at some frequency is associated with resonance. Thus resonance and resonance frequency can be identified using this method. But it cannot identify the component and bus that excites the resonance.

Using modal analysis, this problem can be solved. If we observe closely, input current vector is always set to 1 p.u. during the frequency scan analysis. So the high voltage vector values are associated with the singularity of the admittance matrix $[Y]$. This singularity of $[Y]$ matrix can be found when one of its eigenvalue is close to zero. Now the admittance matrix can be decomposed as,

$$[Z_n]_f = [L]_f [Z_M]_f [T]_f \tag{4-3}$$

where $[Z_M]$ is the diagonal eigenvalue matrix. $[L_f]$ is the left eigenvalue matrix and while $[T_f]$ is the right eigenvalue matrix. This Eigen analysis or modal transformation is basically a matrix decoupling method that transforms the nodal impedance matrix $[Z_N]$ into modal impedance matrix $[Z_M]$ as [103],

$$[Z_N]_f = \begin{bmatrix} Z_{11} & Z_{12} & \vdots & \cdots \\ Z_{21} & Z_{22} & \vdots & \cdots \\ \vdots & \vdots & \vdots & \cdots \\ Z_{N1} & Z_{n2} & Z_{n3} & Z_{nn} \end{bmatrix}_f \tag{4-4}$$

$$\text{while, } [Z_M]_f = \begin{bmatrix} Z_{m,11} & 0 & \vdots & \\ 0 & Z_{m,22} & \vdots & \\ \vdots & \vdots & \vdots & \\ 0 & 0 & 0 & Z_{m,nn} \end{bmatrix}_f \tag{4-5}$$

It can be seen that the modal analysis actually decouples the coupled nodal impedance matrix [Z_N] into decoupled modal impedance matrix [Z_M] in the modal domain. So, while nodal impedance matrix [Z_N] actually shows how the nodes of an electrical system are coupled to each other in nodal coordinate; modal impedance matrix [Z_M] shows the grid configuration in the modal domain. There is no change of the dimension between nodal [Z_N] and modal [Z_M] impedance matrix, hence the number of mode is same as the number of nodes in an electrical system. Modal impedance matrix is diagonally symmetrical:

$$\left[Z_M\right]_f = \left[Z_M\right]_f^T \tag{4-6}$$

And left and right eigenvalue matrices are related as:

$$\left[L\right]_f^{-1} = \left[T\right]_f \tag{4-7}$$

As modal impedance matrix [Z_M] is a diagonal eigenvalue matrix, left and right eigenvalue matrices are also effectively diagonal matrix:

$$\left[L\right]_f^{-1} = \left[T\right]_f = \left[T\right]_f^T \tag{4-8}$$

Substituting (4-8) into (4-1) we get:

$$\left[V\right]_f = \left[L\right]_f \left[Z_M\right]_f^{-1} \left[T\right]_f \left[I\right]_f \tag{4-9}$$

or,

$$\left[T\right]_f \left[V\right]_f = \left[Z_M\right]_f^{-1} \left[T\right]_f \left[I\right]_f \tag{4-10}$$

If modal voltage (v_M) and modal current (i_M) vectors are defined as:

$$\left[v_M\right]_f = \left[T\right]_f \left[V\right]_f \tag{4-11}$$

and,

$$\left[i_M\right]_f = \left[T\right]_f \left[I\right]_f \tag{4-12}$$

Equation (4-10) then reduces to (4-13). Modal analysis in this work will be carried out using equation (4-13)

$$\left[v_M\right]_f = \left[Z_M\right]_f^{-1} \left[i_M\right]_f \tag{4-13}$$

4.3 Distribution System with DG

In this chapter, virtual harmonic impedance based control scheme of DG presented in Section 4.2 will be used to compensate system harmonics. This is implemented by modifying harmonic currents at every frequencies using $I^*_h = V_{G\_h}/R_h$ and the reference harmonic current of the PV system is produced by combining all the individual harmonic references as,

$$I^*_h = I^*_3 + I^*_5 + \ldots.. + I^*_{15} \tag{4-14}$$

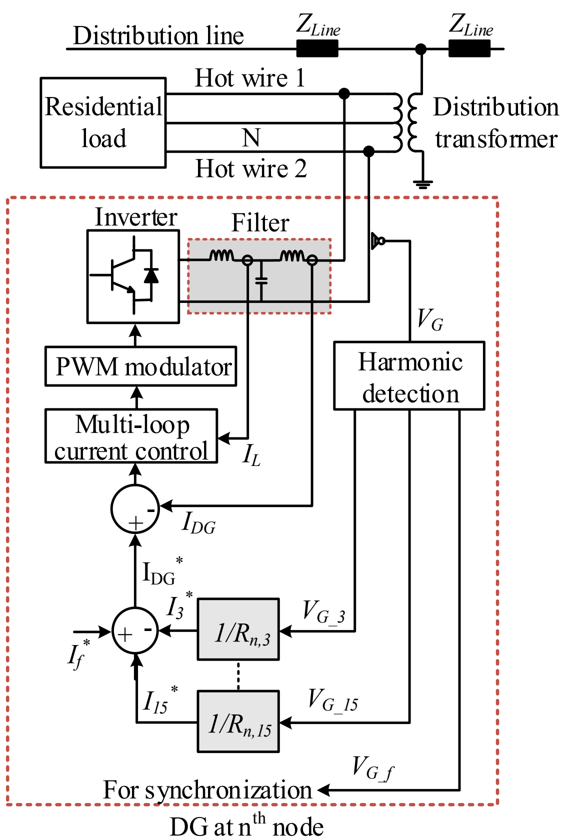

Figure 4.1. Harmonic damping with resistive active filter (R-APF) based DG

Block diagram of the control system of DG unit is shown in Figure 4.1. This DG control system is similar to the one shown in Figure 4.2 except here, every individual harmonic components of DG output current will be controlled to get improved harmonic compensation result. Virtual resistance will be used for controlling overall DG RMS current while compensation priorities will be used to regulate DG currents at different position and harmonic frequencies.

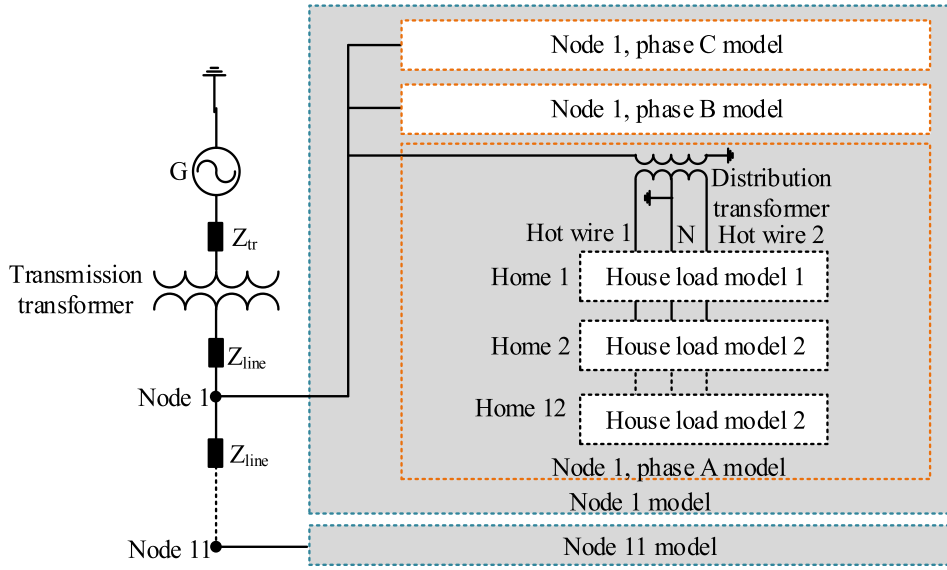

Figure 4.2. Distribution system model

The distribution system used in this work is shown in Figure 4.2. It has a *34.4*KV transmission line which is connected to the *12.47*KV distribution feeders through transmission transformer (Xf_{tr}) [25]. The 3 phase distribution feeder has 11 nodes. On each node, a group of 12 houses are connected to the distribution feeder through distribution transformer (Xf_{dis}) in a way that the load current is balanced (6 home model 1 and 6 home model 2) [34, 35].

To investigate the effectiveness of different harmonic compensation schemes, distribution bus with PFC capacitors is also modeled [2, 21, 22]. To simplify the investigation of the impact of nonlinear loads on distribution system power quality, analysis and simulation will be carried out on a single distribution feeder as shown in Figure 4.3. Here DGs are connected at the secondary side of the distribution transformer. In this model, n = 1, 2, 3……N represents the n^{th} node. Z_{Xn} represents the distribution line impedance, Z_{Yn} represents the distribution transformer impedance. The house load model is comprised of Z_{Ln} which represents the fundamental load impedance and I_{hn} which represents the harmonic current of the non-linear load at n^{th} node. Z_{C1}, Z_{C2}... Z_{Cn} are the impedances of the PFC capacitors respectively at the n^{th} node. Here the DG at nth node is represented by virtual impedance R_n. V_n is the voltage at the n^{th} node.

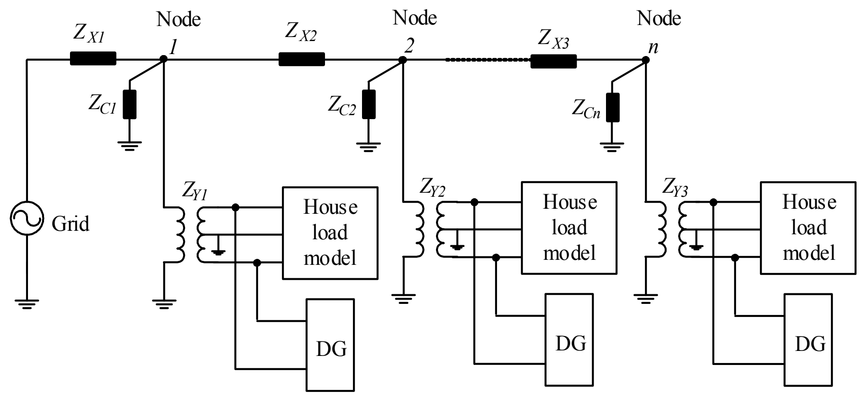

Figure 4.3. Typical distribution feeder with DG

Now the parallel branch connected at each distribution system node can be simplified into a parallel impedance and current source using Norton theorem as shown in Figure 4.4.

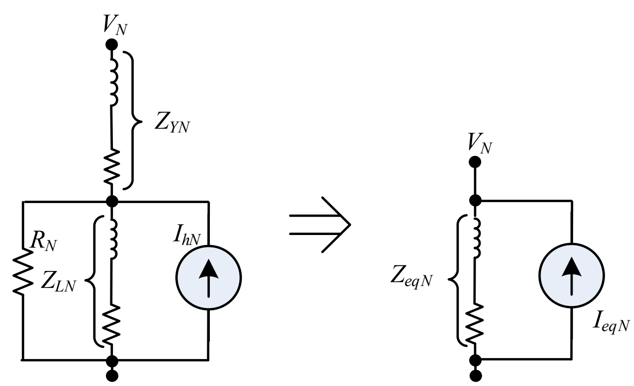

Figure 4.4. Equivalent parallel branch

So, the N node distribution system shown in Figure 4.3 can be simplified into the system shown in Figure 4.5.

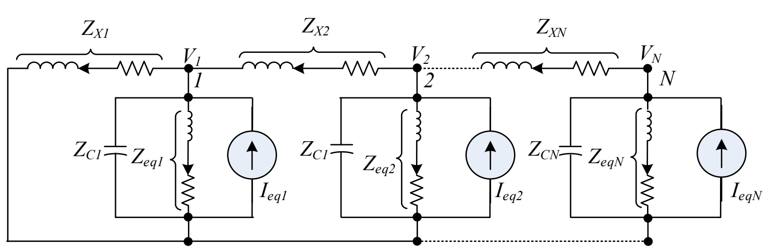

Figure 4.5. Equivalent distribution system model of an N node distribution feeder

From the equivalent distribution system model shown in Figure 4.5, admittance matrix is formed as shown in (4-15). Then modal analysis can be carried out using (5-15) to identify harmonic compensation priorities.

$$\begin{bmatrix} V_1 \\ V_2 \\ \vdots \\ \vdots \\ \vdots \\ V_N \end{bmatrix}_f = \begin{bmatrix} Y_{X1}+Y_{X2}+Y_{eq1}+Y_{C1} & -Y_{X2} & \cdots & 0 \\ -Y_{X2} & Y_{X2}+Y_{X3}+Y_{eq2}+Y_{C2} & \cdots & 0 \\ 0 & -Y_{X3} & \cdots & 0 \\ \cdots & \cdots & \cdots & \\ 0 & 0 & \cdots & Y_{eqN}+Y_{CN} \end{bmatrix}_f^{-1} \begin{bmatrix} I_1 \\ I_2 \\ \vdots \\ \vdots \\ \vdots \\ I_N \end{bmatrix}_f \tag{4-15}$$

4.4 Improved Harmonic Compensation with modal analysis

A comparison of different harmonic compensation methods was carried out in the previous chapter. It was done by keeping the total harmonic RMS current from all the DGs in the system same irrespective of the compensation scheme and distribution system configuration. With this criterion, the analysis of V_h/i_h with different compensation methods but with equal equivalent rating was carried out using an 11 node distribution system. The analysis result shows that:

1. The end-of-line and distributed compensation has a crossover frequency for an N-node distribution feeder. End-of-line compensation is better in the low-frequency region before the crossover frequency, and distributed compensation is better in the high-frequency region after the crossover frequency. As feeder node (length) increases, this crossover frequency moves to the lower-frequency region.
2. PFC capacitors are often installed in distribution systems and they may cause harmonic resonances and affect the harmonic compensation performance. For a distribution system with PFC capacitor, the crossover frequency moves towards the low-frequency region as the capacitor is moved towards the end of the distribution line. When the capacitor is connected at node 11, the crossover frequency moves close to the 7th harmonic frequency. Therefore, harmonic compensation scheme has to be chosen carefully in that situation.

Although the method presented in the previous chapter can identify the better compensation method between end-of-line and distributed compensation, the compensation priorities at each node and at each harmonic frequency cannot be identified. For example, if there are two DGs connected at node 7 and node 11, this method cannot identify which should have the higher compensation priority. To overcome this problem, compensation priorities at each node and at each frequency should be identified. Modal analysis is used in this work to identify the required compensation priorities at each node. Then a selective compensation scheme will be developed to improve the harmonic compensation performance using those priority values.

In this work, modal analysis was carried out at first using the same 11 node distribution model for 1^{st} to 40^{th} harmonic frequencies using (4-13) without PFC capacitor. Figure 4.6 shows the modal impedance for each mode.

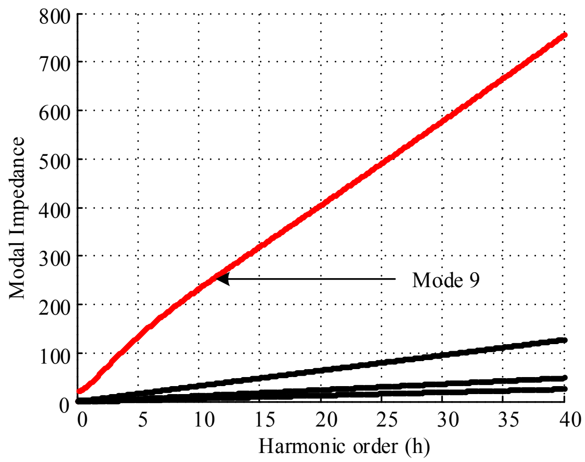

Figure 4.6. Modal impedance for different modes

It can be seen from the modal analysis equation shown in (4-16) that the lowest Eigen value will result in highest modal impedance. And high modal impedance at a particular frequency will result in high modal harmonic voltage for the same input modal harmonic current. In other words, modal impedance can be used to identify the mode that is more prone to harmonic distortion.

$$\underbrace{\begin{bmatrix} V_{m,1} \\ V_{m,2} \\ \vdots \\ V_{m,N} \end{bmatrix}}_{Modal\ Voltage} = \underbrace{\begin{bmatrix} Z^{-1}_{m,11} & 0 & \vdots & \\ 0 & Z^{-1}_{m,22} & \vdots & \\ \vdots & \vdots & \vdots & \\ 0 & 0 & 0 & Z^{-1}_{m,NN} \end{bmatrix}}_{Modal\ impedance} \underbrace{\begin{bmatrix} i_{m,1} \\ i_{m,2} \\ \vdots \\ i_{m,N} \end{bmatrix}}_{Modal\ Current} \tag{4-16}$$

Here, modal current matrix is the multiplication of Eigen vector matrix and physical input current matrix (4-17). Similarly, modal voltage matrix is the multiplication of Eigen vector matrix and physical output voltage matrix (4-18). From (4-17), it can be seen that depending on the Eigen vector values, same physical input current at different nodes will result in different modal input current. And depending on modal impedance value, same modal input current can result in different modal voltage.

$$\underbrace{\begin{bmatrix} i_{m,1} \\ i_{m,2} \\ \vdots \\ i_{m,N} \end{bmatrix}}_{Modal\ Current} = \underbrace{\begin{bmatrix} T_{11} & T_{12} & \vdots & \vdots \\ T_{21} & T_{22} & \vdots & \vdots \\ \vdots & \vdots & \vdots & \vdots \\ \vdots & \vdots & \vdots & \end{bmatrix}}_{Eigen\ Vector} \underbrace{\begin{bmatrix} \\ \\ \vdots \\ I_N \end{bmatrix}}_{Input\ Current} \tag{4-17}$$

$$\underbrace{\begin{bmatrix} v_{m,1} \\ v_{m,2} \\ \vdots \\ v_{m,N} \end{bmatrix}}_{Modal\ Voltage} = \underbrace{\begin{bmatrix} L_{11} & L_{12} & \vdots & \vdots \\ L_{21} & L_{22} & \vdots & \vdots \\ \vdots & \vdots & \vdots & \vdots \\ \vdots & \vdots & \vdots & \end{bmatrix}}_{Eigen\ Vector} \underbrace{\begin{bmatrix} V_1 \\ V_2 \\ \vdots \\ V_N \end{bmatrix}}_{Output\ Voltage} \tag{4-18}$$

The critical modal impedance (highest modal impedance) is much higher than other modal impedances. As a result, if $Z_{m,11}^{-1}$ is the critical modal impedance in (4-16), then we can assume,

$$\underbrace{\begin{bmatrix} Z_{m,11}^{-1} & 0 & \vdots & \\ 0 & Z_{m,22}^{-1} & \vdots & \\ \vdots & \vdots & \vdots & \\ 0 & 0 & 0 & Z_{m,NN}^{-1} \end{bmatrix}}_{Modal\ impedance} \approx \underbrace{\begin{bmatrix} Z_{m,11}^{-1} & 0 & \vdots & \\ 0 & 0 & \vdots & \\ \vdots & \vdots & \vdots & \\ 0 & 0 & 0 & 0 \end{bmatrix}}_{Modal\ impedance} \tag{4-19}$$

Combining (4-16) to (4-19) we get,

$$\begin{bmatrix} V_1 \\ V_2 \\ \vdots \\ V_N \end{bmatrix}_f = Z_{m,11,f}^{-1} \underbrace{\begin{bmatrix} L_{11}T_{11} & L_{12}T_{12} & \vdots & \vdots \\ L_{21}T_{11} & L_{22}T_{12} & \vdots & \vdots \\ \vdots & \vdots & \vdots & \vdots \\ \vdots & \vdots & \vdots & \end{bmatrix}}_{Particapation\ Factor} \begin{bmatrix} \\ \\ \vdots \\ I_N \end{bmatrix}_f \tag{4-20}$$

The Participation Factor (PF) matrix of (4-20) denotes the impact of each bus on the critical mode. Whereas $Z_{m,11,f}^{-1}$ denotes the impact level at different harmonic frequencies. Combining the modal impedance and PF index, we can determine participation of each bus to output harmonic voltage distortion. In this work, this approach will be used to quantify the harmonic compensation priorities at different harmonic frequencies and at different nodes of the distribution system. Then the compensation priority values will be used to implement the selective compensation scheme which will improve the harmonic compensation performance.

From the modal impedance shown in Figure 4.6, harmonic compensation priorities at each frequency of interest in an 11 node distribution system can be calculated from the mode 9 impedance. To do so, modal impedance at frequencies of interests and associated Eigen vector matrix are calculated. In this work, modal impedances at 3rd, 5th, 7th, 9th, 11th, 13th and 15th harmonic frequencies and participation factors of different input harmonic currents at different nodes are calculated.

Although these compensation priority values will ensure improved compensation performance of DGs with selective harmonic compensation, one practical aspect has to be incorporated here. Modal impedance has different percentage values at different harmonics. But in practical residential distribution system, magnitudes of low order harmonics, e.g., 3rd, 5th, 7th etc. are usually much higher. So, the compensation priority values should be modified according to the load harmonic current data for improved compensation result.

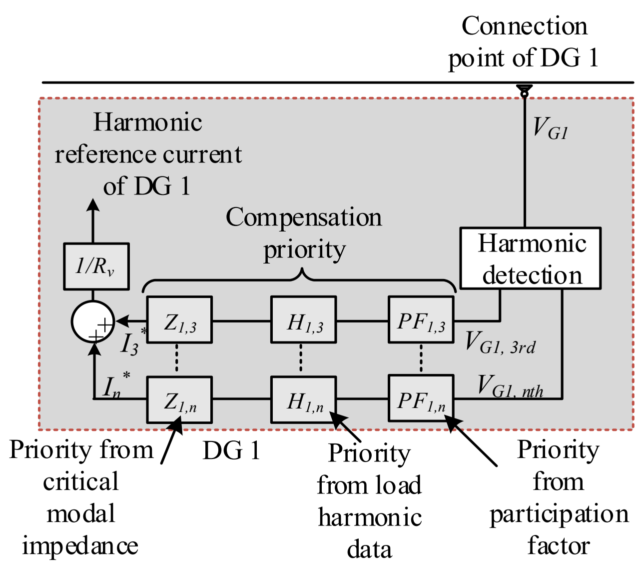

Figure 4.7. Selective compensation scheme with virtual harmonic resistances

To implement the selective harmonic compensation scheme, the distributed compensation structure with different virtual resistance is modified as shown in Figure 4.7. In Figure 4.7, priority from participation factor at each node ($PF_{n,h}$) can be assigned according to the participation factor from Eigen analysis. Then priority from modal impedance ($Z_{n,h}$) and harmonic load data ($H_{n,h}$) can be assigned separately. And virtual resistance (R_V) can be used to control total DG(s) rating. The compensation priority (CP) at different distribution system node and harmonics can be expressed as,

$$CP_{n,h} = \frac{PF_{n,h} \cdot H_{n,h} \cdot Z_{n,h}}{\max\left(\bigcup_{n,h}^{n=1,2..N,h=3,5..15} H_{n,h} \cdot Z_{n,h}\right)} \tag{4-21}$$

here, $n = 1, 2.....N$ represents n^{th} node and $h = 3, 5 .... 15$ represents h^{th} harmonics.

4.5 Harmonic Compensation Performance

Using the previously described model based method, the DG compensation priority values are calculated from the modal analysis participation factor, modal impedance and load harmonic current data. The participation factor modifies compensation priorities according to the DG position at each harmonic frequency. Priority from modal impedance modifies compensation priority according to the impact of each input harmonic current on output voltage distortion. In this section, modal analysis will be used at first to compare the observations found from the previous chapter and then the effectiveness of the developed criterion will be investigated.

4.5.1 Observations with Modal Analysis

To compare the observations obtained using modal analysis with the ones obtained in the previous chapter, modal impedances are calculated at first using the same distribution system model and PFC capacitor value but with different capacitor placements. This is shown in Figure 4.8. As shown, the resonance frequency is lower as the PFC capacitor is moved towards the end of the distribution line. This conclusion is similar to the one obtained in the previous chapter.

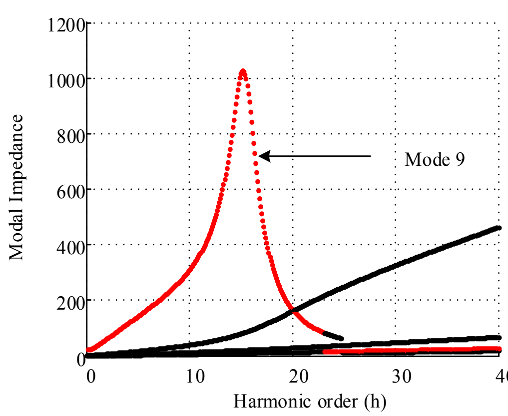

(a)

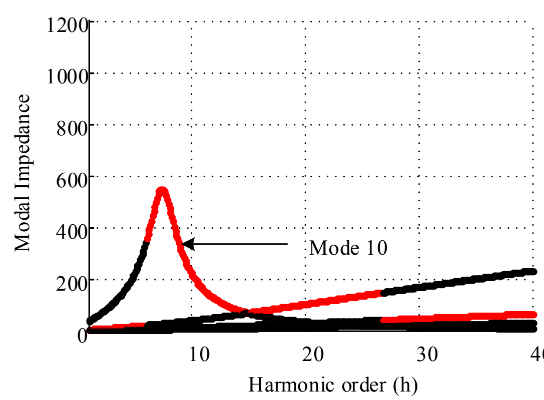

(b)

Figure 4.8. Modal impedance with 8uF capacitor at (a) node 3 and (b) node 11

Modal analysis is used to identify the harmonic compensation priorities at each node for different capacitor position. As an example, normalized values of 7th harmonic participation factor for different capacitor positions are shown in Table 4.1. As seen from Table I, participation factor at node 11 is same for capacitor at node 3 or 11. But the participation factor is higher at node 10 when the capacitor is connected at node 3 than when connected at node 11. So the 7th harmonic compensation priority increases at the end nodes as the PFC capacitor is moved towards the end of the distribution line. In other words, end of line compensation performs better as the PFC capacitor is moved towards the end of the distribution line, which is consistent with the conclusion obtained in the previous chapter.

Similarly, using modal analysis it can be shown that the resonance frequency is lowered when the PFC capacitor value is increased and end of line compensation performs better as the PFC capacitor value is decreased while distributed compensation performs better as the PFC capacitor value is increased, which is consistent with the conclusions obtained in the previous chapter.

Table 4.1: Calculated compensation priority at 7th harmonics with an 8uF capacitor connected at different nodes

Harmonic order		**7th**	**7th**	**7th**
Capacitor	**Value [uF]**	8	8	8
	Position [node]	3	7	11
Participation factor at node	**1**	16.25	14.03	9.42
	2	32.24	27.95	18.82
	3	47.71	41.63	28.18
	4	58.43	54.97	37.5
	5	68.23	67.86	46.75
	6	76.94	80.18	55.92
	7	84.42	91.85	64.99
	8	90.55	95.08	73.95
	9	95.24	97.53	82.78
	10	98.4	99.17	91.47
	11	**100.00**	**100.00**	**100.00**

4.5.2 Selective Harmonic Compensation with Single Resonance

In this section, a distribution system with single resonance is used to investigate the harmonic compensation performance of the developed selective harmonic compensation scheme. To identify the improved compensation scheme in the developed distribution system model, modal impedances for different modes with an 8uF capacitor connected at node 5 are calculated and shown in Figure 4.9. From Figure 4.9, we can see that the capacitor at node 5 introduces a resonance at mode 9.

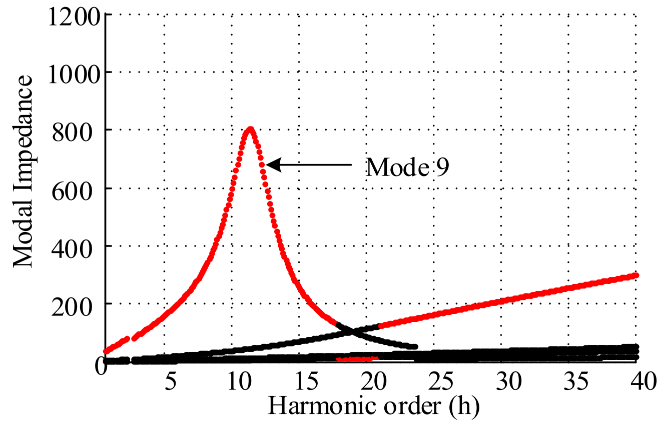

Figure 4.9. Modal impedance for different modes with an 8uF capacitor at node 5 (single resonance)

Now from the Eigen vectors, participation factor of each input harmonic current at each node can be obtained and are shown in Table 4.2, where the modal impedances and input harmonic current for different harmonics are also shown.

Table 4.2. Participation factor, load harmonics and modal impedance data for calculating compensation priority with an 8uF capacitor at node 5

		Harmonic order						
		3rd	**5th**	**7th**	**9th**	**11th**	**13th**	**15th**
Modal Impedance		92.36	160.01	255.04	433.71	784.00	506.15	256.60
Input Current		6.19	0.55	1.67	0.84	0.33	0.32	0.27
Participation Factor at node	**1**	2.10	3.83	6.11	10.23	20.74	16.20	9.83
	2	4.17	7.59	12.15	20.39	41.50	32.61	19.95
	3	6.16	11.25	18.04	30.42	62.28	49.40	30.64
	4	8.05	14.72	23.72	40.22	83.21	66.79	42.21
	5	9.79	17.97	29.10	49.75	104.00	85.00	55.00
	6	11.21	20.17	31.70	52.06	103.51	79.74	48.27
	7	12.44	22.06	33.92	54.02	103.12	75.45	42.94
	8	13.44	23.61	35.73	55.60	102.80	72.10	38.85
	9	14.22	24.80	37.11	56.79	102.58	69.62	35.89
	10	14.74	25.60	38.03	57.60	102.42	67.97	33.96

	11	15.00	26.00	38.50	58.00	102.35	67.16	33.01

Now the harmonic compensation priority can be assigned on a DG connected to different distribution system node according to Table 4.2. According to the parameters listed in Table 4.2, several observations can be made:

1. For low order harmonics, e.g., 3rd order harmonics, compensation at the end will provide better result.
2. For high order harmonics, e.g., 15th order harmonics, compensation at the resonance point will provide better performance.
3. For the 11th order harmonic, compensation at node 5, 6, 7, 8, 9, 10 and 11 will provide better result (since participation factor values are very close for all those 7 nodes).
4. For the same input harmonic current, output voltage distortion will be highest at the 11th harmonic frequency and lowest at 3rd order harmonics. As a result, highest compensation priority should be assigned on 11th order harmonics (from modal impedance values).
5. Load harmonic current has highest magnitude at 3rd harmonic frequency and lowest at 15th harmonics. For improved compensation, the compensation priorities should be modified according to the harmonic load current profile.

To verify these observations, simulation was carried out at first with exaggerated 7th harmonic load and the resultant 7th harmonic voltage throughout the distribution line was recorded. According to Table 4.2, 7th harmonic compensation at node 11 will provide better result than compensation at node 5. To verify this, simulation was run separately with DG connected at node 5 and node 11 with the same RMS DG current. The resultant 7th harmonic voltages throughout the distribution line are shown in Table 4.3. It can be seen that compensation results are better even with the same RMS DG current when DG is connected at node 11. This result verifies the observation about low order harmonics of Table 4.2.

Similarly, simulations with exaggerated 13th harmonic are conducted and the results in Table 4.3 show that 13th harmonic compensation at node 5 will provide better result than compensation at node 11. This result verifies the observation about high order harmonics of Table 4.2.

Table 4.3. 7th and 13th harmonic voltage with different compensation strategies

DG	At node	0		5		11	
	I_{RMS} (A)	0		15		15	
Harmonic order		**7th**	**13th**	**7th**	**13th**	**7th**	**13th**
Harmonic voltage at node	1	249.27	231.62	238.58	**220.61**	**237.64**	220.83
	2	320.50	309.17	306.59	**294.85**	**305.36**	295.15
	3	388.27	395.26	371.15	**377.61**	**369.61**	378.01
	4	452.83	490.44	432.50	**469.43**	**430.63**	469.93
	5	514.42	595.32	490.87	**570.87**	**488.65**	571.5
	6	530.27	538.96	506.93	**514.97**	**503.03**	518.62
	7	543.39	492.6	520.24	**468.98**	**514.64**	475.68
	8	553.83	455.92	530.83	**432.59**	**523.53**	442.41
	9	561.63	428.66	538.75	**405.54**	**529.72**	418.55
	10	566.82	410.61	544.01	**387.63**	**533.26**	403.93
	11	569.40	401.62	546.64	**378.71**	**534.15**	398.4

Finally, simulation was carried out with the same distribution system model with the real residential load. At first, DG was connected at node 11 with same priority at each harmonic frequency (end of line compensation). Then DG was connected to every node of the distribution system with same priority at each harmonic frequency (distributed compensation). Another simulation was carried out where the total DG RMS current is same as end-of-line or distributed compensation. In this case, selective compensation scheme was used. The compensation priorities were assigned according to participation factor, load harmonic data and modal impedance values. Simulation with compensation priority values listed in Table 4.2 results in V_{THD} values shown in Figure 4.10. It can be seen from Figure 4.10 that for the same DG RMS current, V_{THD} values are lower when selective harmonic compensation is used.

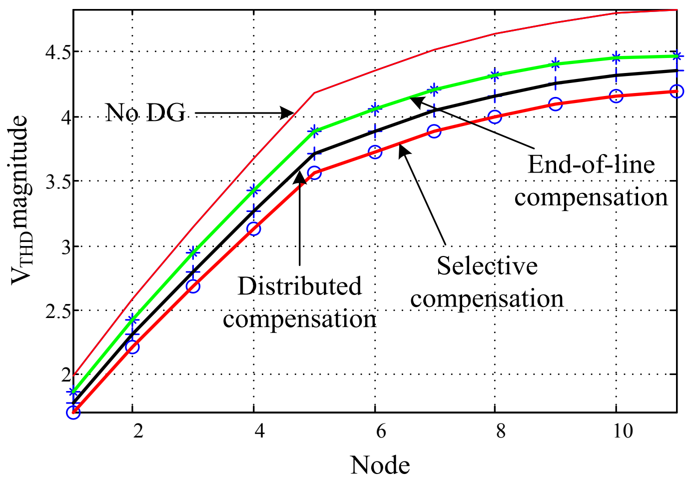

Figure 4.10. Compensation result with different compensation strategies, same DG ratings and an 8uF capacitor at node 5

4.5.3 Selective Harmonic Compensation with Multiple Resonances

To test the effectiveness of the proposed criterion in a system with multiple resonances, modal analysis was carried out with 16uF capacitors connected at node 3 and node 7 (multiple resonance situation). Modal impedances for different modes from that analysis are shown in Figure 4.11. It can be seen that the capacitors at node 3 and node 7 introduce resonances at mode 9 and mode 10.

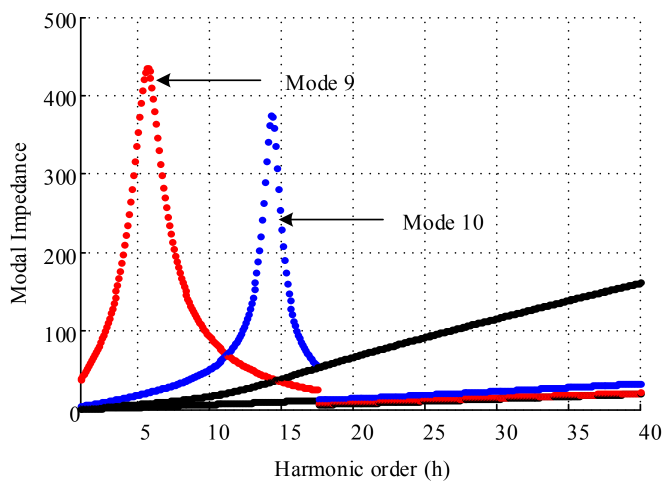

Figure 4.11. Modal impedances for different modes with 16uF capacitors at node 3 and node 7

Now from the Eigen theory, participation factor and modal impedance at different node at different harmonic frequencies can be calculated which is shown in Table 4.4 along with load harmonic data.

Table 4.4. Participation factor, load harmonics and modal impedance data for calculating compensation priority with 16uF capacitors at node 3 and node 7

		Harmonic order						
		3rd	**5th**	**7th**	**9th**	**11th**	**13th**	**15th**
Modal Impedance		116	354	257	121	73	143	229
Input Current		6.19	0.55	1.67	0.84	0.33	0.32	0.27
Participation Factor at node	**1**	0.41	1.42	1.21	0.67	0.44	5.24	8.79
	2	1.61	5.65	4.93	2.79	1.92	20.09	36.44
	3	3.55	12.66	11.38	6.74	4.96	42.10	86.93
	4	5.83	19.59	16.14	8.55	5.52	20.10	33.50
	5	8.49	27.92	22.31	11.43	7.19	5.27	6.05
	6	11.40	37.56	30.31	15.92	10.57	0.02	0.62
	7	14.38	48.41	40.62	22.84	16.88	5.23	16.40
	8	16.11	49.39	36.14	17.07	10.32	8.02	12.81
	9	17.50	50.14	33.01	13.47	6.77	10.69	10.53
	10	18.46	50.65	31.04	11.38	4.94	12.77	9.18
	11	18.96	50.90	30.08	10.43	4.17	13.91	8.56

Priority values for selection harmonic compensation scheme can then be obtained from Table 4.4 according to (4-21). To investigate the harmonic compensation performance with selective compensation, simulations were carried out with the same distribution system model with residential load. At first, DG was connected at node 11 with same priority at each harmonic frequency (end of line compensation). Then DG was connected to every node of the distribution system with same priority at each harmonic frequency (distributed compensation). Then selective harmonic compensation was carried out where the total DG RMS current is same as the distributed compensation. All resultant V_{THD} values are shown in Figure 4.12. From Figure 4.12, it can be seen that for the same DG RMS current, V_{THD} values are lower when selective harmonic compensation is used. These results verify the effectiveness of the proposed selective harmonic compensation strategy.

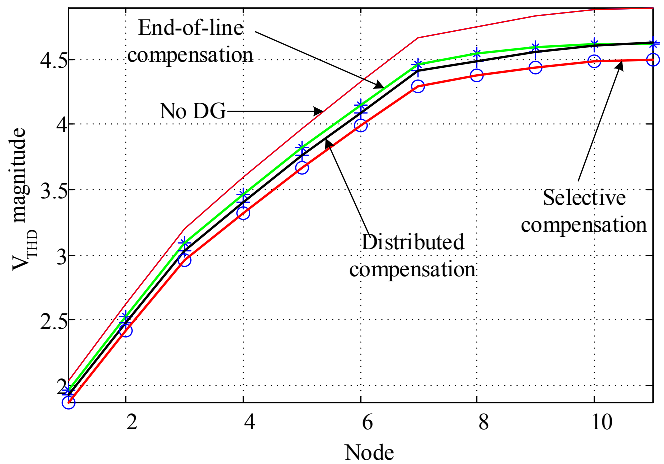

Figure 4.12. Selective harmonic compensation with multiple resonances

4.6 Discussion

The work presented in this thesis is a model based approach and the performance of the method presented here is dependent on system configuration and parameters. The performance of the presented method is most sensitive to the capacity or placement and value in the system as changing capacitor placement or value significantly change the resonance in the system. In real life situation, various distribution network components such as distribution transformer, distribution line impedance, PFC capacitor, transmission transformer etc. are usually fixed. If a new component is installed or existing configuration is changed, that can easily be accounted for in the model. On the other hand, loads are variable in a practical distribution network. To account for this, constant load monitoring system can be installed, assumed load data can be used or historic load data can be used. Just to show the performance of the proposed method with assumed load data, simulation was run again with same load but compensation priority values were calculated assuming 3rd, 5th , 7th and 9th harmonic load currents to be 5 times higher than of 11th, 13th and 15th harmonic currents. Figure 4.16 shows the selective compensation result in such case. As seen from the Figure 4.13, the compensation performance deteriorated compared to the result with actual load data but still the results are better than distributed compensation. If historic load data was used here, the compensation performance would have even closer to the results with actual load data.

It should also be noted that a single phase radial distribution system model is used in this work for sake of simplicity, but the presented method can be applied to any distribution system model.

For example, modal analysis as carried out in a three phase system in [31] and in interconnected system model in [32, 33]. Moreover, to coordinate different DG units under changing available DG rating, multi layered control can be used. In [38], hierarchical decentralized control technique is discussed. An important next step on this could be the multi-layered control where a supervisory layer control can be utilized to adjust selective compensation priorities on-line.

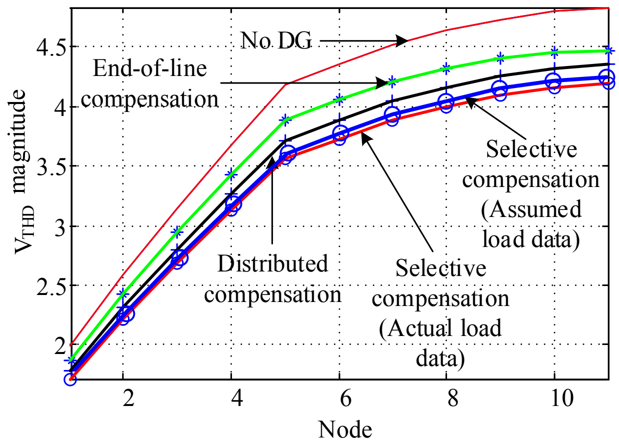

Figure 4.13. Selective harmonic compensation with inaccurate load data

Virtual impedance based DG controllers are used in this work which use connection point voltage THD to generate compensating current and reduces voltage distortion. Although compensating non-linear load current locally would have resulted distortion free voltage, it is not practically feasible in a residential distribution system to compensate all local non-linear load current and make grid current sinusoidal. This is because, the controller of the DG unit needs the load current information to compensate the harmonic current locally. But DG units are usually installed in a house surrounded by a group of house in a residential area, all producing non-liner load currents. In such practical scenario, it is very difficult for the DG controller to know the total non-linear load current information. Figure 4.14 shows a typical residential distribution system scenario where DG is connected to house 1 of house group 1. The controller of that DG have no load current information of house 2 – house n of house group 1 and any house of house group 2.

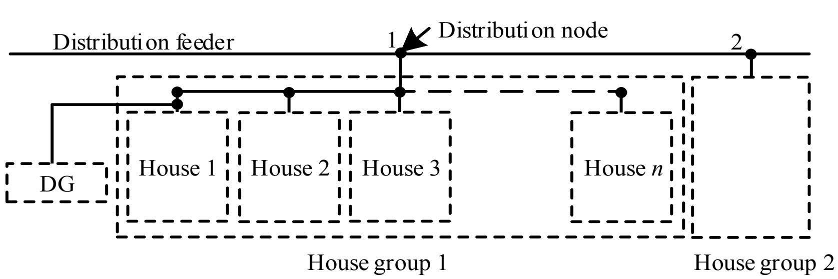

Figure 4.14. Typical residential distribution system configuration with DG

Different available capacity of DGs at different nodes will affect the actual harmonics compensation participation from each DG. However, the DG compensation priorities identified in the proposed method (which does not depend on available DG rating) is still important for the operation of DGs. According to the proposed method, a DG with higher priority should participate more in harmonic compensation compared to a DG with low priority. This is because, DG with higher compensation priority will be able to reduce V_{THD} more compared to a DG with less priority using the same DG capacity. So, it is very important to ensure that the DG with higher priority utilizes more capacity of that particular DG for harmonic compensation. A further consideration of the work is to simultaneously include the compensation priority determined in this chapter and the available DG rating for harmonic compensation to achieve further improved and coordinated compensation.

4.7 Conclusion

In this chapter, a selective harmonic compensation scheme using DG-grid interfacing inverters is developed that improves the harmonic compensation performance on a residential distribution system. Here, compensation priorities for different DG position and harmonic frequency are identified for improved compensation performance compared to traditional distributed compensation. Assigning such compensation priorities on different DG interfacing inverters in the distribution system improves compensation performance. An in-depth analysis, comparison and simulation of the developed selective compensation scheme with different existing harmonic compensation schemes were conducted to identify the performance improvement. To achieve the main objective of this work of improving the harmonic compensation performance in a residential distribution system, a model based approach is adopted where selective harmonic compensation priorities are generated according to the system parameters and load current data. This calculated priority values are used to achieve better compensation. The next chapter will focus on a droop based wireless control system of the DGs that consider both the compensation priority and available aggregated DG rating for harmonic compensation without the need of communication among DG units.

Chapter 5

Priority Driven Droop Controller for Distributed Harmonic Compensation

5.1 Introduction

It was mentioned in the previous chapters, power electronics interfaced DGs provide an excellent solution to the harmonic problem in the residential distribution grid. For implementation of distributed compensation and considering the available aggregated converter rating for harmonic compensation, conductance-power (G-S) based droop controllers have been used to control several active power filters that are installed in different locations [25]. This system is called distributed active-filter system (DAFS) where individual APFs compensates harmonics without any communication among themselves. This communication-less control scheme is implemented by a droop relationship between the harmonic conductance and VA consumption of each individual APF. The droop slope of different AFP is designed according to the VA rating of individual APFs which ensures even sharing of harmonic compensation workload. But this traditional G-S based droop controller has some drawbacks. Due to the approximation and simplification used in the DAFS controller design, significant power sharing error may be introduced among different converters. Moreover, additional power sharing error may be introduced depending on the connection point voltage distortion (due to feeder impedance). Finally, although the droop controller controls the virtual harmonic impedance of the individual converter, the same harmonic impedance is used for all harmonics. But depending on the network

---

Publication out of this chapter:

M.S. Munir, Y.W. Li, "Residential Distribution System Harmonic Compensation using Priority Driven Droop Controller", Submitted, IEEE Trans. Smart Grid, Dec 2017.

configuration, prioritizing the compensation of some specific harmonics at certain location will provide better compensation result. To overcome all these drawbacks associated with traditional G-S droop based controller, a novel priority driven droop controller to implemented the selective harmonic compensation strategy for DG interfacing inverters is proposed in this chapter.

The proposed control method can eliminate power sharing error introduced by the traditional G-S droop method. Also the power sharing error introduced by the feeder impedance are eliminated in the proposed controller. With the harmonic compensation priorities determined by modal analysis, the compensation priority and available aggregated DG rating for harmonic compensation can be combined together in the proposed harmonics droop control. As a result, a system level control and implementation strategy can be developed, where all DGs of a distribution system is controlled without communication among them.

5.2 Traditional Conductance- Power (*G-S*) Based Droop Controller

The traditional conductance-power (*G-S*) based droop algorithm is shown in Figure 5.1 [106-108]. Here, harmonic conductance command is obtained from the output apparent power of DG (S_n), rated capacity (S_{n0}), droop offset (G_{n0}) and G-S droop equation shown in (5-1) and Figure 5.2. The harmonic voltage content at the DG connection point (V_{G_h}) is modified according to the harmonic conductance command (G_n) to generate the harmonic reference current for DG.

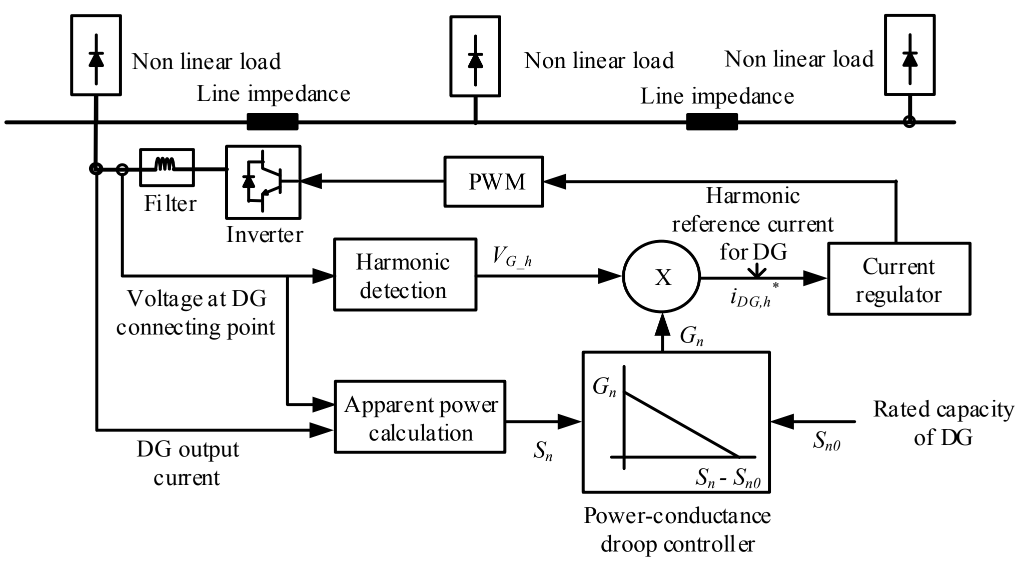

Figure 5.1. Block diagram of G-S droop control

$$G_n = G_{n0} + b_n(S_n - S_{n0}) \tag{5-1}$$

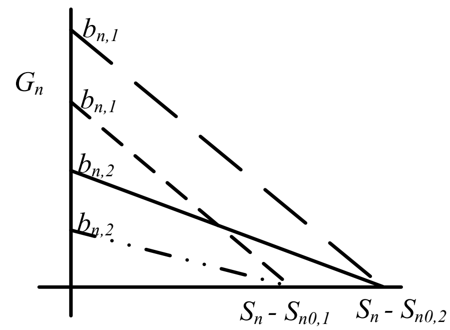

Figure 5.2. Conductance vs power relationship using G-S droop control

Since the main component of the RMS voltage at the point of connection is the fundamental voltage, the output apparent power of DG (S_n) can be expressed as,

$$S_n = |V_n| G_n |V_{n,h}| \approx |V_{n,f}| G_n |V_{n,h}| \tag{5-2}$$

Combining (5-1) and (5-2) we get,

$$S_n = |V_{n,f}| \{G_{n0} + b_n (S_n - S_{n0})\} |V_{n,h}|$$

$$\text{Or, } S_n = \frac{|V_{n,f}|\left(G_{n0} - b_n S_{n0}\right)|V_{n,h}|}{1 - b_n |V_{n,f}||V_{n,h}|} \tag{5-3}$$

In a number of previous works [25, 29, 30], (5-3) is simplified assuming $\left(b_n|V_{n,f}||V_{n,h}|\right) \gg 1$ as,

$$S_n b_n = b_n S_{n0} - G_{n0} \tag{5-4}$$

If there are an *n* number of DGs and their droop characteristics are assigned as,

$$b_1 S_{10} - G_{10} = b_2 S_{20} - G_{20} = \ldots = b_n S_{n0} - G_{n0} \tag{5-5}$$

Then combining (5-4) and (5-5) we get,

$$S_1 b_1 = S_2 b_2 = \ldots = S_n b_n \tag{5-6}$$

So, the output apparent power of the DGs are inversely proportional to the slope of the droop controller according to (5-6). While the slope of the droop controller is also inversely proportional to the apparent power rating of the respective DGs according to (5-5). Combining (5-5) and (5-6), it can be seen that such droop slope allocation will allow proportional sharing of the harmonic filtering workload among different DG units according to the respective DG rating as shown in (5-7).

$$\frac{S_1}{S_{10}} = \frac{S_2}{S_{20}} = \ldots = \frac{S_n}{S_{n0}} \tag{5-7}$$

5.3 Proposed Conductance- Power (*G-S*) Based Droop Controller

In case of the traditional droop controller, (5-6) is derived assuming $\left(b_n|V_{n,f}||V_{n,h}|\right) \gg 1$. But depending on the value of the droop slope (b_n), this assumption may not hold valid. Because of power sharing accuracy and stability concerns, droop slope (b_n) can be very small resulting $\left(b_n|V_{n,f}||V_{n,h}|\right) \approx 1$ which will introduce considerable error in output power sharing among different DG units.

To demonstrate this, Figure 5.3 shows the output power ratio (S_1/S_2) of 2 DGs with S_{10} = 1000VA and S_{20} = 500VA respectively. Here the range of b_2 is double of b_1 since $S_{10} = 2S_{20}$. Now, if b_1 = .005 then according to the traditional droop controller, b_2 =.01. It can be seen from Figure 5.3 that the power sharing accuracy with the traditional droop controller is very poor especially when the droop slope is lower.

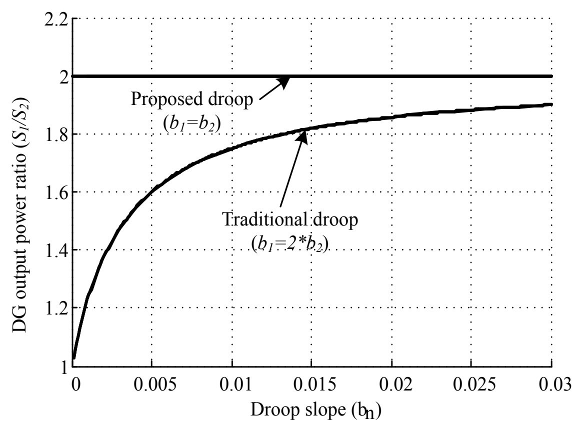

Figure 5.3. Power sharing of DGs with traditional and proposed power-conductance droop controller with G_{n0} = 0.

To overcome this power sharing problem, the DG output power S_n needs to be proportional to the DG rating S_{n0}. Such power sharing problem can be eliminated considering two situations: i) when conductance offset is zero and, ii) when conductance offset is non zero.

5.3.1 With conductance offset 0 (Gn0=0)

If conductance offset is considered 0 (G_{n0} = 0) in (5-3), then (5-3) can be rewritten as,

$$S_n = \frac{-b_n S_{n0}\left|V_{n,f}\right|\left|V_{n,h}\right|}{1-b_n\left|V_{n,f}\right|\left|V_{n,h}\right|} \tag{5-8}$$

If the connection point fundamental and harmonic voltages are constant and droop slope of all DGs are same for all DGs (b_n = const.) then,

$$S_n = const \cdot S_{n0} \tag{5-9}$$

According to (5-9), DG output power will be proportional to DG rating. To demonstrate this, Figure 5.3 shows the output power ratio (S_1/S_2) of 2 DGs with S_{10} = 1000VA and S_{20} = 500VA respectively. According to the proposed droop controller, when droop slope for different DGs are kept same then the DG outputs should be proportional to the respective DG ratings. It can be seen from Figure 5.3 that the power sharing is always accurate and independent of the value of b_n.

5.3.2 With nonzero conductance offset (Gn0≠0)

According to the traditional droop controller, the conductance offset should be constant across n number of DGs to make the droop characteristics relationship shown in (5-5) valid when ($G_{n0} \neq 0$). But when the droop offset is constant across n number of DGs, the output power of all DGs will be same irrespective of their rating and this will introduce power sharing error. If conductance offset is nonzero ($G_{n0} \neq 0$) while the connection point fundamental and harmonic voltages are constant and droop slopes of all DGs are same for all DGs (b_n = const.) in (5-3), then (5-3) can be rewritten as,

$$S_n = \frac{\left|V_{n,f}\right|\left(G_{n0} - b_n S_{n0}\right)\left|V_{n,h}\right|}{1 - b_n\left|V_{n,f}\right|\left|V_{n,h}\right|} \tag{5-10}$$

To make the DG output power S_n proportional to the DG rating S_{n0}, G_{n0} has to be proportional to DG rating S_{n0} as,

$$G_{n0} = K_G S_{n0} \tag{5-11}$$

where K_G is the conductance offset constant and has the same value for all DGs. Then (5-11) becomes,

$$S_n = S_{n0} \cdot \left(K_G - b_n\right)$$

$$S_n \propto S_{n0} \tag{5-12}$$

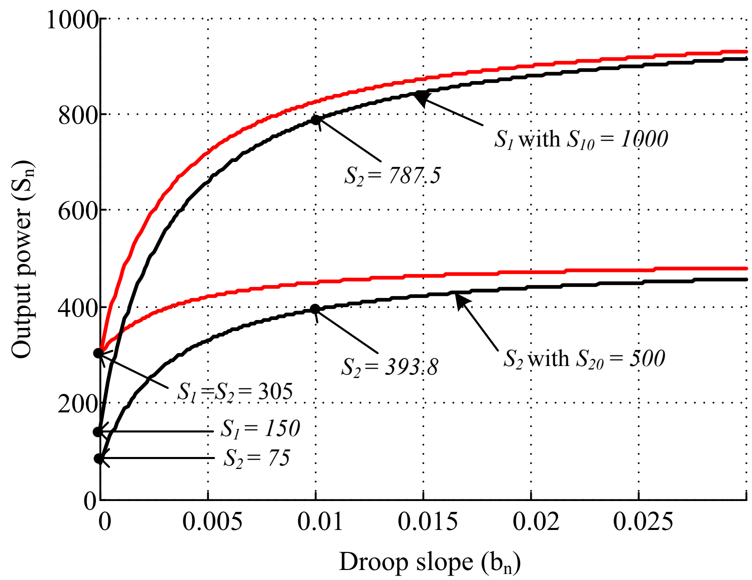

Figure 5.4. Power sharing error with traditional droop controller when $G_{n0} \neq 0$ (red plots) and elimination of power sharing error with proposed power-conductance based droop controller with $G_{n0} \neq 0$ (black plots).

Again, according to (5-12), DG output power will be proportional to DG rating when (K_G+b_n) is a constant. To demonstrate this, Figure 5.4 shows the output power (S_n) of 2 DGs with S_{10} = 1000VA and S_{20} = 500VA respectively. It can be seen from Figure 5.4 that when droop slope is zero then both DGs will have the same output power irrespective of DG ratings when traditional droop controller is used. This will introduce significant power sharing error. According to the proposed droop controller, when droop slope and conductance offset constant for different DGs are kept same then the DG output should be proportional to the DG rating. It can be seen from Figure 5.4 that S_1 = 787.5VA and S_2 = 393.8VA when droop slopes, b_1=b_2=.01 and the power sharing is accurate.

5.3.3 Verification of the power sharing accuracy of the proposed droop controller

To show how the proposed droop controller will ensure proper power sharing, two DGs are considered to be operating at the same connection point where, $S_{10} = nS_{20}$. So, DG power outputs should be $S_1 = nS_2$ and the conductance relationship should be $G_1 = nG_2$. According to modified droop controller, droop slope should be same for both DGs, b_c in this case. So the modified droop equation becomes (5-13) where b_c stands for common droop slope for all DGs and the ratings of different DGs are related as,

$$G_1 = b_c\left(S_1 - S_{10}\right) = b_c\left(nS_2 - nS_{20}\right) = nG_2 \tag{5-13}$$

It can be seen from (5-13) that the desired conductance relationship can be achieved with the modified droop controller. In case of the traditional droop controller, both DGs should have different slopes and slope relationship should have been $nb_1 = b_2$. Then droop equation would be,

$$G_1 = b_1\left(S_1 - S_{10}\right) = \left(b_2 / n\right)\left(nS_2 - nS_{20}\right) = G_2$$

This conductance relationship will introduce power sharing error in the system. To verify this, simulation was run using the circuit configuration shown in Figure 5.5 and parameters listed in Table 5.1. Here a single residential house load model was used as each load.

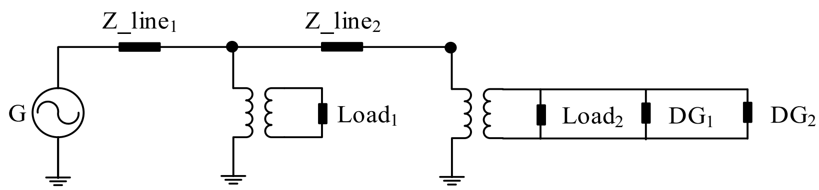

Figure 5.5. Test circuit for comparison of power sharing accuracy of the traditional and modified droop controller when DGs are connected to the same node.

Table 5.1: Circuit parameters

Circuit Parameters	**Value**
Generator	34.5KV
Distribution transformer	7200V/120V, 0.015+0.03j p.u
Distribution line impedance	.43Ω/km, 150µH/km

In the simulation, $S_{10} = 100$ and $S_{20} = 400$. If we assign $b_1 = 0.08V^{-2}$ then $b_2 = 0.02V^{-2}$ (case 1). Simulation was first run with these droop parameters (case 1). Then simulation was run again where $b_1 = 0.008V^{-2}$ and $b_2 = 0.002V^{-2}$ (case 2) then $b_1 = 0.0008V^{-2}$ then $b_2 = 0.0002V^{-2}$ (case 3) while S_{10} and S_{20} remains same as before. Finally, simulation was run again with fixed droop slope for both DGs where $b_1 = 0.008V^{-2}$ and $b_2 = 0.008V^{-2}$ (case 4) $b_1 = 0.002V^{-2}$ and $b_2 = 0.002V^{-2}$ (case 5) while S_{10} and S_{20} remains same as before. The results are listed in Table 5.2. As shown in Table 5.2, the power sharing is accurate. As the droop slope is lowered, sharing error becomes greater. On the other hand, power sharing remains very accurate with the modified droop controller even with very low droop slope (case 5).

Table 5.2: Comparison of power sharing accuracy among different DGs with traditional and proposed conductance-power based droop controller

Scenario	S_{10}	S_{20}	S_{20}/S_{10}	b_1	b_2	S_1	S_2	S_2/S_1
(case 1)	100	400	4.00	0.08	0.02	98.1	380.0	3.87
(case 2)	100	400	4.00	0.008	0.002	89.2	269.0	3.01
(case 3)	100	400	4.00	0.0008	0.0002	45.6	69.5	1.51
(case 4)	100	400	4.00	0.008	0.008	89.2	356.5	4.00
(case 5)	100	400	4.00	.0002	.0002	17.3	69.5	4.00

5.4 Mitigation of Power Sharing Error Introduced by Feeder Impedance

It should be noted here that the proposed droop controller is implemented using (5-14) where the apparent power at different nodes (S_n) are calculated using (5-3). Now, the fundamental component of line voltage is almost same at different DG connection point throughout the distribution system. But the node harmonic voltage at different nodes ($V_{n,h}$) can vary due to the feeder impedance of the distribution system. As a result, sharing error may be introduced even when the proposed droop controller is used. This sharing error wasn't apparent in Table 5.2 because both DGs were connected at the same node and both experienced same $V_{n,h}$. To see how node harmonic voltage affects the power sharing accuracy, simulation was run again with DGs connected at different nodes as shown in Figure 5.6 while the results are listed in Figure 5.7.

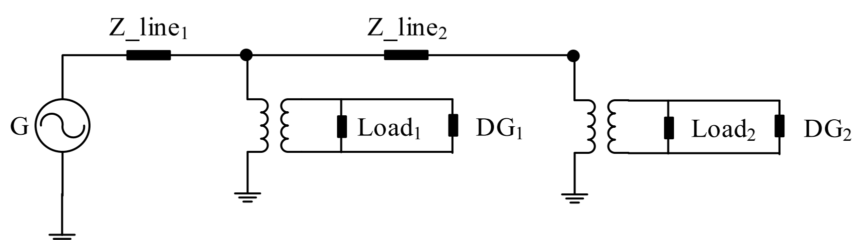

Figure 5.6. Test circuit for verification of power sharing accuracy of modified droop controller when DGs are connected at different nodes.

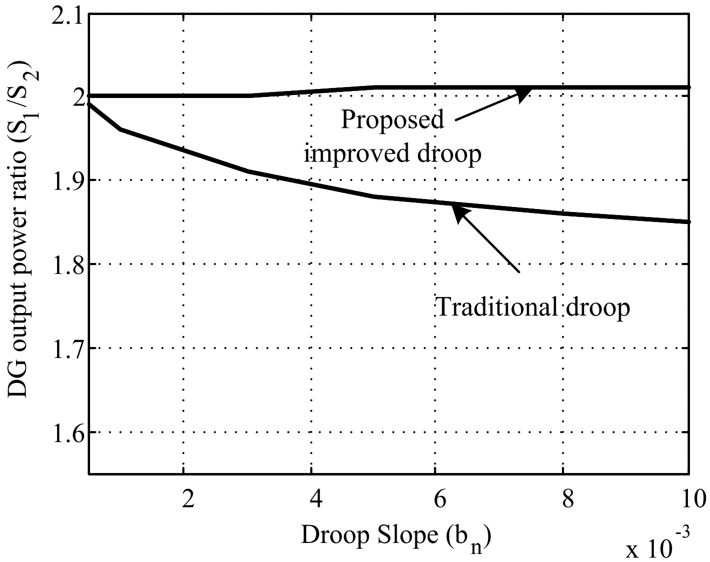

Figure 5.7. Power sharing error introduced by feeder impedance and mitigation of that error using proposed improved droop controller.

It can be seen from Figure 5.7 that the sharing error increases as the droop slope value is increased. This can be explained using (5-3). It can be seen from (5-3) that higher droop slope will try to increase DG output power S_n. Increasing DG output power S_n will result in lower harmonic voltage ($V_{n,h}$) at connecting node with larger percentage of harmonics variations at different nodes. As a result, power sharing error increase as droop slope value is increased. Moreover, the DG systems are usually connected in the secondary side of the distribution transformer. Since the transformer impedance is much higher compared to distribution line impedance, the voltage distortion difference can be significant at the connection point of different DGs which makes sharing error worse. In this power sharing error can be removed by implementing an additional control block that will automatically adjust the droop slope in a small range according to the node harmonic voltage ($V_{n,h}$) variation using (5-14).

$$\bigcup_{h=3,5\ldots}^{h_{\max}} \quad h \quad \frac{V_{n0,h,rms}}{V_{n,h,rms}} \tag{5-14}$$

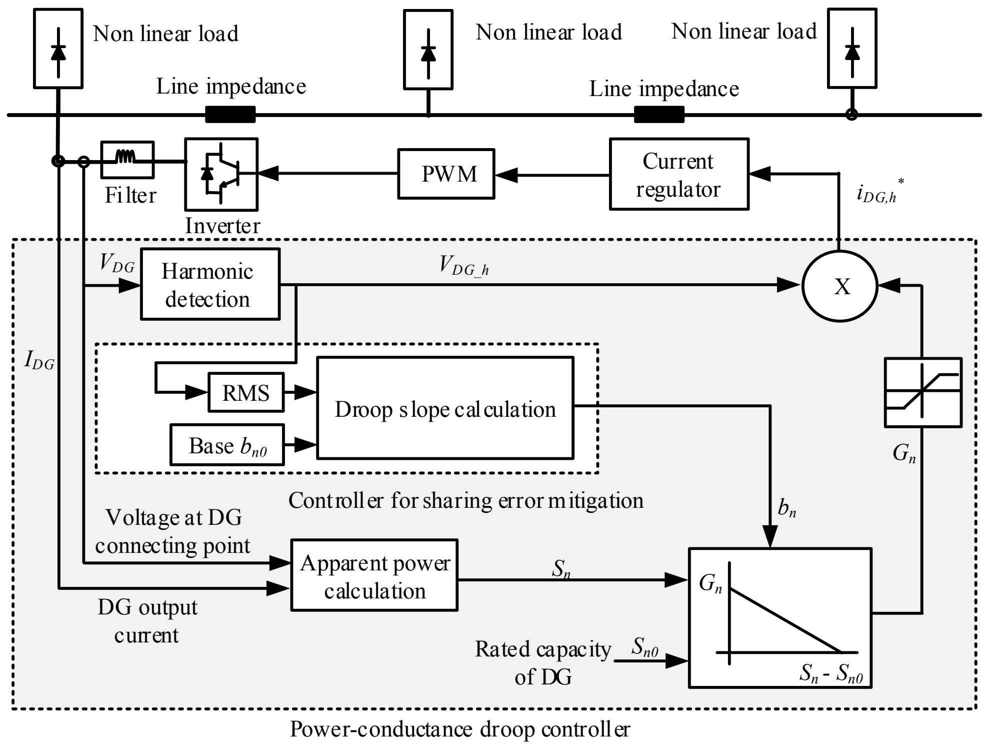

Figure 5.8. Block diagram of the modified droop controller with constant $b_n{*}V_{n,h}$ controller.

Here, $b_{n0,h}$ is the base droop slope at different harmonics and $V_{n,h,rms}$ is the h^{th} harmonic voltage at n^{th} node. By doing this, $b_{n,h}{*}V_{n,h}$ of (5-3) will become a constant and remove any effect of varying $V_{n,h}$ on sharing error which is shown in Figure 5.7. It should be noted that the sharing error results shown in Figure 5.7 will be even greater if they had significantly different connection point harmonics. This power sharing error can be improved using the controller shown in Figure 5.8. Figure 5.7 shows the improved sharing error condition when the controller shown in Figure 5.8 was implemented to improve sharing error. It can be seen from Figure 5.7 that the controller shown in Figure 5.8 can greatly improve the sharing error.

5.5 Implementation of the Modified Conductance- Power Based Priority Driven Droop Controller

While the proposed droop controller can eliminate power sharing error among different DGs operating at different nodes of the distribution system, the controller can be further improved to obtain better harmonics compensation results. To obtain better harmonic compensation result, harmonic compensation priorities at different nodes and at different harmonic frequencies of the distribution system can be identified first. Then the proposed droop controller can be realized using those identified priority values. The droop equation shown in (5-1) has three degree of freedom which can be modified using the results obtained from modal analysis to obtain improved harmonic compensation results. They are, droop slope (b_n), conductance offset (G_{n0}) and DG rated capacity (S_{n0}). In this section, the harmonic compensation priorities will be identified first and then the droop variables will be analyzed to see which one is most suitable. Then the proposed droop controller will be implemented using the selected modified variable for better compensation results.

5.5.1 Resonance Mode Analysis and Priority Calculation

Traditionally, frequency scan analysis is used in an electrical network to identify resonance phenomena and resonance frequency. To carry out frequency scan analysis, an electrical network of n node is represented by an $n \times n$ admittance matrix $[Y]$ at first. Then voltage vector of the system is calculated from the following equation:

$$[V]_f = [Z_N]_f [I]_f \tag{5-15}$$

$$\text{Or, } \begin{bmatrix} V_1 \\ V_2 \\ \vdots \\ V_N \end{bmatrix}_f = \begin{bmatrix} Y_{11} & Y_{12} & \vdots & \cdots \\ Y_{21} & Y_{22} & \vdots & \cdots \\ \vdots & \vdots & \vdots & \vdots \\ Y_{N1} & Y_{n2} & \vdots & \cdots \end{bmatrix} \begin{bmatrix} I_1 \\ I_2 \\ \vdots \\ I_N \end{bmatrix}_f \tag{5-16}$$

Here, $[V]$, $[Z_N]$ and $[I]$ are nodal voltage vector, nodal impedance and nodal current vector respectively while subscript f denotes the frequency. For every frequency, the voltage vector can be calculated for 1 p.u. current injection. The voltage vector that has very high value at some frequency is associated with resonance. Thus resonance and resonance frequency can be identified using this method. But it cannot identify the component and bus that excites the resonance. Using modal analysis, this problem can be solved. Here the high voltage vector values are associated with the singularity of the admittance matrix $[Y]$. This singularity of $[Y]$ matrix can be found when one of its eigenvalue is close to zero. Now the admittance matrix can be decomposed as,

$$[Z_N]_f = [L]_f [Z_M]_f [T]_f \tag{5-17}$$

Here, $[Z_M]$ is the diagonal eigenvalue matrix. $[L_f]$ is the left eigenvalue matrix and while $[T_f]$ is the right eigenvalue matrix. This Eigen analysis or modal transformation is basically a matrix decoupling method that transforms the nodal impedance matrix [Z_N] into modal impedance matrix [Z_M] as,

$$[Z_N]_f = \begin{bmatrix} Z_{11} & Z_{12} & \vdots & \cdots \\ Z_{21} & Z_{22} & \vdots & \cdots \\ \vdots & \vdots & \vdots & \cdots \\ Z_{N1} & Z_{n2} & Z_{n3} & Z_{nn} \end{bmatrix}_f$$

and,

$$[Z_M]_f = \begin{bmatrix} Z_{m,11} & 0 & \vdots & \\ 0 & Z_{m,22} & \vdots & \\ \vdots & \vdots & \vdots & \\ 0 & 0 & 0 & Z_{m,nn} \end{bmatrix}_f$$

It can be seen that the modal analysis actually decouples the coupled nodal impedance matrix [Z_N] into decoupled modal impedance matrix [Z_M] in the modal domain. So, while nodal impedance matrix [Z_N] actually shows how the nodes of an electrical system are coupled to each other in nodal coordinate; modal impedance matrix [Z_M] shows the grid configuration in the modal domain. Modal impedance matrix is diagonally symmetrical (5-18) and eigenvalue matrices are related as (5-19).

$$[Z_M]_f = [Z_M]_f^T \tag{5-18}$$

$$[L]_f^{-1} = [T]_f \tag{5-19}$$

As modal impedance matrix [Z_M] is a diagonal eigenvalue matrix, left and right eigenectors matrices are also effectively diagonal matrix:

$$[L]_f^{-1} = [T]_f = [T]_f^T \tag{5-20}$$

Substituting (5-20) into (5-15) we get:

$$\text{or, } [T]_f [V]_f = [Z_M]_f^{-1} [T]_f [I]_f \tag{5-21}$$

If modal voltage (v_M) and modal current (i_M) vectors are defined as:

$$\underbrace{\begin{bmatrix} i_{m,1} \\ i_{m,2} \\ \vdots \\ i_{m,N} \end{bmatrix}}_{Modal\ Current} = \underbrace{\begin{bmatrix} T_{11} & T_{12} & \vdots & \vdots \\ T_{21} & T_{22} & \vdots & \vdots \\ \vdots & \vdots & \vdots & \vdots \\ \vdots & \vdots & \vdots & \end{bmatrix}}_{Eigen\ Vector} \underbrace{\begin{bmatrix} \\ \\ \vdots \\ I_N \end{bmatrix}}_{Input\ Current} \tag{5-22}$$

and,
$$\underbrace{\begin{bmatrix} v_{m,1} \\ v_{m,2} \\ \vdots \\ v_{m,N} \end{bmatrix}}_{Modal\ Voltage} = \underbrace{\begin{bmatrix} L_{11} & L_{12} & \vdots & \vdots \\ L_{21} & L_{22} & \vdots & \vdots \\ \vdots & \vdots & \vdots & \vdots \\ \vdots & \vdots & \vdots & \end{bmatrix}}_{Eigen\ Vector} \underbrace{\begin{bmatrix} V_1 \\ V_2 \\ \vdots \\ V_N \end{bmatrix}}_{Output\ Voltage} \tag{5-23}$$

Equation (5-21) then reduces to (5-24). Modal analysis in this work will be carried out using equation (5-24)

$$\left[v_M\right]_f = \left[Z_M\right]_f^{-1} \left[i_M\right]_f \tag{5-24}$$

Expanding (5-24), it can be seen that the lowest Eigen value will result in highest modal impedance. And high modal impedance at a particular frequency will result in high modal harmonic voltage for the same input modal harmonic current. In other words, modal impedance can be used to identify the mode that is more prone to harmonic distortion.

$$\underbrace{\begin{bmatrix} V_{m,1} \\ V_{m,2} \\ \vdots \\ V_{m,N} \end{bmatrix}}_{Modal\ Voltage} = \underbrace{\begin{bmatrix} Z_{m,11}^{-1} & 0 & \vdots & \\ 0 & Z_{m,22}^{-1} & \vdots & \\ \vdots & \vdots & \vdots & \\ 0 & 0 & 0 & Z_{m,NN}^{-1} \end{bmatrix}}_{Modal\ impedance} \underbrace{\begin{bmatrix} i_{m,1} \\ i_{m,2} \\ \vdots \\ i_{m,N} \end{bmatrix}}_{Modal\ Current} \tag{5-25}$$

The critical modal impedance (highest modal impedance) is much higher than other modal impedances. As a result, we can assume,

$$\underbrace{\begin{bmatrix} Z_{m,11}^{-1} & 0 & \vdots & \\ 0 & Z_{m,22}^{-1} & \vdots & \\ \vdots & \vdots & \vdots & \\ 0 & 0 & 0 & Z_{m,NN}^{-1} \end{bmatrix}}_{Modal\ impedance} \approx \underbrace{\begin{bmatrix} Z_{m,11}^{-1} & 0 & \vdots & \\ 0 & 0 & \vdots & \\ \vdots & \vdots & \vdots & \\ 0 & 0 & 0 & 0 \end{bmatrix}}_{Modal\ impedance} \tag{5-26}$$

Combining (5-25)-(5-26) we get,

$$\begin{bmatrix} V_1 \\ V_2 \\ \vdots \\ V_N \end{bmatrix}_f = Z^{-1}_{m,11,f} \underbrace{\begin{bmatrix} L_{11}T_{11} & L_{12}T_{12} & \vdots & \vdots \\ L_{21}T_{11} & L_{22}T_{12} & \vdots & \vdots \\ \vdots & \vdots & \vdots & \vdots \\ \vdots & \vdots & \vdots & \end{bmatrix}}_{Particapation\ Factor} \begin{bmatrix} \\ \\ \vdots \\ I_N \end{bmatrix}_f \tag{5-27}$$

The Participation Factor (PF) matrix of (5-27) denotes the impact of each bus on the critical mode. Whereas $Z^{-1}_{m,11,f}$ denotes the impact level at different harmonic frequencies. Combining the modal impedance and PF index, we can determine participation of each bus to output harmonic voltage distortion. In this work, this approach will be used to quantify the harmonic compensation priorities at different harmonic frequencies and at different nodes of the distribution system.

5.5.2 Analysis of the Variables of the Droop Controller

As mentioned before, the droop equation has three degree of freedoms which can be modified using the compensation priority values to obtain improved harmonic compensation results. In this section, these variables are analyzed to identify the most suitable one for proposed priority driven droop controller implementation.

5.5.2.1 Modification of droop slope (b_n)

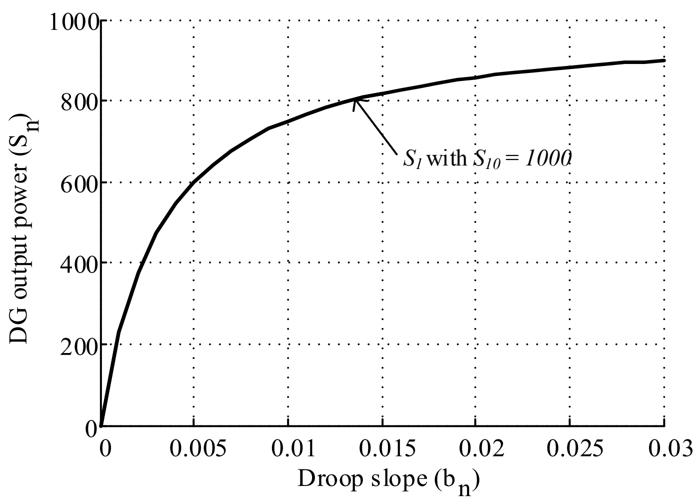

Figure 5.9: Variation of DG output power (S1) with different droop slopes (bn), zero conductance offset (Gn0 = 0) and same DG rating (S10 = const.).

Figure 5.9 shows the DG output power variation with different droop slope (b_n) for the same DG rating (S_{n0}) and zero conductance offset ($G_{n0}=0$). To control the DG output using droop slope, droop slope should be kept within the linear range (0 to .0025 in this case) and changed according to the identified priority values from modal analysis. But it can be seen from Figure 5.9 that when droop slope is in the linear range (0 to .0025), the DG output power is very low and most of the DG rating will remain unused. When droop slope value is high, the output DG power remains almost constant even if the droop slope is changed. So, modifying the droop slope according to the compensation priority value is not ideal.

5.5.2.2 Modification of conductance offset (G_{n0})

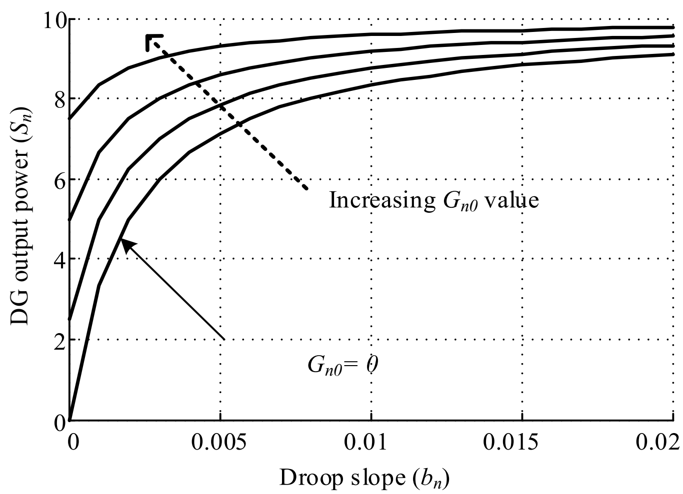

Figure 5.10. DG output power variation with varying droop slope offset (Gn0) and same DG rating (S10 = const.).

Figure 5.10 shows the DG output power variation with different conductance offset (G_{n0}) and same DG rating (S_{n0}) while Table IV lists the output power ratio. It can be seen from this Figure 5.10 that the conductance offset (G_{n0}) can be used to modify the DG output power. However, when conductance offset is used, DG output power is not zero even when droop slope is zero. So, using nonzero values for conductance offset can cause DG overloading. Additionally, Table 5.3 shows that the increased G_{n0} introduces output power sharing error. Hence, modifying conductance offset (G_{n0}) according to identified compensation priority values is not ideal either.

Table 5.3: Comparison of power sharing accuracy among different DGs with varying conductance offset (Gn0)

Scenario	S_{10}	S_{20}	S_{20}/S_{10}	b_1	b_2	G_{10}	G_{20}	S_1	S_2	S_2/S_1
(case 1)	5000	2500	2.0	0.005	0.005	0.0	0.0	3480	1850	1.88
(case 2)	5000	2500	2.0	0.005	0.005	4.0	2.0	3730	2040	1.86
(case 3)	5000	2500	2.0	0.005	0.005	8.0	4.0	3920	2210	1.77
(case 4)	5000	2500	2.0	0.005	0.005	12.0	6.0	4000	2350	1.70

5.5.2.3 Modification of DG rating (S_{n0})

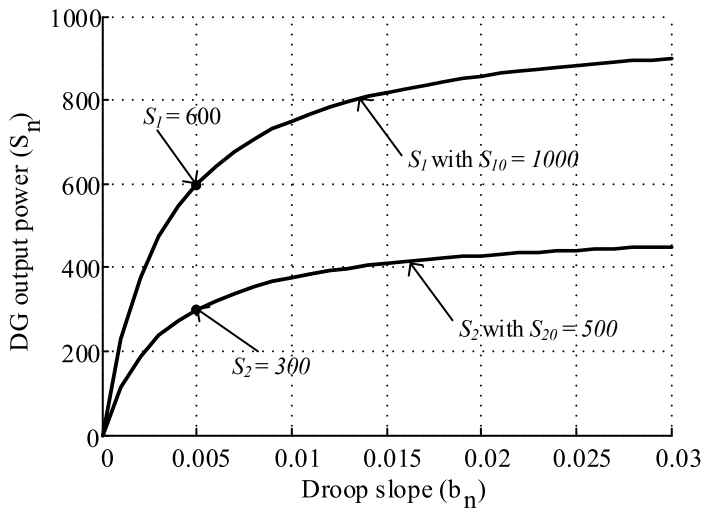

Figure 5.11. DG output power variation with varying DG rating (Sn0)

Figure 5.11 shows the DG output power variation with zero conductance offset ($G_{n0}=0$), same droop slope (b_n) different DG ratings (S_{n0}). It can be seen from Figure 5.11 that the DG output can be effectively controlled using different DG rating values in the droop equation. For example, when S_{20} is reduced by 50% of S_{10}, the DG output S_2 is also reduced by 50% of S_{10} when same droop slope is used. The power sharing is accurate in this case and this hold valid for entire range of droop slope. Hence, modifying DG rating at different nodes and at different harmonics according to the identified priority values will be effective for achieving improved compensation result.

5.5.3 Implementation

Finally, the modified droop controller is implemented with droop parameters obtained using modal analysis. Applying the modal analysis on an 11 node system with a PFC capacitor at node 7 gives the compensation priority values (CPV) listed in Table 5.4.

Table 5.4: DG compensation priority values (PV)

		Harmonic order						
		3rd	**5th**	**7th**	**9th**	**11th**	**13th**	**15th**
Priorities at node	**1**	0.08	0.17	0.37	0.38	0.19	0.11	0.07
	2	0.10	0.21	0.46	0.47	0.24	0.14	0.09
	3	0.12	0.25	0.55	0.57	0.30	0.18	0.12
	4	0.14	0.29	0.64	0.67	0.35	0.22	0.15
	5	0.15	0.32	0.72	0.78	0.42	0.26	0.19
	6	0.17	0.36	0.81	0.89	0.49	0.32	0.23
	7	0.18	0.39	0.89	1.00	0.57	0.38	0.29
	8	0.19	0.40	0.90	0.98	0.54	0.35	0.25
	9	0.19	0.41	0.91	0.97	0.51	0.32	0.22
	10	0.20	0.41	0.91	0.96	0.50	0.30	0.20
	11	0.20	0.42	0.91	0.95	0.49	0.29	0.19

Now these priority values can be used to implement the proposed droop controller with modified rating at each harmonics and at each node. If the available DG ratings of different DGs are S_{n0} then the reference DG ratings (S_{n0}^{*}) can be identified using (5-3). Here, the DG with the highest priority will use most of its rating for harmonic compensation. While DG with less priority will not use all of its rating for harmonic compensation. Thus effective utilization of DG rating will be ensured and even the DG with highest priority will not be overloaded. Once the reference DG ratings (S_{n0}^{*}) is identified, the rating is distributed at different harmonics according to the compensation priority values at the same node and different harmonics. This is shown in (5-28) and (5-29).

$$S_{n0}^{*} = S_{n0} \frac{\sum_{h=3,5,7\ldots}^{h_{\max}} PV_{k,h}}{\sum_{n=1,2,3\ldots}^{N} \sum_{h=3,5,7\ldots}^{h_{\max}} PV_{n,h}} \tag{5-28}$$

and, $$S_{n0,h}^{*} = S_{n0}^{*} \frac{PV_{k,h}}{\sum_{h=3,5,7\ldots}^{h_{\max}} PV_{k,h}} \tag{5-29}$$

here, priority values at different node and different harmonics ($Z_{n,h}$) are obtained from the priority from critical modal impedance ($H_{n,h}$), priority from load harmonic data and priority from participation factor ($PF_{n,h}$).

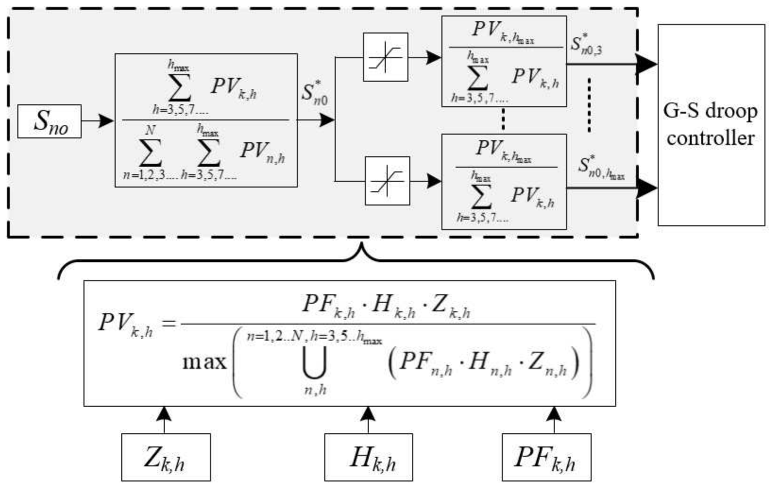

Figure 5.12. Block diagram of the proposed droop controller.

The compensation results with different methods are shown in Figure 5.13. For a fair comparison, harmonic compensation were carried out using traditional and proposed droop controller keeping the total capacity same. It can be seen from Table V that the compensation result using the proposed droop controller is better compared to using traditional droop controller.

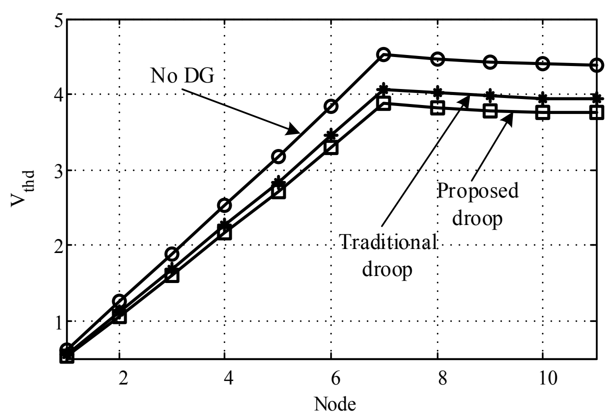

Figure 5.13. V_{THD} values at different distribution system nodes using different compensation schemes.

5.6 Modelling and Stability Analysis

In this section, the dynamic behavior of an N node distribution system will be investigated to determine the minimum virtual harmonic impedance required for stable inverter operation. To do so, a typical distribution system with DG is modelled first and then, stability analysis was carried out using the developed model. This is implemented by modifying harmonic currents at every frequencies using $I^*_h = V_{G\_h}/R_h$ and the reference harmonic current of the PV system is produced by combining all the individual harmonic references as,

$$I^*_h = I^*_3 + I^*_5 + \ldots.. + I^*_{15}$$

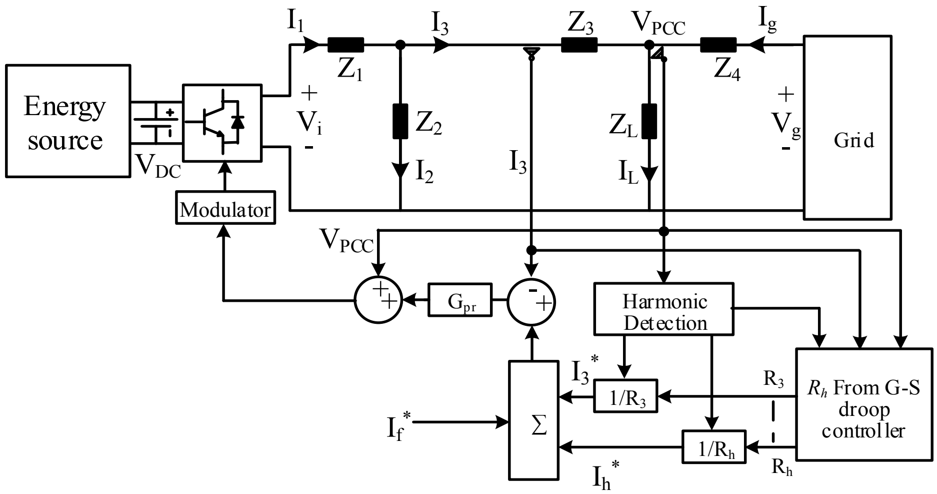

Figure 5.14. Harmonic damping with resistive active filter (R-APF) based DG.

Block diagram of the control system of DG unit is shown in Figure 5.14.

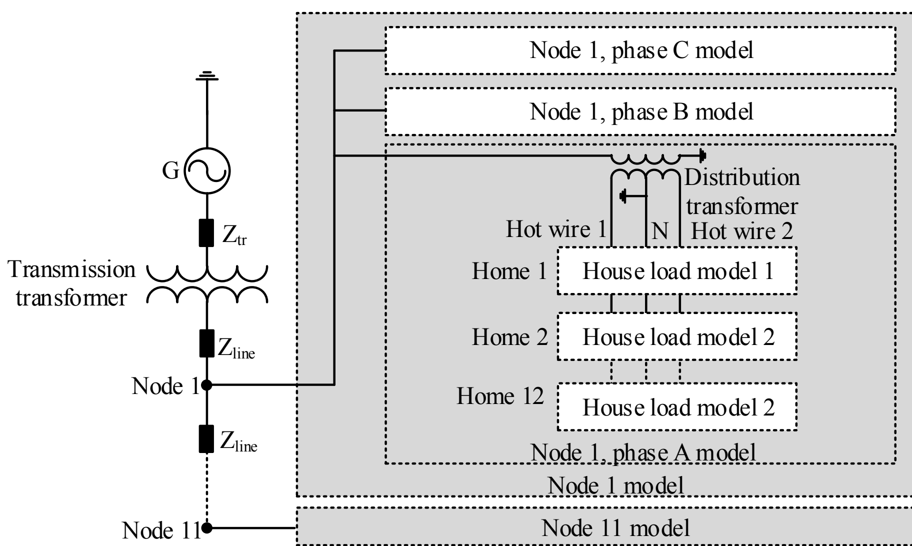

Figure 5.15: Distribution system model.

The distribution system used in this work is shown in Figure 5.15. It has a *34.4*KV transmission line which is connected to the *12.47*KV distribution feeders through transmission transformer (Xf_{tr}). The 3 phase distribution feeder has 11 nodes. To simplify the investigation of the impact of nonlinear loads on distribution system power quality, analysis and simulation will be carried out on a single distribution feeder as shown in Figure 5.16. Here DGs are connected at the secondary side of the distribution transformer. In this model, n = 1, 2, 3……N represents the n^{th} node. Z_{Xn} represents the distribution line impedance, Z_{Yn} represents the distribution transformer impedance. The house load model is comprised of Z_{Ln} which represents the fundamental load impedance and I_{hn} which represents the harmonic current of the non-linear load at n^{th} node. $Z_{C1}, Z_{C2}... Z_{Cn}$ are the impedances of the PFC capacitors respectively at the n^{th} node. Here the DG at n^{th} node is represented by virtual impedance R_n. V_n is the voltage at the n^{th} node. From the impedance matrix of the system shown in Figure 5.16 and (5-33), compensation priority can be identified.

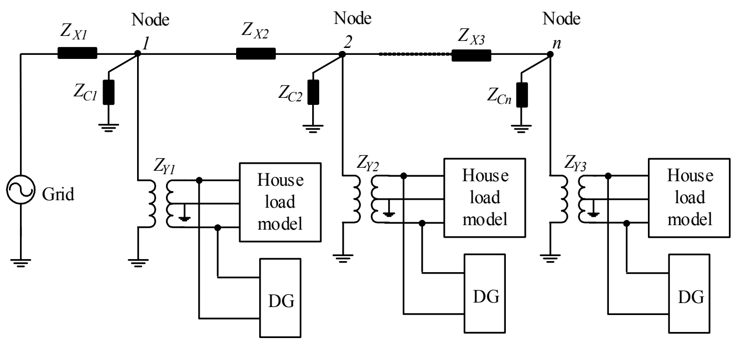

Figure 5.16. Simplified single distribution feeder.

Figure 5.17 shows the equivalent block diagram of the current controller used in this work.

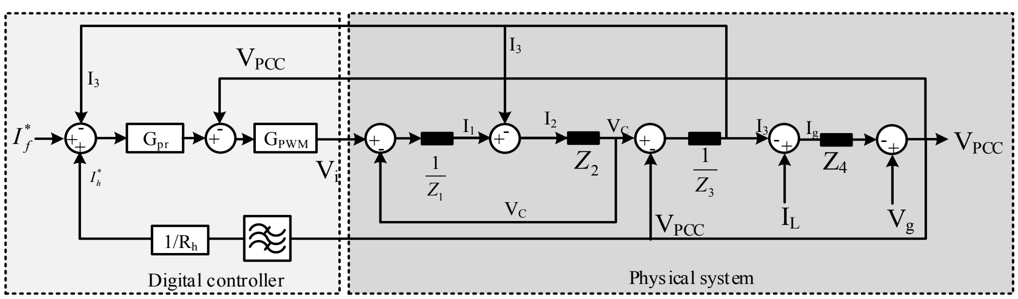

Figure 5.17. Equivalent block diagram of the inverter controller with virtual harmonic resistance and power-conductance droop controller.

This inverter controller can be expressed as Norton equivalent circuit model shown in Figure 5.18 according to equation (5-30).

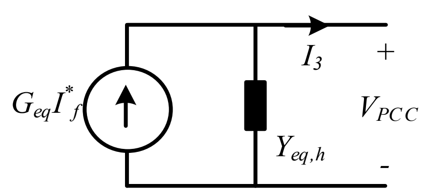

Figure 5.18. Norton equivalent circuit of the inverter controller

$$I_3 = V_{PCC} Y_{eq,h} + I_f^* G_{eq} \tag{5-30}$$

where,

$$Y_{eq,h} = \frac{\left(1 + sC_f R_d\right)\left(G_{\Sigma h} G_{PWM} G_{PR,h} + G_{PWM} - 1\right) - L_1 C_f s^2}{\left(G_{PWM} G_{PR,h} + L_1 s - L_2 s\right)\left(1 + sC_f R_d\right) - L_1 L_2 C_f s^3} \tag{5-31}$$

and,

$$G_{eq} = \frac{G_{PWM} G_{PR,h} \left(1 + sC_f R_d\right)}{\left(G_{PWM} G_{PR,h} + L_1 s - L_2 s\right)\left(1 + sC_f R_d\right) - L_1 L_2 C_f s^3} \tag{5-32}$$

This virtual harmonic impedance can be used in the equivalent model of an N node distribution system as shown in Figure 5.19 that is obtained from Figure 5.16.

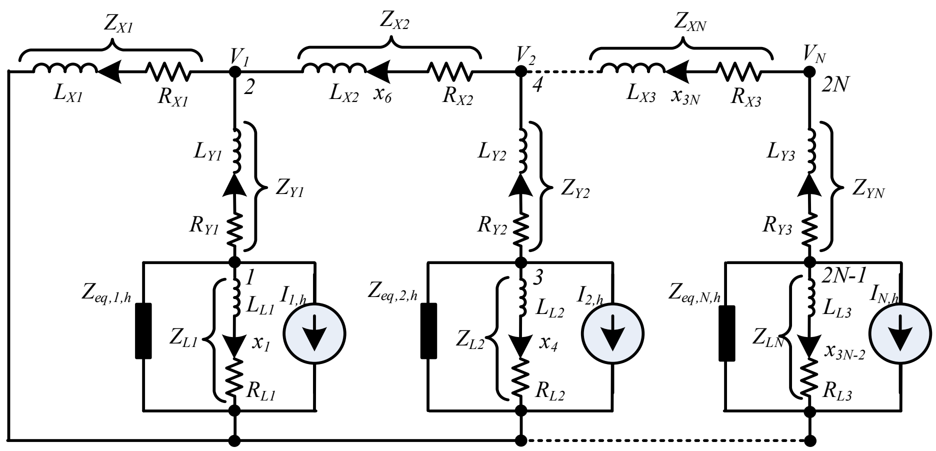

Figure 5.19. Equivalent model of an N node distribution feeder with virtual harmonic impedance.

As the analysis here focuses on harmonic frequencies, the source is shorted in Figure 5.20). Additionally, V_n is the voltage at the n^{th} node. x_1, x_4... x_{3N-2} are the currents through Z_{L1}, Z_{L2}... Z_{Ln}. x_2, x_5... x_{3N-1} are the currents through Z_{Yn}. x_3, x_6... x_{3N} are the currents through Z_{Xn}. Here, x_1, x_2... x_{3N} are taken to be the state variables, I_{hn} is the input, and V_n is the output of the state space model of the system. Then for a N-node system, there are 3N state equations. The 1-N, N+1 to 2N, and 2N+1 to 3N equations are shown in (5-33)-(5-35), respectively:

$$I_{h\cdot n} = x_{3n-2} + x_{3n-1} + \frac{x_{3n-2} R_{L\cdot n} + \text{[illegible]}}{R_n} \tag{5-33}$$

$$\sum_{n=1}^{N}\left(x_{3\cdot n}R_{X\cdot n} + \dots\right. \tag{5-34}$$

$$x_{3n-1} + x_{3n+3} = x_{3n} \tag{5-35}$$

Solving (5-33) to (5-35) yields the A_N and B_N matrices of the state space model while the equation of the system output yields the C_N and D_N matrices of the state space model.

$$v_n = v_{n-1} + x_{3n}R_{Xn} + \dots \tag{5-36}$$

Hence, the state space model of the system can be obtained as shown in (5-37).

$$\frac{v_n(s)}{I_{hn}(s)} = C_N \phi B_N + D_N \tag{5-37}$$

where, $\phi = (sI - A_N)^{-1}$, n = 1, 2…N, and I is a $3N\times3N$ identity matrix and,

$$\dots \begin{bmatrix} x_1 \\ x_2 \\ \\ . \\ x_{3N} \end{bmatrix} + B_N \begin{bmatrix} I_{h1} \\ I_{h2} \\ . \\ . \\ I_{hN} \end{bmatrix} \quad \text{and} \quad \begin{bmatrix} v_1 \\ v_2 \\ . \\ . \\ v_N \end{bmatrix} = C_N \begin{bmatrix} x_1 \\ x_2 \\ . \\ . \\ x_{3N} \end{bmatrix} + D_N \begin{bmatrix} I_{h1} \\ I_{h2} \\ . \\ . \\ I_{hN} \end{bmatrix}$$

For a typical dynamic behavior analysis, a 2 node system is considered in this work. To simplify the analysis, $Z_{x1} = Z_{x2} = Z_x$, $Z_{Y1} = Z_{Y2} = Z_Y =$, $Z_{L1} = Z_{L2} = Z_L =$ and $I_{h1} = I_{h2} = I_h$ is assumed. Then,

$$\frac{V_1}{I_h} = \frac{Z_X Z_Y Z_2 + 2Z_X Z_1 Z_2 + Z_X^2 Z_1 + Z_X Z_Y Z_1}{Z_Y^2 + 3Z_X Z_Y + Z_X^2 + \left(2Z_X + Z_Y\right)Z_1 + \left(Z_X + Z_Y\right)Z_2 + Z_1 Z_2} \tag{5-38}$$

and,

$$\frac{V_2}{I_h} = \frac{Z_X Z_Y Z_1 + \left(Z_X^2 + 2Z_X Z_1\right)Z_2 + 3Z_X Z_1 Z_2}{Z_Y^2 + 3Z_X Z_Y + Z_X^2 + \left(2Z_X + Z_Y\right)Z_1 + \left(Z_X + Z_Y\right)Z_2 + Z_1 Z_2} \tag{5-39}$$

where,

$$Z_{1(2)} = \frac{\left(R_L + sL_L\right)Z_{eq1(2),h}(s)}{R_L + sL_L + Z_{eq1(2),h}(s)} \tag{5-40}$$

Using equations (5-38) and (5-39), stability analysis can be carried out. Figure 5.15 shows the root locus analysis for 3rd harmonic with DG at node 1. It can be seen from Figure 5.20 that the system is stable when $R_{1,3} > 0.0043\Omega$.

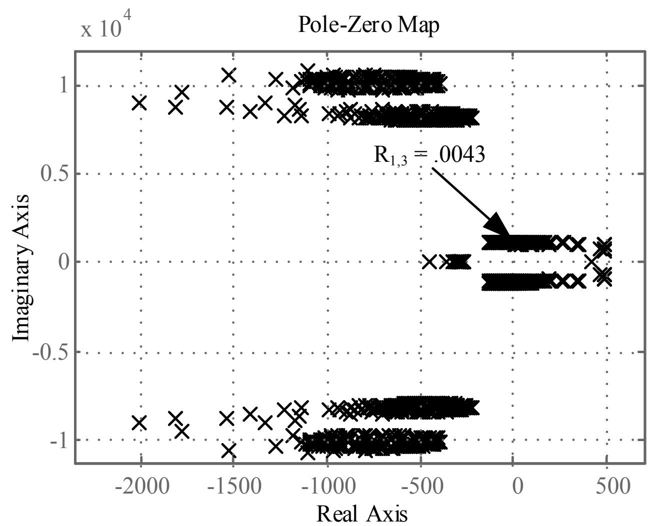

Figure 5.20. Root locus analysis for 3rd harmonic with DG at node 1.

Similarly, the minimum R_V for each dominant harmonic frequency and for each compensation strategy can be obtained (DG no at node 1, DG at node 2 and finally DG at both 1 and 2 node) from stability analysis and are shown in Figure 5.22.

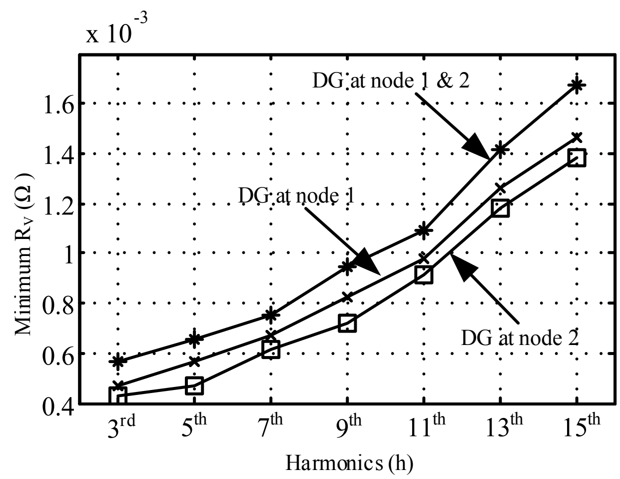

Figure 5.21. Minimum RV for each dominant harmonics when different compensation strategies are used.

It can be seen from Figure 5.21 that different position of DG in the distribution system effects the stability of the system. When the DG is installed at node 2, the minimum virtual harmonic resistance is lower than when DG is connected at node 1. And the required minimum virtual harmonic resistance when DG is connected at both node 1 and 2 is highest among all these the compensation method. So, it can be concluded that the stability margin is largest when end of line compensation is used and smallest when distributed compensation is used. It can be seen from

Figure 5.22 that the minimum R_V ranges between 0.0004Ω to 0.0016Ω depending on the order of the harmonics. This corresponds to maximum droop slope (b_n) of -2.5V-2 to 0.625V-2 when rating is 1000VA. In the simulation, the base droop slope was used to be -5 x 10-3V^{-2} which is well within the maximum droop slope range obtained from stability analysis to avoid instability problem.

5.7 Conclusion

In this chapter, a conductance-power droop based selective harmonic compensation scheme using DG-grid interfacing inverters is developed that improves the harmonic compensation performance on a residential distribution system. Here, harmonic compensation priorities for different DG position and harmonic frequency are identified for improved compensation performance compared to traditional distributed compensation. These priority values were used to implement the proposed droop controller with modified rating at each harmonics and at each node. Here, the available aggregated DG ratings of different DGs are divided among different DGs according to their compensation priorities. As a result, the DG with the highest priority will use most of its rating for harmonic compensation. While DG with less priority will not use all of its rating for harmonic compensation. Thus effective utilization of DG rating will be ensured and even the DG with highest priority will not be overloaded.

In this work, a modification of the G-S droop control method is proposed to eliminate power sharing error introduced by the feeder impedance. Then the proposed G-S droop based selective compensation is implemented by modifying the individual harmonic ratings of the DG-grid interfacing inverters. It should be noted that the work presented in Chapter 4 identifies the harmonic compensation priorities but the implementation scheme determines the virtual harmonic impedance directly with compensation priorities and therefore compensation rating control is not straightforward. On the contrary, the G-S droop method presented in in this chapter utilize the rating (S) directly and can easily control DG compensation level. Here ratings are divided among different DGs according to the compensation priority values and each DGs operate based on the local droop controllers.

An in-depth analysis, comparison and simulation of the developed compensation scheme with different existing harmonic compensation schemes were conducted to identify the performance improvement.

Chapter 6

Conclusion and Future Work

6.1 Thesis Contribution and Conclusion

In this thesis, topics related to the modeling, measurement, and mitigation of residential distribution system harmonics using DG-grid interfacing inverters are addressed. An extensive investigation of different control methods of VSI for power quality improvement was conducted. The attenuation/amplification effects for some of the power electronic-based home appliances were analyzed, and a modeling technique that takes the effects into consideration was proposed. The mitigation schemes for harmonics were investigated. The problem of inter harmonics in distribution systems was also studied.

The main conclusions and contributions of this thesis are summarized as follows:

- Opportunities of distribution system power quality improvement using the DG-grid interfacing inverters are investigated. The idea of using residential DG-grid interfacing inverters as virtual harmonic resistances to damp the system harmonics and improve the power quality was explored. In order to implement harmonic compensation schemes using the DG-grid interfacing inverters, current control method (CCM) and voltage control method (VCM) based VSIs are used. Both the current controlled method and the voltage controlled method are considered and associated power quality compensation schemes are investigated in this work. A comparative analysis of VSI control systems with single and two current sensors are presented. A design criteria for single and multiple-loop feedback method is proposed here to facilitate fair comparison among different control methods. It is shown that multiple-loop feedback system has low line parameter sensitivity which makes the controller suitable to be used in a system with line parameter variation. It was concluded that when CCM based VSI is used as DG interface, the two current sensor scheme with inductor current feedback is recommended considering the superior performance and ability to provide quick protection due to the direct measurement of inverter output current.

- In literature, two different harmonic compensation schemes namely end-of-line and distributed compensation schemes are popular for residential power quality improvement. In this work, the effects of the PV locations on harmonic compensation performance of these schemes are investigated. This analysis then identifies the compensation method that should be used under different grid conditions which lays the groundwork for a priority based improved compensation scheme. It was found that the end-of-line compensation provided better damping for low-order harmonics, whereas distributed compensation provided better damping for high-order harmonics if the equal equivalent rating of the DG was maintained. In the system without PFC capacitors, this crossover frequency was quite high, and end-of-line compensation performed better. However, the presence of capacitor in the system could significantly reduce this crossover frequency and the decision about which compensation strategy to use must be made according to the system load characteristics. Moreover, the effects of capacitor sizes, line impedance, and length on the crossover frequency were also analyzed in this work. With the information about a distribution system, the crossover frequency between the two compensation strategies can be determined by using the model developed in this work, and proper priority can be assigned to the PV inverters at different locations when each DG in the distribution network is assigned the same weight.
- In order to further optimize harmonics compensation with different compensation priority at different nodes and different harmonics, a selective harmonic compensation scheme based on modal analysis is developed that improves the harmonic compensation performance on a residential distribution system. Here, compensation priorities for different DG positions and harmonic frequencies are identified for improved compensation performance compared to traditional distributed compensation. Assigning such compensation priorities on different DG interfacing inverters in the distribution system improves compensation performance. An in-depth analysis, comparison and simulation of the developed selective compensation scheme with different existing harmonic compensation schemes were conducted to identify the performance improvement. To achieve the main objective of this work of improving the harmonic compensation

performance in a residential distribution system, a model based approach is adopted where selective harmonic compensation priorities are generated according to the system parameters and load current data which are used to achieve better compensation results. Although the compensation performance of this proposed selective harmonic control scheme deteriorates when actual load data is not available, the compensation results with inaccurate load data are still better than traditional distributed compensation.

- To facilitate the implementation of priority based selective harmonics compensation, a conductance-power droop based selective harmonic compensation scheme using DG-grid interfacing inverters is developed that improves the harmonic compensation performance on a residential distribution system. Here, harmonic compensation priorities for different DG position and harmonic frequency are identified for improved compensation performance compared to traditional distributed compensation. These priority values were used to implement the proposed droop controller with modified rating at each harmonics and at each node. The available aggregated DG ratings of different DGs are divided among different DGs according to their compensation priorities. As a result, the DG with the highest priority uses most of its rating for harmonic compensation. While DG with less priority does not use all of its rating for harmonic compensation. Thus effective utilization of DG rating is ensured and even the DG with highest priority is not overloaded. Here, a modification of the G-S droop control method is proposed to eliminate power sharing error introduced by the feeder impedance. This proposed G-S droop based selective harmonic compensation scheme also eliminates the power sharing error introduced by the traditional droop control scheme. Moreover, this proposed control scheme can be easily realized as it is a rating based control where each DG calculates the required virtual resistance locally using the droop controller.

6.2 Suggestions for Future Work

As with any study, the work presented in this thesis can be extended. Several extensions and modifications of this thesis can be explored as follows:

- So far, mathematical analysis of selective harmonic compensation and priority driven droop control schemes are presented in this thesis which are then verified using simulation results. In future, these can be implemented using an experimental setup with multi-node system and multiple DGs to analyze the performance.

- In this thesis, compensation priorities are calculated using an offline supervisory control system. An important next step of this work could be to integrate both the supervisory control (done in this thesis thorough offline modeling/analysis) and primary converter control in a multi-layered control scheme.
- Additional case studies for the selective harmonic compensation strategy that include load monitoring data, DG rating variation, historic load data can be conducted to show the benefits of the proposed method.
- Implementation of the proposed priority driven droop controller was shown using a distribution feeder with 11 nodes and one PFC. It will be interesting to see how the proposed controller performs when applied to a more complex real world distribution system model. And eventually, field test on a real distribution system to observe the compensation performance improvement can be considered.
- While this thesis focuses on the harmonic compensation of distribution systems, it is possible to extend the idea of coordinated harmonic compensation presented in this thesis to many other power quality enhancement services, e.g., reactive power support and unbalanced voltage compensation etc.

References

[1] International Energy Agency (IEA), "Distributed Generation in Liberalised Electricity Markets", pp. 23, 2002.

[2] M. G. Simes, F. A. Farret, "Modeling Power Electronics and Interfacing Energy Conversion Systems", pp. 57, Wiley-IEEE Press, 2017.

[3] E.J. Coster, J.M.A. Myrzik, B. Kruimer, and W.L. Kling, "Integration Issues of Distributed Generation in Distribution Grids," Proceedings of the IEEE, vol. 99 no. 1, pp. 28-39, Jan 2011.

[4] F. Wang, J. L. Duarte, M. A. M. Hendrix, and P. F. Ribeiro, "Modeling and analysis of grid harmonic distortion impact of aggregated DG inverters," IEEE Trans. Power Electron, vol. 26, no. 3, pp. 786–797, Mar. 2011.

[5] M. Triggianese, F. Liccardo, and P. Marino, "Ancillary Services performed by Distributed Generation in grid integration," Proc. IEEE International Conference on Clean Electrical Power, 2007, pp. 164–170.

[6] M.I. Marei, T.K. Abdel-Galil, E.F. El-Saadany, and M.M.A. Salama, "Hilbert transform based control algorithm of the DG interface for voltage flicker mitigation," IEEE Trans. Power Delivery, vol. 20, pp. 1129- 1133, April 2005.

[7] M. Prodanovic, K. De Brabandere, J. Van Den Keybus, T. Green, and J. Driesen, "Harmonic and reactive power compensation as ancillary services in inverter-based distributed generation," IEE Proc. Gener. Transm. Distrib., vol.1, pp.432-438, May 2007

[8] N. Pogaku and T.C. Green, "Harmonic mitigation throughout a distribution system: a distributed-generator-based solution," IEE Proc. Gener. Transm. Distrib., vol. 153, no. 3, pp. 350- 358, 11 May 2006.

[9] C.J. Gajanayake, D.M. Vilathgamuwa, P. C. Loh, R. Teodorescu, and F. Blaabjerg, "Z-Source-Inverter-Based Flexible Distributed Generation System Solution for Grid Power Quality Improvement," IEEE Trans. Energy Conversion, vol.24, pp.695-704, Sept. 2009.

[10] Y. W. Li, D. M. Vilathgamuwa and P. C. Loh, "Microgrid Power Quality Enhancement Using A Three-Phase Four-Wire Grid-Interfacing Compensator," IEEE Trans. Ind. Applicat., vol. 41, pp. 1707-1719, Nov-Dec. 2005.

[11] C.H. Lin, W.L. Hsieh, C.S. Chen, C.T. Hsu and T.T. Ku, "Optimization of Photovoltaic Penetration in Distribution Systems Considering Annual Duration Curve of Solar Irradiation," IEEE Transactions on Power Systems, vol.27, no.2, pp.1090-1097, May 2012.

[12] A. Capasso, W. Grattieri, R. Lamedica, and A. Prudenzi, "A bottom-up approach to residential load modeling," IEEE Transactions on Power Systems, vol.9, no.2, pp.957-964, May 1994.

[13] Renewable Energy policy network for the 21st century, "Renewables 2016 – Global status report", pp. 17, 2016.

[14] "Modeling and simulation of the propagation of harmonics in electric power networks. I. Concepts, models, and simulation techniques," Power Delivery, IEEE Transactions on, vol. 11, pp. 452-465, 1996.

[15] A. E. Emanuel, J. Janczak, D. J. Pileggi, E. M. Gulachenski, C. E. Root, M. Breen, and T. J. Gentile, "Voltage distortion in distribution feeders with nonlinear loads," IEEE Trans. Power Del., vol. 9, no. 1, pp. 79–87, Jan. 1994.

[16] R. Dwyeret al., "Evaluation of harmonic impacts from compact fluorescent lights on distribution systems," IEEE Trans. Power Syst., vol.10, no. 4, pp. 1772–1779, Nov. 1995.. I. Concepts, models, and simulation techniques," Power Delivery, IEEE Transactions on, vol. 11, pp. 452-465, 1996.

[17] N. R. Watson, T. L. Scott, and S. Hirsch, "Implications for distribution networks of high penetration of compact fluorescent lamps," IEEE Trans. Power Del., vol. 24, no. 3, pp. 1521–1528, Jul. 2009.

[18] D. Salles, C. Jiang, W. Xu, W. Freitas and H. Mazin,"Assessing the Collective Harmonic Impact of Modern Residential Loads – Part I: Method," IEEE Trans. Power Del., vol.27, no.4, pp.1937-1946, Oct. 2012.

[19] D. J. Pileggi, E. M. Gulachenski, C. E. Root, T. J. Gentile, A. E. Emanuel, "The Effect of Modern Compact Fluorescent Lights on Voltage Distortion," IEEE Trans. Power Del., vol. 8, no. 3, July 1993, pp. 1451-1459.

[20] W.E. Reid, "Power Quality Issues-Standards and Guidelines," IEEE Trans. Industry Applications, vol. 32, no. 3, May/June 1996.

[21] R. Dwyer, A. K. Khan, M. McGranaghan, L. Tang, R. K. McCluskey, R. Sung, T. Houy, "Evaluation of Harmonic Impacts from Compact Fluorescent Lights on Distribution Systems," IEEE Trans. Power Syst., vol. 10, no. 4, Nov. 1995, pp. 1772-1779.

[22] A. Antonopoulos, G. Mörée, J. Soulard, L. Ängquist and H. P. Nee, "Experimental evaluation of the impact of harmonics on induction motors fed by modular multilevel converters," 2014 International Conference on Electrical Machines (ICEM), Berlin, 2014, pp. 768-775.

[23] M. N. D. Dang, N. Al-Mutawaly and J. Lepoutre, "From transmission to distribution networks-harmonic impacts on modern grid," 2015 IEEE 28th Canadian Conference on Electrical and Computer Engineering (CCECE), Halifax, NS, 2015, pp. 452-459.

[24] P. S. Moses and M. A. S. Masoum, "Three-Phase Asymmetric Transformer Aging Considering Voltage-Current Harmonic Interactions, Unbalanced Nonlinear Loading, Magnetic Couplings, and Hysteresis," in IEEE Transactions on Energy Conversion, vol. 27, no. 2, pp. 318-327, June 2012.

[25] R. Sarathi, A. Nandini and T. Tanaka, "Understanding electrical treeing phenomena in XLPE cable insulation under harmonic AC voltages adopting UHF technique," in IEEE Transactions on Dielectrics and Electrical Insulation, vol. 19, no. 3, pp. 903-909, June 2012.

[26] H. Hu, Q. Shi, Z. He, J. He and S. Gao, "Potential Harmonic Resonance Impacts of PV Inverter Filters on Distribution Systems," in IEEE Transactions on Sustainable Energy, vol. 6, no. 1, pp. 151-161, Jan. 2015.

[27] S. Yanchenko and J. Meyer, "Harmonic emission of household devices in presence of typical voltage distortions," 2015 IEEE Eindhoven PowerTech, Eindhoven, 2015, pp. 1-6.

[28] H. Wang, "Harmonic Impact of Modern Residential Loads on Distribution Power System and Mitigation Solutions," MSc. thesis, University of Alberta, Canada, 2011.

[29] Gonzalez, A. Damian, McCall, C. John, "Design of Filters to Reduce Harmonic Distortion in Industrial Power Systems," IEEE Trans. Industry Applications, vol.IA-23, no.3, pp.504-511, May 1987.

[30] Chang, G.W., Hung-Lu Wang, Shou-Yung Chu, "Strategic placement and sizing of passive filters in a power system for controlling voltage distortion," IEEE Trans. Power Del., vol.19, no.3, pp. 1204- 1211, July 2004.

[31] Mau Teng Au, Jovica V. Milanovic, "Planning Approaches for the Strategic Placement of Passive Harmonic Filters in Radial Distribution Networks," IEEE Trans. Power Del., vol.22, no.1, pp.347-353, Jan. 2007.

[32] Chang, G.W., Shou-Yung Chu, Hung-Lu Wang, "Sensitivity-based approach for passive harmonic filter planning in a power system," Power Engineering Society Winter Meeting, 2002. IEEE, vol.2, no., pp. 937- 940 vol.2, 2002.

[33] Chi-Jui Wu, Jung-Chen Chiang, Shih-Song Yen, Ching-Jung Liao, Jin-ShyrYang, Tzong-Yih Guo, "Investigation and mitigation of harmonic amplification problems caused by single-tuned filters," IEEE Trans. Power Del., vol.13, no.3, pp.800-806, Jul 1998.

[34] J. M. Guerrero, L. Hang, and J. Uceda, "Control of distributed uninterruptible power supply systems," IEEE Trans. Ind. Electron., vol. 55, no. 8, pp. 2845–2859, Aug. 2008.

[35] J. C. Vasquez, J. M. Guerrero, A. Luna, P. Rodriguez, and R. Teodorescu, "Adaptive droop control applied to voltage-source inverters operating in grid-connected and islanded modes," IEEE Trans. Ind. Electron., vol. 56, no. 10, pp. 4088–4096, Oct. 2009.

[36] Y. W. Li and C. N. Kao, "An accurate power control strategy for powerelectronics-interfaced distributed generation units operating in a lowvoltagemultibus microgrid," IEEE Trans. Power Electron., vol. 24, no. 12, pp. 2977–2988, Dec. 2009.

[37] J. He, Y. W. Li and M. S. Munir, "A Flexible Harmonic Control Approach Through Voltage-Controlled DG–Grid Interfacing Converters," in IEEE Transactions on Industrial Electronics, vol. 59, no. 1, pp. 444-455, Jan. 2012.

[38] B. P. Mcgrath, D. G. Holmes, and J. J. H. Galloway, "Power converter line synchronization using a discrete Fourier transform (DFT) based on a variable sample rate," IEEE Transaction on Power Electronics., vol. 20, no. 4, pp. 877-884, Apr. 2005.

[39] H. Akagi, Y. Kanazawa, and A. Nabae, "Instantaneous reactive power compensation comprising switching devices without energy storage components, " IEEE Transaction on Industry Application., vol. 20, no. 3, pp. 625-630, Mar/Apr. 1984.

[40] P. Rodríguez, A. Luna, I. Candlea, R. Mujal, R. Teodorescu, and F. Blaabjerg, "Multiresonant frequency-locked loop for grid synchronization of power converters under distorted grid conditions," IEEE Transaction on Industrial Electronics., vol. 58, no. 1, pp. 127–138, Jan. 2011.

[41] Y. Wang and Y. W. Li, “Three-phase cascaded delayed signal cancellation PLL for fast selective harmonic detection,” IEEE Transaction on Industrial Electronics., vol. 60, no. 4, pp. 1452–1463, Apr. 2013.

[42] H. Akagi, H. Fujita, and K. Wada, “A shunt active filter based on voltage detection for harmonic termination of a radial power distribution line,” IEEE Trans. Ind. Appl., vol. 35, no. 3, pp. 6138–645, May/Jun. 1999.

[43] S. Alyasin, S2. Hoffman, R. Sasaki, “The identification of the true energy savings realized from high efficiency electronic loads”, Proceedings of the IEEE PES T & D, April 10-15, 1994 pp. 79-85.

[44] A. Domijan, O. Hancock, C. Maytrott, “A study and evaluation of power electronic based adjustable speed motor drives for air conditioners and heat pumps with an example utility case study of the Florida Power and Light Company”, IEEE Transactions on Energy Conversion, vol. 7, no. 3, Sept. 1992, pp. 396-404.

[45] L. E. Sulfstede, “Applying Power Electronics to Residential HVAC – The Issues”, IEEE Transactions on Industry Applications, vol. 29, no. 2, March/April 1993, pp. 300-305.

[46] A. M. Jungreis, A. W. Kelley, “Adjustable Speed Drive for Residential Applications”, IEEE Transactions on Industry Applications, vol. 31, no. 6, Nov./Dec. 1995, pp. 1315-1322.

[47] M.I. Marei, T.K. Abdel-Galil, E.F. El-Saadany, and M.M.A. Salama, “Hilbert transform based control algorithm of the DG interface for voltage flicker mitigation,” IEEE Trans. Power Delivery, vol. 20, pp. 1129- 1133, April 2005.

[48] M. Prodanovic, K. De Brabandere, J. Van Den Keybus, T. Green, and J. Driesen, “Harmonic and reactive power compensation as ancillary services in inverter-based distributed generation,” IEE Proc. Gener. Transm. Distrib., vol.1, pp.432-438, May 2007

[49] N. Pogaku and T.C. Green, “Harmonic mitigation throughout a distribution system: a distributed-generator-based solution,” IEE Proc. Gener. Transm. Distrib., vol. 153, no. 3, pp. 350- 358, 11 May 2006.

[50] C.J. Gajanayake, D.M. Vilathgamuwa, P. C. Loh, R. Teodorescu, and F. Blaabjerg, “Z-Source-Inverter-Based Flexible Distributed Generation System Solution for Grid Power Quality Improvement,” IEEE Trans. Energy Conversion, vol.24, pp.695-704, Sept. 2009.

[51] Y. W. Li, D. M. Vilathgamuwa and P. C. Loh, “Microgrid Power Quality Enhancement Using A Three-Phase Four-Wire Grid-Interfacing Compensator,” IEEE Trans. Ind. Applicat., vol. 41, pp. 1707-1719, Nov-Dec. 2005.

[52] Q. Zeng, L. Chang, "Study of advanced current control strategies for three-phase grid-connected pwm inverters for distributed generation," IEEE Conference on Control Applications, pp.1311-1316, Aug. 2005.

[53] M. David, W. Donald, "Current Control of VSI-PWM Inverters," IEEE Trans on Industry App., , vol.IA-21, no.3, pp.562-570, May 1985

[54] G. Wang; Y.W. Li; "Parabolic PWM for Current Control of VSCs," IEEE Trans on Industrial Elec., v.57, n10, pp.3491-3496, Oct. 2010.

[55] A.N. Rahim, J.E. Quaicoe, "Modeling and analysis of a feedback control strategy for 3-phase voltage-source utility interface systems," Industry Application Society Annual Meeting, 1994, pp.895-902 vol.2, Oct 1994.

[56] G. Shen, D. Xu, Luping Cao, Xuancai Zhu, “An mproved control strategy for Grid-connected voltage source inverters with an LCL filter”, IEEE Trans. on Industrial Elec., vol.23, no.4, pp.1899-1906, July 2008.

[57] G. Shen, X. Zhu, J. Zhang, D. Xu, ``A New Feedback Method for PR Current Control of LCL-Filter-Based Grid-Connected Inverter," IEEE Trans. on Industrial Electronics, vol.57, no.6, pp.2033-2041, June 2010.

[58] T. Erika, D.G. Holmes, "Grid current regulation of a 3-phase voltage source inverter with an LCL input filter," IEEE Transactions on Power Electronics, vol.18, no.3, pp. 888- 895, May 2003.

[59] J. He, Y.W. Li, “GCC Schemes with Embedded Virtual Imepdance for Voltage Source Converters with LC or LCL Filters”, Submitted, Energy Conversion Congress and Exposition (ECCE 2011), Phoenix, USA,

[60] P. Jintakosonwit, H. Akagi, H. Fujita, and S. Ogasawara, “Implementation and performance of automatic gain adjustment in a shunt-active filter for harmonic damping throughout a power distribution system,” IEEE Trans. Power Electron., vol.17, pp. 438-447, May 2002.

[61] L. Asiminoaei, F. Blaabjerg, and S. Hansen, “Evaluation of harmonic detection methods for active power filter applications,” IEEE APEC- 2005, pp. 635- 641.

[62] E. Jacobsen and R. Lyons, "The Sliding DFT," IEEE Signal Processing Magazine, vol 20, pp. 74-80, Mar. 2003.

[63] D. N. Zmood, D. G. Holmes and G. H. Bode, "Stationary frame current regulation of PWM inverters with zero steady-state error," IEEE Trans. Power Electron., vol. 18, pp. 814–822, Mar. 2003.

[64] P. Mattavelli, "Synchronous-frame harmonic control for high-performance AC power supplies," IEEE Trans. Ind. Applicat., vol. 37, pp. 864–872, May/Jun. 2001.

[65] R. Lasseter, "Microgrids," Proc. IEEE Power Engineering Society Winter Meeting, 2002, pp. 305–308.

[66] Y. W. Li, D. M. Vilathgamuwa, and P. C. Loh, "Design, Analysis and Real-Time Testing of Controllers for Multi-Bus Microgrid System," IEEE Trans. Power Electron., vol. 19, pp. 1195-1204, Sep. 2004.

[67] Y. W. Li and C. N. Kao, "An Accurate Power Control Strategy for Power-Electronics-Interfaced Distributed Generation Units Operating in a Low-Voltage Multibus Microgrid," IEEE Trans. Power Electron., vol. 24, pp. 2977-2988, Dec. 2009.

[68] A. Domijan, O. Hancock, C. Maytrott, "A study and evaluation of power electronic based adjustable speed motor drives for air conditioners and heat pumps with an example utility case study of the Florida Power and Light Company", IEEE Transactions on Energy Conversion, vol. 7, no. 3, Sept. 1992, pp. 396-404.

[69] S. Alyasin, S. Hoffman, R. Sasaki, "The identification of the true energy savings realized from high efficiency electronic loads", Proceedings of the IEEE PES T & D, April 10-15, 1994 pp. 79-85.

[70] L. E. Sulfstede, "Applying Power Electronics to Residential HVAC – The Issues", IEEE Transactions on Industry Applications, vol. 29, no. 2, March/April 1993, pp. 300-305.

[71] A. M. Jungreis, A. W. Kelley, "Adjustable Speed Drive for Residential Applications", IEEE Transactions on Industry Applications, vol. 31, no. 6, Nov./Dec. 1995, pp. 1315-1322.

[72] C. Jiang (Spring 2012), "A Probabilistic Bottom-up Technique for Modeling and Simulation of Residential Distributed Harmonic Sources", PhD Thesis, pp 100-105, Electrical and Computer Engineering Department, University of Alberta, Canada.

[73] J. Arrillaga and N.R. Watson, "Power System Harmonics", Second Edition, 2003, pp. 176-180, John Wiley & Sons, Ltd.

[74] K. Wada, H. Fujita, H. Akagi, "Considerations of a shunt active filter based on voltage detection for installation on a long distribution feeder," IEEE Transactions on Industry Applications, vol.38, no.4, pp. 1123- 1130, Jul/Aug 2002.

[75] European Photovoltaic Industry Association (EPIA), "Annual report - 2011", pp. 5-7, March 2012.

[76] Global Wind Energy Council (GWEC), "Global wind report, annual market update - 2011", pp. 4-7, March 2012.

[77] C.H. Lin, W.L. Hsieh, C.S. Chen, C.T. Hsu and T.T. Ku, "Optimization of Photovoltaic Penetration in Distribution Systems Considering Annual Duration Curve of Solar Irradiation," IEEE Transactions on Power Systems, vol.27, no.2, pp.1090-1097, May 2012.

[78] A. Capasso, W. Grattieri, R. Lamedica, and A. Prudenzi, "A bottom-up approach to residential load modeling," IEEE Transactions on Power Systems, vol.9, no.2, pp.957-964, May 1994.

[79] C. Zhe, F. Blaabjerg and J.K. Pedersen, "Hybrid compensation arrangement in dispersed generation systems," IEEE Transactions on Power Delivery, vol.20, no.2, pp. 1719- 1727, April 2005.

[80] Y.A.-R.I. Mohamed, "Mitigation of Dynamic, Unbalanced, and Harmonic Voltage Disturbances Using Grid-Connected Inverters With Filter," Industrial Electronics, IEEE Transactions on , vol.58, no.9, pp.3914-3924, Sept. 2011.

[81] M. Prodanovic, K.D. Brabandere, J.V.D. Keybus, T. Green and J. Driesen, "Harmonic and reactive power compensation as ancillary services in inverter-based distributed generation," Generation, Transmission & Distribution, IET , vol.1, no.3, pp.432-438, May 2007.

[82] A.B. Nassif, J. Yong, W. Xu. “Measurement-based Approach for Constructing Harmonic Models of Electronic Home Appliances”. IET Generation, Transmission & Distribution. Vol. 4(3):363-375.

[83] Y.J. Wang, R.M. O'Connell, G. Brownfield, “Modeling and Prediction of Distribution System Voltage Distortion Caused by Non-linear Residential Loads," IEEE Power Engineering Review, vol.21, no.7, pp.71, July 2001.

[84] P.T. Cheng, T.L. Lee, "Distributed Active Filter Systems (DAFSs): A New Approach to Power System Harmonics," IEEE Transactions on Industry Applications, vol.42, no.5, pp.1301-1309, Sept.-Oct. 2006.

[85] T.L. Lee, J.C. Li, P.T. Cheng , "Discrete Frequency Tuning Active Filter for Power System Harmonics," IEEE Transactions on Power Electronics, vol.24, no.5, pp.1209-1217, May 2009.

[86] Y. W. Li and C. N. Kao, “An Accurate Power Control Strategy for Power-Electronics-Interfaced Distributed Generation Units Operating in a Low-Voltage Multibus Microgrid,” IEEE Transactions on Power Electronics, vol. 24, pp. 2977-2988, Dec. 2009.

[87] J. He and Y. W. Li, “Analysis, Design and Implementation of Virtual Impedance for Power Electronics Interfaced Distributed Generation,” IEEE Transactions on Industry Application, vol. 47, pp. 2525-2538, Nov/Dec. 2011.

[88] D. M. Vilathgamuwa, P. C. Loh and Y. W. Li, “Protection of Microgrids during Utility Voltage Sags,” IEEE Transactions on Industrial Electronics, vol. 53, pp. 1427-1436, Oct. 2006.

[89] J. He, Y. W. Li, D. Bosnjak, and B. Harris, “Investigation and Active Damping of Multiple Resonances in a Parallel-Inverter Based Microgrid,” IEEE Transactions on Power Electronics, in press, 2012.

[90] Y. W. Li, “Control and Resonance Damping of Voltage Source and Current Source Converters with LC Filters,” IEEE Transactions on Industrial Electronics, vol. 56, pp. 1511-1521, May 2009.

[91] J. He, Y. Li and S. Munir, "A Flexible Harmonic Control Approach through Voltage Controlled DG-Grid Interfacing Converters," IEEE Transactions on Industrial Electronics, vol.59, no.1, pp.444-455, Jan. 2012.

[92] N. Pogaku and T.C. Green, “Harmonic mitigation throughout a distribution system: a distributed-generatorbased solution,” IEE Proc. Gener. Transm. Distrib., vol. 153, no. 3, pp. 350- 358, 11 May 2006.

[93] C.J. Gajanayake, D.M. Vilathgamuwa, P. C. Loh, R. Teodorescu, and F. Blaabjerg, “Z-Source-Inverter-Based Flexible Distributed Generation System Solution for Grid Power Quality Improvement,” IEEE Trans. Energy Conversion, vol.24, pp.695-704, Sept. 2009.

[94] P. Jintakosonwit, H. Akagi, H. Fujita, and S. Ogasawara, “Implementation and performance of automatic gain adjustment in a shunt-active filter for harmonic damping throughout a power distribution system,” IEEE Trans. Power Electron., vol.17, pp. 438-447, May 2002.

[95] D. N. Zmood, D. G. Holmes and G. H. Bode, “Stationary frame current regulation of PWM inverters with zero steady-state error,” IEEE Trans. Power Electron., vol. 18, pp. 814–822, Mar. 2003.

[96] P. Mattavelli, “Synchronous-frame harmonic control for high-performance AC power supplies,” IEEE Trans. Ind. Applicat., vol. 37, pp. 864–872, May/Jun. 2001.

[97] R. Dwyer, A.K. Khan, M. Mcgranaghan, L. Tang, R.K. Mccluskey, R. Sung, and T. Houy, "Evaluation of harmonic impacts from compact fluorescent lights on distribution systems," IEEE Transactions on Power Systems, vol.10, no.4, pp.1772-1779, Nov. 1995.

[98] E.J. Currence, J.E. Plizga and H.N. Nelson, "Harmonic resonance at a medium-sized industrial plant," Industry Applications, IEEE Transactions on, vol.31, no.4, pp.682-690, Jul/Aug 1995.

[99] M. Saito, T. Takeshita, N. Matsui, "Modeling and harmonic suppression for power distribution systems", IEEE Transactions on Industrial Electronics, Volume.50, Issue.6, pp.1148, 2003

[100] I. Bucatariu and F.D. Surianu, "Optimal Placement of Fixed Series Capacitor in Distribution Networks", Proceedings of the 9th WSEAS/IASME International Conference on Electric Power Systems, High Voltages and Electric Machines, pp. 65-70, Genova, Italy, October 17-19, 2009.

[101] H.D. Chiang, J.C. Wang, O. Cockings and H.D. Shin, "Optimal capacitor placements in distribution systems: Part I and Part 11," IEEE Transaction on Power Delivery, vol. 5, No. 2, pp. 634- 649, January 1990.

[102] M. Bradt, B. Badrzadeh, E. Camm, D. Mueller, J. Schoene, T. Siebert, T. Smith, M. Starke, R. Walling, “Harmonics and resonance issues in wind power plants”, in Proc. IEEE PES General Meeting, vol., no., pp.1,8, 24-29 July 2011.

[103] Wilsun Xu; Zhenyu Huang; Yu Cui; Haizhen Wang, "Harmonic resonance mode analysis," Power Delivery, IEEE Transactions on , vol.20, no.2, pp.1182,1190, April 2005

[104] Md Hasan, K.; Rauma, K.; J., I.; Luna, A.; rodriquez, P., "Harmonic Compensation Analysis in Offshore Wind Power Plants using Hybrid Filters," Industry Applications, IEEE Transactions on , vol.PP, no.99, pp.1,1,

[105] J. He, Y. W. Li, J. Guerrero, F. Blaabjerg, and J. Vasquez, “An Islanding Microgrid Power Sharing Approach Using Enhanced Virtual Impedance Control Scheme,” IEEE Transactions on Power Electronics, vol. 28, pp. 5272-5282, Nov. 2013.
[106] P.T. Cheng, T.L. Lee, "Distributed Active Filter Systems (DAFSs): A New Approach to Power System Harmonics," IEEE Transactions on Industry Applications, vol.42, no.5, pp.1301-1309, Sept.-Oct. 2006.
[107] T. L. Lee, P. T. Cheng, H. Akagi and H. Fujita, "A Dynamic Tuning Method for Distributed Active Filter Systems," in IEEE Transactions on Industry Applications, vol. 44, no. 2, pp. 612-623, March-april 2008.
[108] T. L. Lee and P. T. Cheng, "Design of a New Cooperative Harmonic Filtering Strategy for Distributed Generation Interface Converters", in IEEE Trans. on Power Elec., vol. 22, no. 5, pp. 1919-1927, Sept. 2007.

Appendix

Table A1: Distribution system model parameters

Circuit Parameters	Value
Generator	34.5KV
Distribution transformer	7200V/120V, 0.015+0.03j p.u
Distribution line impedance	.43Ω/km, 150µH/km
Number of nodes	11
Number of House loads at each node	12

Table A2: DG compensation priority calculated from Table 4.2.

		Harmonic order						
		3rd	5th	7th	9th	11th	13th	15th
Priorities at node	1	0.04	0.01	0.10	0.14	0.20	0.10	0.03
	2	0.09	0.02	0.19	0.28	0.40	0.20	0.05
	3	0.13	0.04	0.29	0.41	0.60	0.30	0.08
	4	0.17	0.05	0.38	0.54	0.80	0.40	0.11
	5	0.21	0.06	0.46	0.67	1.00	0.51	0.14
	6	0.24	0.07	0.50	0.70	1.00	0.48	0.12
	7	0.26	0.07	0.54	0.73	0.99	0.45	0.11
	8	0.29	0.08	0.57	0.75	0.99	0.43	0.10
	9	0.30	0.08	0.59	0.77	0.99	0.42	0.09
	10	0.31	0.08	0.60	0.78	0.98	0.41	0.09
	11	0.32	0.09	0.61	0.79	0.98	0.40	0.08

Table A3: DG compensation priority calculated from Table 4.4.

		Harmonic order						
		3rd	5th	7th	9th	11th	13th	15th
Priorities at node	1	0.02	0.02	0.03	0.00	0.00	0.01	0.03
	2	0.07	0.06	0.12	0.02	0.00	0.05	0.13
	3	0.15	0.14	0.28	0.04	0.01	0.11	0.31
	4	0.24	0.22	0.40	0.05	0.01	0.05	0.12
	5	0.35	0.31	0.55	0.07	0.01	0.01	0.02
	6	0.47	0.42	0.75	0.09	0.01	0.01	0.01
	7	0.59	0.54	1.00	0.13	0.02	0.01	0.06
	8	0.66	0.55	0.89	0.10	0.01	0.02	0.05
	9	0.72	0.56	0.81	0.08	0.01	0.03	0.04
	10	0.76	0.57	0.76	0.07	0.01	0.03	0.03
	11	0.78	0.57	0.74	0.06	0.01	0.04	0.03

Table A4: V_{THD} values in Figure 4.10.

Compensation strategy	V_{THD} at node										
	1	2	3	4	5	6	7	8	9	10	11
No DG	1.99	2.58	3.14	3.67	4.18	4.36	4.51	4.64	4.73	4.80	4.83
End of line	1.87	2.42	2.94	3.43	3.89	4.06	4.20	4.32	4.40	4.45	4.47
Distributed	1.78	2.31	2.80	3.27	3.71	3.88	4.04	4.16	4.26	4.32	4.36
Selective	1.74	2.25	2.73	3.18	3.61	3.78	3.94	4.06	4.15	4.22	4.25

Table A5: V_{THD} values in Figure 4.12.

Compensation strategy	V_{THD} at node										
	1	2	3	4	5	6	7	8	9	10	11
No DG	2.03	2.62	3.20	3.60	3.97	4.33	4.66	4.75	4.83	4.88	4.90
End of line	1.96	2.53	3.09	3.46	3.82	4.15	4.46	4.54	4.59	4.62	4.62
Distributed	1.92	2.48	3.03	3.40	3.76	4.09	4.41	4.49	4.56	4.61	4.63
Selective	1.90	2.46	3.00	3.37	3.72	4.05	4.36	4.44	4.50	4.55	4.57

Table A5: V_{THD} values in Figure 4.13.

Compensation strategy	V_{THD} at node										
	1	2	3	4	5	6	7	8	9	10	11
No DG	1.99	2.58	3.14	3.67	4.18	4.36	4.51	4.64	4.73	4.80	4.83
End of line	1.87	2.42	2.94	3.43	3.89	4.06	4.20	4.32	4.40	4.45	4.47
Distributed	1.78	2.31	2.80	3.27	3.71	3.88	4.04	4.16	4.26	4.32	4.36
Selective (actual)	1.74	2.25	2.73	3.18	3.61	3.78	3.94	4.06	4.15	4.22	4.25
Selective (assumed)	1.76	2.28	2.76	3.21	3.64	3.82	3.98	4.11	4.21	4.27	4.30